System Simulation of Partially Premixed Combustion in Heavy-Duty Engines

Gas Exchange, Fuels and In-cylinder Analysis

Svensson, Erik

2019

Document Version:
Publisher's PDF, also known as Version of record

System Simulation of Partially Premixed Combustion in Heavy-Duty Engines

Gas Exchange, Fuels and In-cylinder Analysis

System Simulation of Partially Premixed Combustion in Heavy-Duty Engines

Gas Exchange, Fuels and In-cylinder Analysis

by Erik Svensson

LUND
UNIVERSITY

Thesis for the degree of Doctor of Philosophy in Engineering
Thesis advisor: Associate Professor Sebastian Verhelst
Thesis co-advisor: Professor Martin Tunér
Faculty opponent: Dr. Andrew Smallbone

To be presented, with the permission of the Faculty of Engineering of Lund University, for public criticism in the M:B lecture hall at the Department of Energy Sciences on Thursday, the 13th of June 2019 at 10:15.

Organization
LUND UNIVERSITY

Department of Energy Sciences
Box 188
SE–221 00 LUND
Sweden

Author(s)
Erik Svensson

Document name
DOCTORAL DISSERTATION

Date of disputation
2019-06-13

Sponsoring organization
Swedish Energy Agency
KCFP Engine Research Center

Title and subtitle
System Simulation of Partially Premixed Combustion in Heavy-Duty Engines: Gas Exchange, Fuels and In-cylinder Analysis

Abstract
The concept of partially premixed combustion (PPC), applied to conventional diesel engines, has shown to yield high gross efficiencies and low emissions of oxides of nitrogen and soot. PPC emerged from the knowledge gained from homogeneous charge compression ignition (HCCI) research. To extend the load range and thus reduce cylinder pressure rise rates, the fuel is directly injected during the compression stroke, instead of in the intake port as is common with HCCI. In contrast to conventional diesel combustion, there is a separation between the fuel injection event and the start of combustion in PPC. Furthermore, the PPC concept relies on a high degree of dilution with exhaust gas recirculation (EGR) and air. This dilution and premixedness lead to a lower global temperature, which reduces NO_x emissions and wall heat transfer which therefore results in a high thermodynamic efficiency. However, a high level of dilution reduces the exhaust temperature and thus leads to a lower gas exchange efficiency because the turbine needs to compensate by generating a higher exhaust back pressure. This thesis therefore focuses on expanding the system boundary of PPC, to facilitate a commercial application. This has been conducted in several studies which targeted the brake efficiency, instead of the gross. The work was conducted with a combination of engine modeling and simulations. Moreover, the in-cylinder combustion was taken from experimental measurements or predicted using a stochastic reactor model. The first part of the work investigated the influence of dilution on the gas exchange performance. The gas exchange efficiency was seen to decrease exponentially at high levels of dilution. In addition, a low inlet temperature led to an increase in both brake and gross efficiencies. Furthermore, an evaluation of turbocharger configurations revealed that, although a two-stage turbocharger only negligibly increased the brake efficiency, it enabled a substantially higher engine load than the two single-stage turbochargers. Finally, the gas exchange efficiency was increased with 4 %pt. by using a combined low and high-pressure EGR system. The second part focused on optimizing the engine boundary conditions, choice of fuels, and injection strategy. The results showed that by using methanol, an increase in brake efficiency of 2.2 %pt. was possible compared to gasoline. The reason was a higher gross efficiency which resulted from an improved compromise between combustion duration, heat transfer, and NO_x emissions, as well as lower compression work and favorable ratio of specific heats. Increasing the engine's compression ratio, facilitated a lower inlet temperature with methanol and this led to a 1.4 %pt. further increase in brake efficiency.

Key words
Partially premixed combustion, Compression ignition, Direct injection, Methanol, Engine optimization, Stochastic reactor model, Gas exchange, $T - \phi$-diagrams

Classification system and/or index terms (if any)

Supplementary bibliographical information

Language
English

ISSN and key title
0282-1990

ISBN
978-91-7895-129-1 (print)
978-91-7895-130-7 (pdf)

Recipient's notes

Number of pages
170

Price

Security classification

Signature _____ Date May 20, 2019

System Simulation of Partially Premixed Combustion in Heavy-Duty Engines

Gas Exchange, Fuels and In-cylinder Analysis

by Erik Svensson

LUND
UNIVERSITY

A doctoral thesis at a university in Sweden takes either the form of a single, cohesive research study (monograph) or a summary of research papers (compilation thesis), which the doctoral student has written alone or together with one or several other author(s).

In the latter case the thesis consists of two parts. An introductory text puts the research work into context and summarizes the main points of the papers. Then, the research publications themselves are reproduced, together with a description of the individual contributions of the authors. The research papers may either have been already published or are manuscripts at various stages (in press, submitted, or in draft).

Funding information: The thesis work was financially supported by the Swedish Energy Agency, grant numbers P38272-1 and P22485-4, and the KCFP Engine Research Center.

Faculty of Engineering, Department of Energy Sciences

ISBN: 978-91-7895-129-1 (print)
ISBN: 978-91-7895-130-7 (pdf)
ISRN: LUTMDN/TMHP-19/1151-SE
ISSN: <0282-1990>

Printed in Sweden by Tryckeriet i E-huset, Lund University, Lund 2019

Till Katja

Contents

List of publications iii
Acknowledgments v
Abstract vii
Populärvetenskaplig sammanfattning på svenska viii
Abbreviations & Symbols x

1 Introduction **1**
1.1 Motivation and Scope 3
1.2 Thesis Contributions 6
1.3 Thesis Outline 6

2 Partially Premixed Combustion in Heavy Duty Engines **9**
2.1 Distinction between Combustion Modes 9
2.2 Mechanisms for Reducing NO_x and Soot 11
2.3 Means to achieve Partially Premixed Combustion 13
2.4 Alternative Fuels 15
2.5 Engine Energy Flows and Efficiency Definitions 17

3 Models and Validation **23**
3.1 Gas Dynamic Multi Cylinder Engine Model 23
3.2 Gas Dynamic Single Cylinder Engine Model 28
3.3 Stochastic Reactor Model 30
3.4 Full Engine Cycle Simulation 34

4 Gas Exchange Analysis **39**
4.1 Influence of Engine Parameters on Gas Exchange Efficiency 39
4.2 Evaluation of Turbochargers for Partially Premixed Combustion . . . 43
4.3 Application of Dual Loop EGR 58
4.4 Summary 62

5 Re-Optimization of the Engine Settings to achieve Maximum Engine Brake Efficiency **65**
5.1 Operating Points 69
5.2 Optimization Strategy 71
5.3 Optimization Results 74

5.4 Limitations of the Approach 87
5.5 Influence of Optimization Constraints 93
5.6 Summary 98

6 Emission Formation and Ignition Location on the $T - \phi$ Plane 101
6.1 $T - \phi$ Map Methodology 102
6.2 SRM Particle Trajectories during Optimal Combustion 106
6.3 Sensitivity of Start of Injection on Ignition Timing 110
6.4 The Effect of Thermal Stratification 111
6.5 Summary 116

7 Summary and Conclusions 119
7.1 Contributions 119
7.2 Outlook 122

Appendix A 125

Bibliography 127

Summary of Papers 141

List of publications

This thesis is based on the following publications, referred to by their Roman numerals:

I **Evaluation of Different Turbocharger Configurations for a Heavy-Duty Partially Premixed Combustion Engine**

E. Svensson, L. Yin, P. Tunestål, M. Thern, M. Tunér
SAE International Journal of Engines vol. 10, no. 5 (2017)

II **Combined Low and High Pressure EGR for Higher Brake Efficiency with Partially Premixed Combustion**

E. Svensson, L. Yin, P. Tunestål, M. Tunér
SAE Technical Paper, 2017-01-2267, 2017

III **Simulation Based Investigation of achieving Low Temperature Combustion with Methanol in a Direct Injected Compression Ignition Engine**

E. Svensson, S. Verhelst
SAE Technical Paper, 2019-01-1152, 2019

IV **Numerical Optimization of Compression Ratio for a PPC Engine running on Methanol**

E. Svensson, S. Verhelst
Paper accepted for publication at JSAE/SAE PFL, Kyoto, Japan

V **Evaluation of Injection Strategies at Maximum Brake Efficiency for a Methanol PPC Engine**

E. Svensson, M. Tunér, S. Verhelst
Paper submitted to NASAE/SAE, Capri, Italy

VI **Potential Levels of Soot, NO_x, HC and CO for Methanol Combustion**

E. Svensson, C. Li, S. Shamun, B. Johansson, M. Tunér, C. Perlman, H. Lehtiniemi, F. Mauss,
SAE Technical Paper, 2016-01-0887, 2016

Other non-related publications:

Investigation of Late-Cycle Soot Oxidation Using Laser Extinction and In-Cylinder Gas Sampling at Varying Inlet Oxygen Concentrations in Diesel Engines

Y. Gallo, V. Malmborg, J. Simonsson, **E. Svensson**, M. Shen, P-E Bengtsson, J. Pagels, M. Tunér, A. Garcia, Ö. Andersson
Fuel, vol. 193, pp. 208-314, 2017

Alternative Fuels for Particulate Control in CI Engines

S. Shamun, P. Garcia, **E. Svensson**
Springer, Engine Exhaust Particulates, pp. 181-197, 2018

Investigating the Potential of an Integrated Coolant Waste Heat Recovery System in an HD Engine using PPC Operation

V. Singh, **E. Svensson**, S. Verhelst, M. Tunér
ASME Conference Proceedings, ICEF 2018-9708, 2018

Acknowledgments

I would like to begin by thanking Martin Tunér, who gave me this job and the opportunity to pursue a Ph.D. in the field of combustion engines. You were my main supervisor for the first part of my Ph.D. studies, and the one who introduced me to the world of engine simulations and chemical kinetics. The freedom that you allowed me in my research was invaluable. Moreover, I always felt your support when I wanted to spend time on reading up on things, which were not necessarily related to my research, but which improved my general technical knowledge. Furthermore, your optimism and the way that you always stand up for your students are admirable. Finally, I would like to thank you for allowing me the privilege of having two main supervisors during these years.

Next, I want to thank Sebastian Verhelst who took over my supervision for the final one and a half years. My thesis would not have been possible without your guidance, and I'd even go as far as to say that you taught me what it means to be a researcher. Although, you made me frustrated at times by always questioning and challenging my every move, you always managed to do it in a constructive way. Moreover, there are very few times when your suggestions did not make sense in hindsight. Your high expectations pushed me to work harder than anything else and I would like to thank you for that. Finally, I don't think I can thank you enough for all your comments and corrections to my texts.

I would like to express my deepest gratitude to Marcus Thern. You have been a true mentor for me and the way that you have always been available to answer every single one of my stupid questions is truly remarkable. Furthermore, you were the one who convinced me to apply for the Ph.D. position. At the time I did not know anything about combustion engines, but you encouraged me by asking rhetorically: how hard can it be? And that mentality is something that I have embraced and what made me complete this journey. I'm truly going to miss stopping by your office for a casual one-hour talk about everything from politics to thermodynamics to latex peculiarities.

Furthermore, I would like to thank Per Tunestål and Öivind Andersson. Per, our common interest in football and beer has led to very joyful discussions. I expect us to see each other at Stadion when di blåe are playing! Öivind, your way of teaching the scientific methodology, going from experimental design to scientific writing, is something that I have benefited from greatly. I hope you will continue with your podcast as I have really enjoyed listening to those episodes.

Magnus Genrup and Jens Klingmann deserve to be thanked. They, together with Marcus, taught me everything I know about turbo machines. Magnus, you got me

the position at Volvo for my Master's thesis project, which led to my interest in trucks and engines.

I would like to thank Harry, Cathleen and Andrea at Loge. Harry for all our interesting discussions on the bus from Malmö, and Cathleen, and Andrea for the quick and great support I always got.

I also want to thank Robert and Krister. You helped me with all the IT related issues. Also, you trusted me to have access to the license server which was very convenient.

Many thanks to Catarina, Elna, Gity, and Isabelle for always having time to help me with any questions or issues I had.

I did not spend too much time in the lab over the years. But, whenever I did, I always received help from our technicians. Thank you, Mats, Tommy, Tomas, Anders, and Patrik. Moreover, you were always very nice to talk to.

If it had not been for all my great colleagues, these years would have seemed so much more. Specifically, I want to thank Nhut Lam. We shared an office for my whole time, and he made me feel welcome from the first second. A special thanks also go to Kenan, Niko, Vikram, Xinda, Changle, Sam, Ashish, Christian, Thommie, and Mateusz. Spending time in the office, during lunch, and going to conferences with you guys have been a pleasure.

Naturally, I would not have been where I am if it were not for my family. Mamma and Pappa, you have made me into the person that I am today. Without you, none of this would have been possible, and your complete and unconditional support in everything I have ever wanted to do, is something that I can't thank you for enough. Henrik, Andreas, and Markus, to spend time with you has been something that I have really looked forward to.

Katja, I don't think it is possible to describe what your support and understanding have meant to me during these four years. Through all the late nights and weekends, the knowledge that you were waiting for me was the thing that kept me going. Jag älskar dig!

Abstract

The concept of partially premixed combustion (PPC), applied to conventional diesel engines, has shown to yield high gross efficiencies and low emissions of oxides of nitrogen and soot. PPC emerged from the knowledge gained from homogeneous charge compression ignition (HCCI) research. To extend the load range and thus reduce cylinder pressure rise rates, the fuel is directly injected during the compression stroke, instead of in the intake port as is common with HCCI. In contrast to conventional diesel combustion, there is a separation between the fuel injection event and the start of combustion in PPC. Furthermore, the PPC concept relies on a high degree of dilution with exhaust gas recirculation (EGR) and air. This dilution and premixedness lead to a lower global temperature, which reduces NO_x emissions and wall heat transfer which therefore results in a high thermodynamic efficiency. However, a high level of dilution reduces the exhaust temperature and thus leads to a lower gas exchange efficiency because the turbine needs to compensate by generating a higher exhaust back pressure.

This thesis therefore focuses on expanding the system boundary of PPC, to facilitate a commercial application. This has been conducted in several studies which targeted the brake efficiency, instead of the gross. The work was conducted with a combination of engine modeling and simulations. Moreover, the in-cylinder combustion was taken from experimental measurements or predicted using a stochastic reactor model.

The first part of the work investigated the influence of dilution on the gas exchange performance. The gas exchange efficiency was seen to decrease exponentially at high levels of dilution. In addition, a low inlet temperature led to an increase in both brake and gross efficiencies. Furthermore, an evaluation of turbocharger configurations revealed that, although a two-stage turbocharger only negligibly increased the brake efficiency, it enabled a substantially higher engine load than the two single-stage turbochargers. Finally, the gas exchange efficiency was increased with 4 %pt. by using a combined low and high-pressure EGR system.

The second part focused on optimizing the engine boundary conditions, choice of fuels, and injection strategy. The results showed that by using methanol, an increase in brake efficiency of 2.2 %pt. was possible compared to gasoline. The reason was a higher gross efficiency which resulted from an improved compromise between combustion duration, heat transfer, and NO_x emissions, as well as lower compression work and favorable ratio of specific heats. Increasing the engine's compression ratio, facilitated a lower inlet temperature with methanol and this led to a 1.4 %pt. further increase in brake efficiency.

Populärvetenskaplig sammanfattning på svenska

De skadliga effekterna av global uppvärmning är välkända samt starkt kopplade till en ökning av växthusgaser och framför allt utsläpp av CO_2. Från 1970 till 2010 fördubblades dessa utsläpp till följd av förbränning av fossila bränslen, industriprocesser, skogsavverkning och lantbruk. Transportsektorn står för en stor och ökande del av alla CO_2-utsläpp och enligt en prognos från internationella energiorganisationen IEA kommer lastbilar att stå för hälften av alla CO_2-utsläpp från transportsektorn år 2050. Eftersom mängden CO_2-utsläpp är nästan direkt proportionell mot bränsleförbrukningen är det av största vikt att öka motorns effektivitet för denna grupp fordon.

Den konventionella dieselmotorn dominerar lastbilsmarknaden på grund av dess låga bränsleförbrukning och hållbarhet. Bränsleförbrukningen för dieselmotorer har minskat stadigt under lång tid som följd av en rad tekniska innovationer. En stor nackdel för dieselmotorn är emellertid att det under förbränningen skapas stora mängder av skadliga utsläpp. Fordonstillverkare har behövt använda tekniker som leder till höjd bränsleförbrukning och ökad kostnad för att kunna minimera dessa utsläpp. Detta har i förlängningen gjort att minskningen av bränsleförbrukningen har avtagit under de senaste åren.

Som en motpol har forskare på senare år börjat utveckla nya avancerade förbränningskoncept med målet att eliminera de skadliga utsläppen men ändå uppnå samma låga bränsleförbrukning. Dessa koncept kombinerar på olika sätt val av bränsle, strategier för direktinsprutning och utspädning med luft. Dessutom använder man sig av så kallad EGR-teknik (vilket står för exhaust gas recirculation) som innebär att avgaser tas från motorns utlopp och förs tillbaka till inloppet. Även om koncepten skiljer sig åt är det gemensamma målet att minska temperaturen under förbränningen för att på så sätt sänka nivåerna av utsläpp. En lägre temperatur under förbränningen har även fördelen att det kan minska värmeöverföringen till motorns väggar vilket kan leda till ännu lägre bränsleförbrukning. För att nå målet om nollutsläpp krävs dock mycket mer forskning.

I det här arbetet har ett koncept som heter partiellt förblandad förbränning (vilket har förkortningen PPC) studerats. Skillnaden mellan detta koncept och konventionell dieselförbränning är att tidpunkten för insprutning av bränslet är tidigarelagd så att bränsle och luft har mer tid att blandas. På så sätt kan en mer optimal förbränning uppnås. Utöver förblandning av luft och bränsle används EGR-system för att reducera förbränningstemperaturen. För att detta ska fungera krävs en väldigt effektiv turbo som levererar stora mängder luft till motorns inlopp. Test i laboratoriemiljö har visat att PPC kan reducera de skadliga utsläppen till nivåer långt under lagkraven. Problemet som uppstår när PPC ska testas på en riktigt lastbil är dock att dagens turbos inte

är tillräckligt effektiva och därför inte klarar av att leverera så stora mängder av luft som krävs. Följaktligen har än så länge inte en lägre bränsleförbrukning kunnat uppnås. Ett av huvudmålen med det här arbetet har därför varit att analysera hur man kan gå tillväga för att uppnå en balans av höga mängder luft och låg bränsleförbrukning. Vidare gjordes en optimering av val av bränsle, randvillkor, och bränsleinsprutningsinställningar med målet att åstadkomma en så hög motorverkningsgrad som möjligt.

I den första delen av arbetet studerades olika sorters turbo-konfigurationer samt olika EGR-system. En turbo kan leverera stora mängder luft genom att en kompression av luften sker i turbons kompressor. Vanligtvis sker den här kompressionen i ett steg. Det visade sig emellertid att om kompressionen delas upp i två steg kan en något lägre bränsleförbrukning uppnås. Dessutom kunde motorns lastområde förstoras, det vill säga den maximala effekten blev högre. Det finns olika EGR-system men de kan i huvudsak delas in i två grupper. I den ena gruppen leds avgaserna om innan turbon medan avgaserna tillåts strömma genom turbon i den andra gruppen. I det här arbetet jämfördes ett system från bådadera grupper. Dessutom simulerades en hybrid, alltså ett system där det var möjligt att både ta avgaser före men även efter turbon. Med hybridsystemet var det möjligt att minska motorns bränsleförbrukning signifikant eftersom turbon kunde göras mer effektiv. Slutligen visade det sig att matchningen av turbon bör ske på annat sätt för ett förbränningssystem som applicerar PPC än för ett med konventionell dieselförbränning.

I den andra delen av arbetet gjordes optimeringar av olika nyckelparametrar för motorn med målet att minimera bränsleförbrukningen. Dessutom jämfördes metanol med två olika slags bensinbränslen. Resultaten visade att metanol kunde ge en ordentlig sänkning av bränsleförbrukningen jämfört med bensin. Dessutom kunde en ändring av motorns geometri leda till en ytterligare sänkning av bränsleförbrukningen med metanol eftersom det var möjligt att reducera temperaturen på den inkommande luften och därmed öka luftmassan.

Abbreviations & Symbols

$\dot{m}$	Mass flow
ϵ	Turbulent kinetic energy dissipation
η_{brake}	Brake efficiency
η_{comb}	Combustion efficiency
η_{c}	Compressor efficiency
$\eta_{\text{gas exchange}}$	Gas exchange efficiency
η_{gross}	Gross indicated efficiency
η_{is}	Isentropic efficiency
η_{mech}	Mechanical efficiency
η_{net}	Net indicated efficiency
η_{tc}	Turbocharger efficiency
η_{t}	Turbine efficiency
η_{vol}	Volumetric efficiency
γ	Ratio of specific heats
λ	Normalized air-fuel ratio
ω	Rotational speed
ϕ	Equivalence ratio
Π	Pressure ratio
ρ	Density
σ	Compressor slip factor
τ	Turbulent mixing time, ignition delay time
d	Diameter
θ	Crank angle degree
ε	Engine compression ratio

A	Cylinder surface area
c	Absolute velocity
c_p	Specific heat capacity at constant pressure
c_v	Specific heat capacity at constant volume
h	Enthalpy
h_0	Total enthalpy
h_t	Heat transfer convection coefficient
k	Turbulent kinetic energy
m	Mass
P	Power
p	Pressure
p'_{max}	Maximum cylinder pressure rise rate
p_0	Total pressure
p_{em}	Exhaust manifold pressure
p_{im}	Intake manifold pressure
p_{inj}	Injection pressure
p_{max}	Maximum cylinder pressure
Q	Heat
Q_{LHV}	Lower heating value
R	Gas constant
R^2	Coefficient of determination
s	Stoichiometric
SS	Sum of squares
T	Temperature
T_0	Total temperature

T_{dew}	Dew point temperature
T_{em}	Exhaust manifold temperature
T_{exh}	Exhaust temperature
T_{im}	Intake manifold temperature
T_{max}	Maximum cylinder temperature
T_{wall}	Cylinder wall surface temperature
U	Turbine tip speed
V	Cylinder volume
V_d	Displacement volume
Y	Mass fraction
0-D	Zero dimensional
1-D	One dimensional
NO_x	Oxides of nitrogen
°ca	Crank angle degree
aTDC	After top dead center
BC	Boundary conditions
BDC	Bottom dead center
BSR	Blade speed ratio
CA-C	Charge air cooler
CDC	Conventional diesel combustion
EGR	Exhaust gas recirculation
EGR-C	Exhaust gas recirculation cooler
EOI	End of injection
EVO	Exhaust valve opening
HCCI	Homogeneous charge compression ignition

HP	High pressure
IPCC	Intergovernmental Panel on Climate Change
IVC	Inlet valve closing
LP	Low pressure
MCE	Multi cylinder engine
MEP	Mean effective pressure
n	Engine speed
PDF	Probability density function
PPC	Partially premixed combustion
PRF	Primary reference fuel
RCCI	Reactivity controlled compression ignition
RON	Research octane number
s	Stroke
sNO_x	Specific oxides of nitrogen
SCE	Single cylinder engine
SET	Supplemental emission test
SOC	Start of combustion
SOI	Start of injection
SRM	Stochastic reactor model
TC	Turbocharger
TDC	Top dead center
VGT	Variable geometry turbine
WG	Waste gate

Chapter 1

Introduction

The adverse effects of global warming are well known and strongly linked to the increase of green-house gas emissions [1]. From 1970 to 2010 the annual total emitted green-house gases, which include CO_2 emissions from combustion of fossil fuel, industrial processes, forestry and land use as well as CH_4 and N_2O emissions, increased with 81 % to yield 49 Gt CO_2 equivalents per year. With 66 % in 2016, the CO_2 emissions from combustion of fossil fuels accounted for the largest part of green-house gas emissions [2]. The majority of CO_2 emissions came from the electricity and heat production, transport, and industrial process sectors as seen in Figure 1.1.

The 2 degree scenario, suggested by the Intergovernmental Panel on Climate Change (IPCC), states that by 2050, the CO_2 emissions from combustion of fossil fuels must be more than halved, in order to prevent the global temperature to rise more than

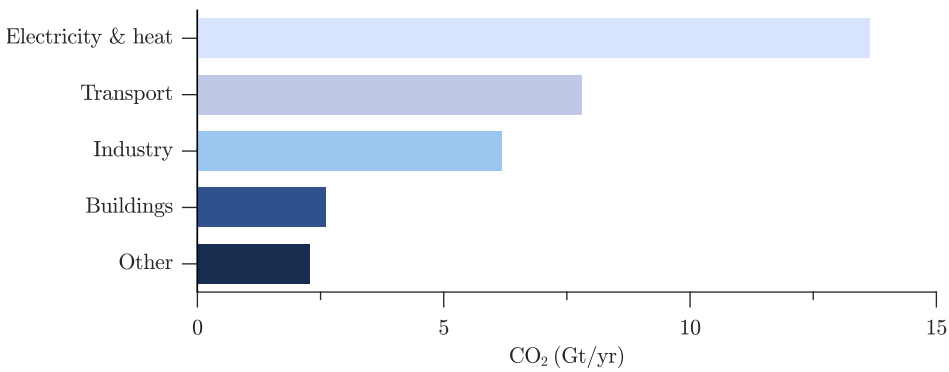

Figure 1.1: Total CO_2 emissions from fuel combustion in 2016 for the following economic sectors: 1) electricity and heat production, 2) transport, 3) industry, 4) buildings, and 5) energy production other than electricity and heat production [2].

2 °C. This can be done via an almost complete decarbonization of the electricity and heat production sector achieved through a transition from coal and gas to renewable fuels as well as carbon capture and storage [3]. The demand of transporting people and goods is increasing at a pace which is yielding a total surplus of emitted CO_2 emissions, despite an increasing share of renewables. Thus, the impact from the transport sector is expected to take up a larger fraction of the total CO_2 emissions.

Figure 1.2 shows the predicted 2050 CO_2 emissions, from the transport sector in the 2 degree scenario, split into the largest categories, namely 1) heavy-duty vehicles which include long haul and mid-sized trucks and buses, 2) light-duty vehicles such as small trucks and cars, 3) shipping, 4) aviation, and 5) rail. The heavy-duty and light-duty vehicles account for 74 % in total and as a consequence the largest impact can be achieved by focusing on these categories. Moreover, it is arguably easier to apply electrification and hybridization to the fleet of light-duty vehicles than the heavy-duty segment because of the difference in power requirement and hence battery size. Consequently, a high emphasis should be put on increasing the efficiency of heavy-duty vehicles, as tail-pipe CO_2 emissions are nearly proportional to the fuel consumption.

Compression ignition engines running on diesel fuel dominate the heavy-duty market because of their high brake efficiency and robustness [4]. The evolution of engine efficiency for the conventional diesel engine is presented in Figure 1.3. The brake efficiency has increased over time due to the implementation of for instance charge air cooling, combustion system optimization, high pressure common rail fuel injection, and variable geometry turbochargers. However, the combustion in diesel engines gives rise to substantial amounts of harmful emissions such as oxides of nitrogen (NO_x), particulate matter, and soot. The ever-stricter regulation limits for these emissions has led manufacturers to implement innovations such as cooled exhaust gas recirculation,

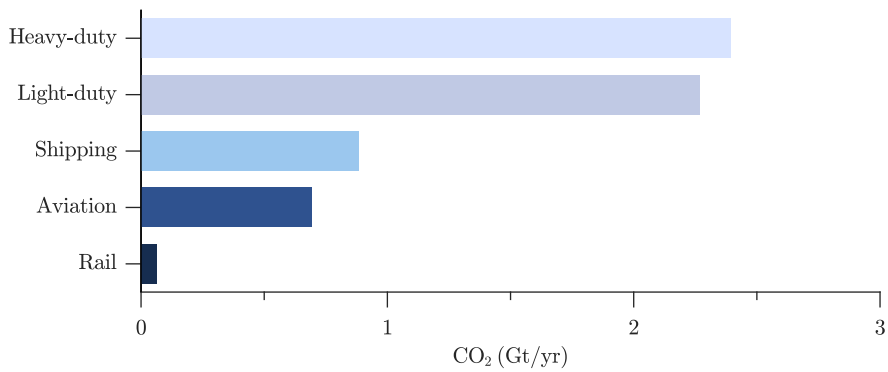

Figure 1.2: Predicted CO_2 emissions from combustion of fossil fuels in 2050 for the transport sector based on the 2 degree scenario (2DS) [3]. Division is made into the following categories: 1) heavy-duty vehicles, 2) light-duty vehicles, 3) shipping, 4) aviation, and 5) rail.

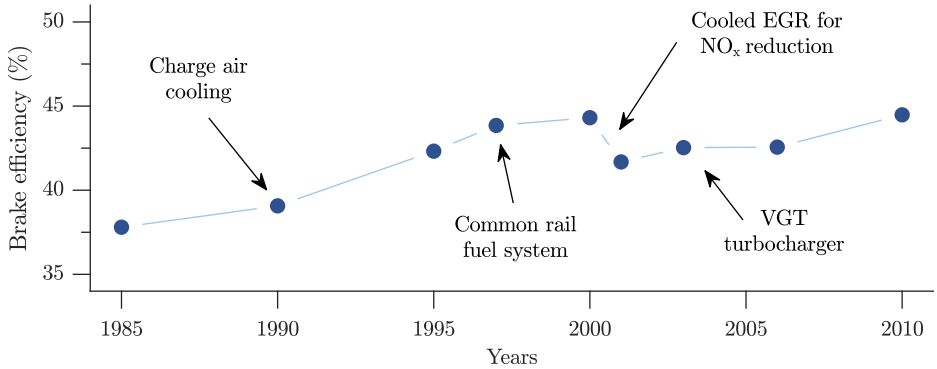

Figure 1.3: Evolution of heavy-duty engine brake efficiency at highway cruising conditions [4].

selective catalytic reduction, and particulate filters. Despite reducing emissions, these innovations have led to a reduction in the attainable brake efficiency and an increased operational cost [5].

In an attempt at reducing the amount of NO_x and soot emissions and hence cost of an advanced exhaust aftertreatment system, but still maintaining the low fuel consumption of the compression ignition engine, several advanced combustion concepts for the conventional diesel engine have been proposed in recent years.

1.1 Motivation and Scope

Advanced diesel engine combustion concepts such as homogeneous charge compression ignition (HCCI) and partially premixed combustion (PPC) all focus on reducing the emissions of NO_x and soot [6–10]. Although the concepts apply slightly different means to achieve low levels of these emissions, a common feature is the application of a high degree of dilution.

This work focuses on the partially premixed combustion concept applied to the conventional diesel engine. Partially premixed combustion emerged from the knowledge that has been gained from researching homogeneous charge compression ignition. In homogeneous charge compression ignition, the fuel is typically injected in the intake port a long time prior to the opening of the intake valves, or very early in the compression stroke, which creates an almost completely homogeneous mixture of fuel and bulk gas at the start of combustion. A certain degree of inhomogeneities exist, however, mainly in temperature because of wall heat transfer and turbulent mixing during the compression stroke [11]. In homogeneous charge compression ignition, the combustion proceeds as a series of sequential auto ignition events. This yields

a short combustion duration and, combined with the high dilution, a high thermal efficiency. However, the load range with homogeneous charge compression ignition, is limited by excessive pressure rise rates which cause engine knock. The partially premixed combustion concept attempts to expand the limited load range. Like homogeneous charge compression ignition, the partially premixed combustion concept applies a large degree of dilution to reduce global temperatures, but in contrast utilizes direct injection of the fuel during the compression stroke. The purpose of this is to create a less homogeneous mixture, which typically reduces pressure rise rates, but which still achieves the advantages of premixed combustion [12, 13]. To separate partially premixed combustion from conventional diesel combustion (CDC), I will use the definition of ignition dwell which is a measure of the difference between the end of fuel injection and start of combustion. A positive ignition dwell is obtained if the total amount of fuel has been injected before the start of combustion, otherwise the ignition dwell is negative.

The partially premixed combustion concept has received continuous focus since its introduction in the mid-2000. Low emissions of NO_x and soot have been achieved [14]. Furthermore, it has been found that the high degree of dilution and prolonged ignition dwell, can lead to lower combustion temperatures which due to a lower heat transfer to the cylinder wall, leads to a higher thermodynamic efficiency [15]. However, most of the research has been conducted in research laboratories where researchers make use of single cylinder engines. In a single cylinder engine, there is combustion in only one cylinder which is beneficial for at least two reasons. First, because only one cylinder is active, less fuel must be supplied. Secondly, there are fewer parameters to control which makes it easier to create an experiment which can single out various phenomena. In contrast to an engine installed on a vehicle, the boundary conditions are typically achieved by external means which for instance can mean that an external compressor is used to increase the inlet pressure, or that the inlet temperature is adjusted by means of an electric heater. Although single cylinder engines are very useful for studying and developing new combustion concepts, there is a risk that the applied boundary conditions cannot be fulfilled for a real application. For example, most heavy-duty vehicles have a turbocharger which extracts energy from the exhaust gases (which are hot) and converts this energy into an elevated pressure via a compressor. Except increasing the density of the incoming charge, the turbocharger takes care of the gas exchange, that is the supply of incoming gas and expulsion of burned gas. However, for this to be successful the exhaust gas has to contain a sufficient level of energy. This can lead to a problem for the partially premixed combustion concept as it relies on high levels of dilution, which reduce the exhaust energy. As a result, the higher potential in thermodynamic conversion inside the cylinder might be lost in gas exchange losses.

Therefore, this thesis presents studies which had the goal of expanding the system boundary of partially premixed combustion, in order to make it commercially applicable. This has been done in several studies which targeted the brake efficiency, instead of the gross indicated efficiency. First, a study was conducted which investigated and attempted to quantify the effect of dilution on the gas exchange performance, for a multi cylinder engine for which realistic boundary conditions were imposed. Secondly, the engine settings were optimized for the purpose of maximizing the engine brake efficiency, which means that the conditions were found which achieve the best trade-off between thermodynamic and gas exchange efficiencies. Thirdly, the in-cylinder processes and emission potential were studied at the conditions for the highest brake efficiency. In terms of fuels, the focus was put on two different gasoline fuels, one with a research octane number (RON) of 76 and one with 97, as well as on methanol. The gasoline fuels were modeled as surrogates because of the difficulty to accurately determine their composition. The choice of these fuels is motivated as follows. First, a fuel with higher research octane number facilitates a positive ignition dwell, hence the choice of the RON 97 gasoline fuel [16–18]. Secondly, in order to extend the operating range (increase the engine load at which PPC can be employed) multiple authors have advocated a fuel with RON of 65-80 [19–21]. Thirdly, the use of renewable fuels will enable a faster reduction of the CO_2 emissions, from the transport sector, than it will to only focus on fuel efficiency. Thus, methanol was targeted in this work as it is the simplest fuel which can be produced from renewable sources and which is liquid at atmospheric conditions [22, 23].

The work was conducted with a combination of engine modeling and simulations. Engine experiments have not been a part of this work, however, experimental data have been used to calibrate and validate the models. The in-cylinder combustion was predicted with a stochastic reactor model or taken from measured experimental data. The stochastic reactor model was also able to satisfactorily predict additional in-cylinder processes such as the injection and vaporization of fuel as well as mixing and emission formation. Two complete engine models were built in the engine modeling framework GT-suite. These models represent two different Scania D13 engines, one in a multi and one in a single cylinder configuration. This engine is representative of a typical engine for a long-haul truck. The multi cylinder engine model was used in the work described previously, while the single cylinder engine model was only used to predict the boundary conditions for the validation of the stochastic reactor model.

1.2 Thesis Contributions

The presented work has resulted in a number of specific contributions:

- A simulation study, evaluating different turbocharger configurations for the partially premixed combustion concept. The main limitation for achieving higher brake efficiencies, was found to be the reduced exhaust enthalpy which arises because of high levels of dilution.
- A simulation study which compared three exhaust gas recirculation (EGR) configurations. The turbocharger had to be redesigned for each configuration, due to the large difference in mass flow. It was found that a combined low and high pressure EGR configuration led to the highest brake efficiency, because more of the engine operating conditions could be run inside the compressor's highest efficiency region.
- An optimization study, where methanol was compared with two gasoline fuels. Realistic constraints were applied, and the brake efficiency was targeted. This study showed the benefits of using methanol in a partially premixed combustion engine.
- The compression ratio for a partially premixed combustion engine running on methanol was optimized for the highest brake efficiency. The optimum compression ratio was higher than the standard one. In addition, with a higher compression ratio the intake manifold temperature could be reduced, which would facilitate cold starts.
- The influence of start of injection strategies on brake efficiency was quantified for methanol. Furthermore, this study provided knowledge about the sensitivity of combustion stability to the inlet conditions.
- The potential levels of soot, NO_x, CO, and CO_2 emissions were investigated using the concept of temperature and equivalence ratio ($T-\phi$) diagrams. The diagrams could also be used to visualize the in-cylinder conditions in the $T-\phi$ domain which allowed an explanation of the previously observed trends.

1.3 Thesis Outline

This thesis is organized into seven chapters including the present introduction. A short description of the content of every chapter is provided here. Chapter 2 presents

a short literature review of the partially premixed combustion concept and describes the issues and potential improvements. In Chapter 3 the various models are presented and validation is provided. Chapter 4 presents the results from the gas exchange studies. Furthermore, Chapter 5 presents the results from the optimization of engine settings, aimed at maximizing the engine brake efficiency, where also a comparison between methanol and the two gasoline fuels is conducted. Chapter 6 provides an analysis of the in-cylinder conditions, which prevailed in the optimum cases found in Chapter 5. Finally, Chapter 7 provides a summary and conclusions of the results and discusses pathways for future work.

Chapter 2

Partially Premixed Combustion in Heavy Duty Engines

This chapter aims to provide an overview of the partially premixed combustion (PPC) concept and its application in heavy duty engines which applies direct injection and compression ignition. For this purpose, this chapter will begin with a discussion on the distinction between the different combustion modes. The mechanism for reducing soot and NO_x are important and will therefore be given a section, as well as the means of how to achieve PPC. Furthermore, the possibility to use alternative fuels will be highlighted. This chapter will conclude with a discussion on the various energy flows and efficiency definitions, as they have a central part throughout this thesis.

2.1 Distinction between Combustion Modes

The conventional diesel engine is used by heavy-duty truck engines because of its ability to reach a good trade-off between high efficiency, specific power and relatively low cost [4]. Irrespective of what combustion concept, advanced or conventional, this engine operates with, it uses the compression ignition combustion system applied to the classical four-stroke cycle which was invented already in the 19^{th} century. As the name suggests, this cycle consists of four different phases, illustrated in Figure 2.1 which shows the cylinder pressure as a function of volume for the four strokes. Conventional diesel combustion (CDC), in the compression ignition combustion system, is an efficient way of converting the energy in the fuel to useful work. However, CDC often generates significant amounts of harmful exhaust emissions such as oxides of nitrogen (NO_x) as well as soot and particulate matter. As mentioned in Chapter 1, the

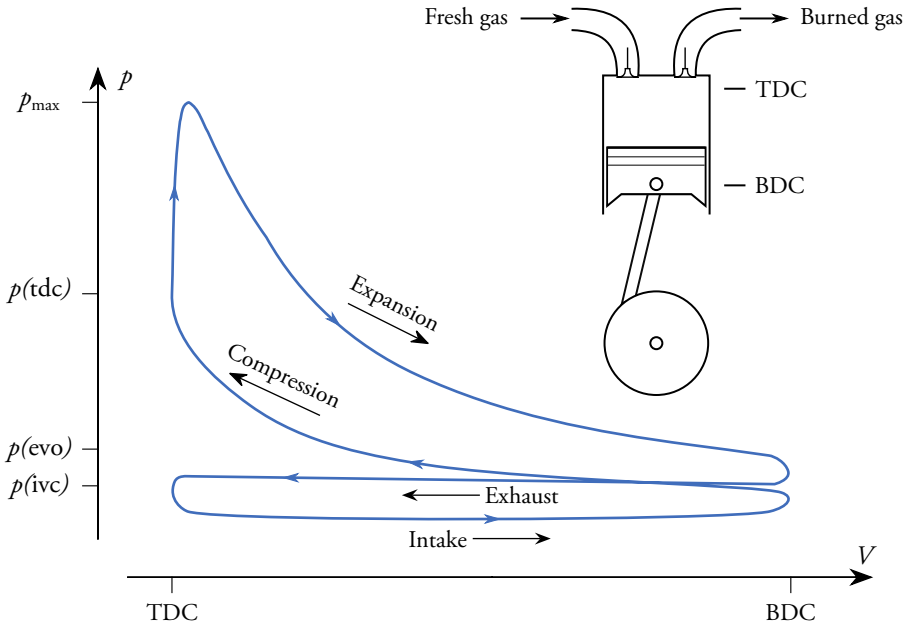

Figure 2.1: Illustration of the in-cylinder pressure as a function of in-cylinder volume as the piston moves through its four strokes: 1) Intake, 2) Compression, 3) Expansion, and 4) Exhaust. Top right corner shows a piston and cylinder which are linked via the connecting rod to the rotating crank-shaft. Fresh gas comes in through the intake valve and the burned gas is let out through the exhaust valve.

PPC concept applies an advanced type of combustion mode to mitigate this drawback. The ultimate goal of PPC is to achieve ultra-low engine-out NO_x and soot emissions, while reaching the same or even higher level of engine efficiency. Consequently the goal is to reduce both local (NO_x, soot) and global-emissions (CO_2), compared to CDC. The concept builds on a single fuel which is most often a gasoline fuel with a relatively low research octane number (RON). Nonetheless, other fuels have been researched with PPC, for instance diesel, gasoline, ethanol, or methanol. The fuel is injected during the compression stroke and is then allowed to mix with the bulk gas. The distinction between CDC and PPC, used in this thesis[1], is that the latter has to fulfill the requirement of a positive ignition dwell. Ignition dwell is defined in Equation (2.1) and is the difference between the start of combustion (θ_{soc}) and the end of fuel injection (θ_{eoi}). Consequently, in order for the ignition dwell to be positive, all of the fuel must be injected before the start of combustion.

$$\text{Ignition dwell} = \theta_{soc} - \theta_{eoi} \tag{2.1}$$

[1]Other definitions exist and are used in the literature.

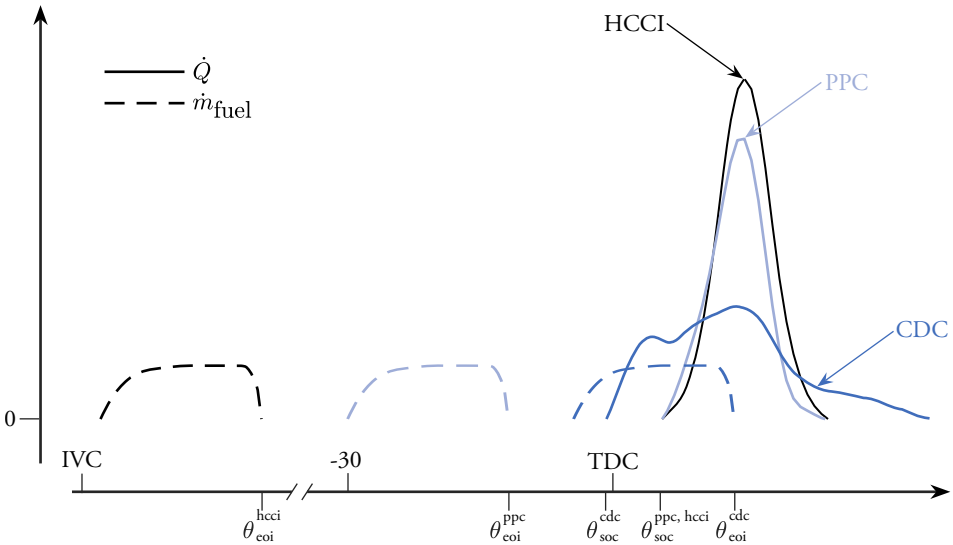

Figure 2.2: Illustrative example of the fuel injection profile ($\dot{m}_{\text{fuel}}$) and rate of combustion ($\dot{Q}$) as a function of crank angle degree (θ) comparing CDC with HCCI, and PPC.

The difference between positive and negative ignition dwell is illustrated in Figure 2.2. This figure uses crank angle degrees (θ) on the x-axis as a measure of time. By convention the crank angle degree has a value of zero when the piston is at top dead center (TDC) between the compression and expansion strokes. Figure 2.2 shows the rate of fuel injection ($\dot{m}_{\text{fuel}}$) and the resulting rate of combustion ($\dot{Q}$). As can be seen, the start of combustion occurs before the end of fuel injection in the CDC case, while there is a separation between these curves for the case with PPC. For the case with homogeneous charge compression ignition (HCCI), the fuel injection occurs a long time prior to TDC, and thus there is an even longer time for the fuel and bulk gas to mix.

2.2 Mechanisms for Reducing NO_x and Soot

The purpose of achieving a positive ignition dwell is to allow for more mixing of the fuel and bulk gas and thereby reduce soot emissions and obtain a lower global combustion temperature [24]. In addition to calculating the ignition dwell, the equivalence ratio (ϕ) can be used to determine how much of the fuel and oxidizer have mixed locally inside the cylinder. The equivalence ratio is defined in Equation (2.2) and is a measure of the ratio between the mass of fuel (m_{fuel}) and the mass of oxidizer[2]

[2]Oxidizer is most often the oxygen in the air but can be other chemical species which include oxygen atoms.

(m_{oxidizer}). Specifically, the equivalence ratio compares the real ratio of fuel and oxidizer to the stoichiometric (s) one.

$$\phi = \frac{\dfrac{m_{\text{fuel}}}{m_{\text{oxidizer}}}}{\left(\dfrac{m_{\text{fuel}}}{m_{\text{oxidizer}}}\right)_s} \tag{2.2}$$

The combination of local equivalence ratio and temperature inside the cylinder can be useful when comparing different combustion modes and concepts. Figure 2.3 shows, for every combination of equivalence ratio and temperature, the formation of NO_x and soot which would result from a homogeneous reaction between air and a gasoline surrogate consisting of iso-octane, toluene, and n-heptane, at 100 bar and a residence time of (2 ms). This type of figure is commonly called a $T-\phi$ diagram and behind the islands of NO_x and soot are a large number of simulations with a detailed chemical kinetic model [25–28]. Figure 2.3 furthermore shows examples of the local conditions of temperature and equivalence ratio for three different combustion concepts, namely CDC, PPC, and HCCI. These cases correspond to the same fuel injection and combustion rates from Figure 2.2, and show the distribution of temperature and equivalence ratio at θ_{50}, which is the crank angle degree at which 50 % of the fuel energy has been released.

For the case with CDC, fuel injection is ongoing at the same time as there is combustion and all of the fuel is not injected before θ_{50}. As a result, the injected fuel starts to oxidize at a high equivalence ratio, and while it mixes with the bulk gas, it moves through the soot island which suggests that this case forms a significant amount of soot[3]. The combustion then goes to completion at an equivalence ratio of one, and thus in addition to forming soot, this case will likely produce a substantial amount of NO_x emissions as the local temperatures are well above 2500 K where $\phi = 1$ [30]. By comparing this case with the PPC case, several things can be noted. First, by letting the fuel and bulk gas mix, the highest equivalence ratio is below the soot island and hence the likeliness for forming soot is lower. Furthermore, by recirculating a large part of the exhaust gas, so called exhaust gas recirculation (EGR), it is possible to reduce the oxygen concentration and the local flame temperatures and thereby reduce NO_x emissions [31–33]. In fact, EGR is fundamental to achieving low emissions of NO_x and in the case shown here, 50 % of the exhaust gas is circulated to the intake manifold. For the case with HCCI, the fuel injection is placed early enough for the stratification in equivalence ratio to be almost negligible. As can be seen this

[3]During the exhaust stroke the soot that has been formed will be oxidized. However this oxidation rate depends on a number of factors and does not correlate well with the amount of formed soot and it is therefore difficult to decide how much exhaust soot this case would produce just by analyzing this figure [29]. Nevertheless, it works well for illustrating how the soot can be formed.

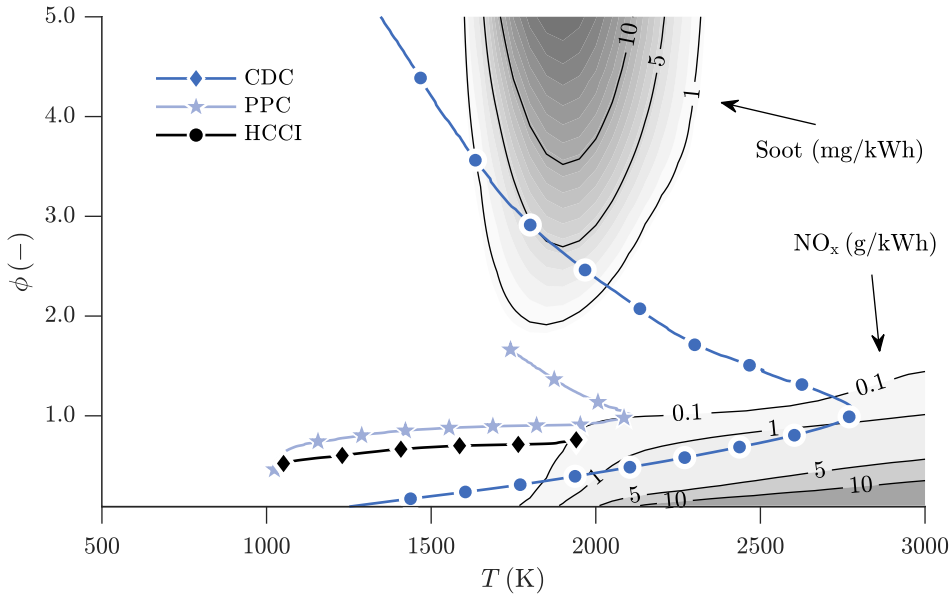

Figure 2.3: Distribution of local in-cylinder conditions as equivalence ratio and temperature for three different combustion modes: CDC, PPC, and HCCI. The figure shows the distribution at θ_{50} which is the crank angle degree at which 50 % of the fuel energy has been converted into heat. Moreover the emission yields of NO_x and soot are shown resulting from a homogeneous reaction between air and a gasoline surrogate consisting of iso-octane, n-heptane and toluene. These emission yields were computed using a detailed chemical kinetic mechanism [28].

eliminates the potential for formation of soot and further reduces the maximum in-cylinder temperature. However, to achieve a reasonable maximum pressure rise rate with HCCI, a higher amount of air was needed. Not only is there a potential for reducing NO_x and soot with PPC and HCCI, but the lower in-cylinder temperature will likely lead to a lower heat transfer to the cylinder walls, which in turn could lead to a higher gross indicated efficiency of the engine [15]. The PPC concept has, however, a greater likeliness for being commercially achievable than HCCI because of the issues with poor combustion efficiency at low load, excessive pressure rise rate at high load, and combustion phasing control of HCCI [11].

2.3 Means to achieve Partially Premixed Combustion

PPC is realized through a positive ignition dwell and there are several ways that this can be achieved. A reduction of the oxygen concentration of the bulk gas has shown to be very effective for increasing the ignition dwell, thus achieving PPC [34, 35]. This reduction can be achieved, at constant fuel flow, by increasing the inlet pressure and adding EGR (at constant λ), replacing air with EGR at constant intake mani-

fold pressure, or reducing the inlet pressure (at constant EGR) and thus reducing the global air-fuel ratio (λ). This has been shown experimentally in both single- and multi cylinder research engines and with a variety of gasoline and diesel fuels. For instance increasing the EGR from 30 % to 48 % can yield an increase in ignition dwell by 3°ca [35]. Furthermore, a reduction of λ from 1.74 to 1.05 was seen to result in an increase of the ignition dwell in the range of 4°ca to 7°ca. There are several mechanisms behind this increase in ignition dwell [36]. First, by substituting air with exhaust gas, the heat capacity of the bulk gas increases and thus a lower temperature after the compression stroke results. This in turn increases the ignition delay time of the fuel-bulk gas mixture and therefore prolongs the ignition dwell. Secondly, by reducing the inlet pressure, the pressure at TDC is reduced and this increases the ignition delay. Thirdly, the reduction of oxygen concentration results in a suppression of the reactions leading to hot ignition. This effect is especially apparent for fuels with a strong low temperature chemistry [36]. A significant disadvantage with increasing the level of EGR, or effectively increasing the inlet pressure is that the gas exchange performance typically deteriorates [37].

A reduction of the intake manifold temperature, or effectively the temperature at intake valve closing, is another effective way of increasing the ignition dwell and thus provide a separation between the start of combustion and end of fuel injection [38, 39]. Reducing the inlet temperature, reduces the temperature at the end of the compression stroke and thus prolongs the ignition delay time. For instance, a reduction of the inlet temperature by 10 K can yield a 30 K lower temperature at TDC with a compression ratio of 17.3. Naturally, how much the start of combustion is retarded will depend on the fuel as well as the engine load and speed. To give an example, a 10 K reduction of the inlet temperature has been shown to result in a 2°ca retardation of the start of combustion [38]. Furthermore, a lower intake temperature is beneficial for reducing the fuel consumption because the charge density increases, the ratio of specific heats is higher and heat transfer can be reduced [38]. On the other hand, there is a large risk that issues due to water condensation, arise when the intake temperature is reduced to levels below the dew point of the gas. These issues include corrosion and fouling of the heat exchangers, and in the case of low pressure EGR, damage to the compressor [40].

The most effective measure to increase the ignition dwell is to use a fuel with higher RON [16–18]. However, by increasing the RON, it is often found that the maximum pressure rise rates increase and that low load combustion stability reduces. Excessive pressure rise rates are detrimental for the engine, leading to damage and can cause premature failure. This issue can be mitigated by using a multiple-injection strategy and hence the maximum pressure rise rate can be reduced [19, 41]. On the other hand, researchers are advocating a fuel with a RON of 65-80 to be optimal for PPC [19–21].

The reason for this is two-fold. First, because it could balance the trade-off between good combustion stability at low loads and excessive peak pressure rise rates at high loads. Secondly, it is argued that the demand for middle distillates (such as diesel and jet fuels) is expected to rise, while the demand for gasoline with high RONs is not expected to increase at the same rate and therefore could lead to a surplus of components with low RON (around 60-70) [21]. However, it is questionable if a RON this low, is enough to yield a combustion rate profile which fulfills the requirement of having a positive ignition dwell. This is especially true if an actual multi cylinder engine is considered, for which the oxygen concentration and intake temperature cannot be set arbitrarily. This was demonstrated recently in a study which compared Swedish MK1 diesel with a primary reference fuel (PRF) with a RON of 70 on a multi cylinder Volvo production engine [42]. Tests were performed at medium and high engine load and varying fuel injection pressure and comparing the soot-NO_x trade-off, combustion characteristics and engine efficiencies for both fuels. A similar rate of combustion was achieved comparing the two fuels for the high engine load and the same ignition dwell was achieved. For the medium load there was a slightly longer ignition dwell for the PRF fuel, however, the equivalent fuel consumption was the same.

In conclusion, there are several ways of achieving a prolonged ignition dwell. Nevertheless, as has been described there are advantages and disadvantages for every one. Thus, to find the best combination an optimization of fuel, boundary conditions, and injection strategy is arguably needed and this is therefore provided in Chapter 5 of this thesis. Regarding fuels, the next section will discuss the possibility of using alternative fuels with PPC.

2.4 Alternative Fuels

The practical aim of PPC is effectively to improve the trade-off between efficiency and NO_x and soot emissions. Ultimately this is about reducing primary energy use. However, this should ultimately be complemented by moving away from fossil fuels. Not only because it would lead to a faster and larger reduction of CO_2 emissions, but also because of the finite resources of fossil fuels. Furthermore, it is preferable if these alternative fuels are liquid, and additionally of sufficient energy density. As such, methanol might be a suitable and viable alternative [23]. As a fuel, methanol has received renewed interest, for instance in shipping but also in automotive applications in China [43–46]. From a practical point of view, methanol has both advantages and disadvantages. A big advantage is that methanol can be produced in large scale from renewable sources which would increase its sustainability and help decrease the net CO_2 emissions for the transport sector [22]. However, the lower heating value of methanol is less than half that of diesel and gasoline and means that a significantly

larger fuel storage is required in order to achieve similar driving range. Moreover, the choice of material for the fuel injection system must be cautiously determined. Finally, issues with cold starts could complicate the use of methanol.

For spark ignition engines, methanol might be considered the optimal fuel. The reason is that the RON is higher than for regular gasoline which means that a higher compression ratio can be used without running into problems with engine knock. Moreover, the higher heat of vaporization, wider flammability limits and increased burning velocities also provides further knock resistance [47, 48]. Another interesting feature of methanol is that the molar expansion is above one (1.07) which means that the number of moles during the combustion increases and therefore gives a theoretically higher expansion ratio of the products [49]. On the other hand, in premixed engines the lower air-to-fuel ratio of methanol counteracts this by leading to a lower and less favorable ratio of specific heats of the overall air-fuel mixture [49].

The performance and emission characteristics for methanol in spark ignition engines are well studied. On the other hand, the literature on methanol in compression ignition engines is limited. A large part of the reason is likely that the properties which make methanol a suitable fuel for spark ignition combustion, can be seen to be inversely unfavorable when it comes to compression ignition combustion. For instance, the RON of methanol is 109 and hence auto ignition of the fuel-oxidizer mixture at an appropriate timing could pose a serious issue. In a research environment this will probably not be an issue because it would be possible to heat the air prior to the engine, however, for a real application it could be a showstopper. A potential remedy would be to increase the engine compression ratio because it would increase the temperature at TDC and therefore reduce the ignition delay time. Nevertheless, there are a few studies with neat methanol in compression ignition engines and they show promising results when it comes to engine efficiency and emissions [50–53]. For instance, a gross indicated efficiency of 52.8 % with a high compression ratio piston but without any optimization of the engine settings was shown in [53]. Furthermore, these studies show that the production of soot and particulate matter for typical engine conditions is negligible. In fact, there is evidence suggesting that methanol does not produce soot even for a global ϕ as high as 1.1 [50]. This has the implication that there might not be any reason to apply PPC with methanol. On the other hand, it is possible that the high heat of vaporization of methanol helps to reduce the piston boundary work during the compression. The reason is that the latent heat helps to cool the gas and therefore reduces its temperature. For this to have a practical effect, it is likely that the start of injection must be placed relatively earlier and hence will fulfill the definition of PPC that way. The amount of NO_x emission produced is likely more dependent on the operating conditions than on the choice of fuel. However, there is a potential to reach lower NO_x emissions with methanol because of the lower adiabatic flame

temperature and the fact that a higher level of exhaust gas recirculation could be used without the usual addition of higher soot formation.

2.5 Engine Energy Flows and Efficiency Definitions

In order to compare different fuels and methods for achieving PPC, as well as to investigate advantages and disadvantages, there needs to be a framework in terms of energy flows to differentiate between the losses and gains. Figure 2.4 shows a Sankey diagram of the energy flows through the engine. The aim of the internal combustion engine is to convert the chemical energy contained inside the fuel to useful work on the crank-shaft. In order to be able to compare various engines of different size, the mean effective pressure (MEP) is often used within the combustion engine research field to normalize various energy flows by the engine's displacement volume (V_d). Consequently, mean effective pressures have the unit bar. As can be seen in Figure 2.4, all the energy flows therefore have names which end with MEP. For instance fuelmep describes the fuel energy normalized by the displacement volume as defined

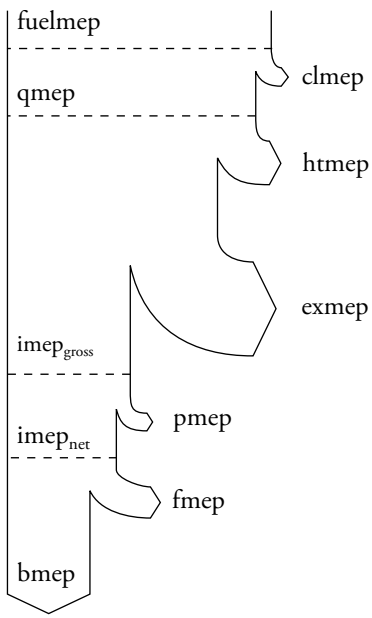

Figure 2.4: Sankey diagram of the engine energy distribution.

in Equation (2.3) where $\dot{m}_{\text{fuel}}$ is the mass of fuel injected every four stroke cycle and Q_{LHV} is the lower heating value of the fuel.

$$\text{fuelmep} = \frac{\dot{m}_{\text{fuel}} \cdot Q_{\text{LHV}}}{V_d} \tag{2.3}$$

The chemical energy in the fuel is converted into internal energy (qmep) in the burned products which are for example CO_2, H_2O, O_2, and N_2. Depending on the engine operating conditions there might be an amount of the fuel which does not turn into complete combustion products. Instead this fuel leaves the cylinder as unburned intermediate species such as hydrocarbon species (HC) and CO and ultimately this is lost energy. In the Sankey diagram this loss is called the combustion loss mean effective pressure or clmep. The combustion efficiency is defined as the ratio between qmep and fuelmep as shown in Equation (2.4).

$$\eta_{\text{comb}} = \frac{\text{qmep}}{\text{fuelmep}} = 1 - \frac{\text{clmep}}{\text{fuelmep}} \tag{2.4}$$

For a combustion efficiency of 100 %, all the energy in the fuel is converted into internal energy of the products which effectively is an increase in their specific heat capacity and temperature. During the expansion stroke the goal is to convert the internal energy into boundary work ($\text{imep}_{\text{gross}}$) on the piston. The $\text{imep}_{\text{gross}}$ is defined in Equation (2.5) where p is the cylinder pressure and V is the cylinder volume. By comparing with Figure 2.1 we can see that the $\text{imep}_{\text{gross}}$ is the integrated boundary work, or the encircled curve, during the compression and expansion stroke.

$$\text{imep}_{\text{gross}} = \frac{1}{V_d} \int_{\text{BDC}}^{\text{BDC}} p(\theta) \, \frac{\mathrm{d}V}{\mathrm{d}\theta} \, \mathrm{d}\theta \tag{2.5}$$

However, as the temperature is high inside the cylinder, but not on the outside, a part of the internal energy is lost as heat transfer (htmep). The internal energy which is still contained in the products when the exhaust valves open is lost and in the Sankey diagram this is called exmep. Consequently, the gross indicated efficiency (η_{gross}) can be defined as the ratio between $\text{imep}_{\text{gross}}$ and fuelmep, see Equation (2.6).

$$\eta_{\text{gross}} = \frac{\text{imep}_{\text{gross}}}{\text{fuelmep}} = 1 - \frac{\big(\text{exmep} + \text{htmep} + \text{clmep}\big)}{\text{fuelmep}} \tag{2.6}$$

Even though, the exhaust energy is lost with respect to the cylinder, all this energy is not considered a loss. Instead this energy can be used to drive the turbine of a turbocharger. The turbine in turn delivers power to the compressor which converts it

to yield a higher intake manifold pressure which is a must if a high level of dilution is required. Because the intake and exhaust valves are open during the intake and exhaust stroke, the pressure in the intake and exhaust manifold will affect the work on the piston. For instance, a positive work on the piston and hence energy to the crank-shaft can be achieved if the pressure in the exhaust manifold is lower than in the intake manifold. However, to achieve this the exhaust gas needs to contain a high level of energy in combination with an efficient turbine and compressor, and thus such a situation is seldom achieved. Therefore, the gas exchange or pump mean effective pressure (pmep) (Equation (2.7)), is often a loss, as it is depicted both in the $p-V$-diagram in Figure 2.1, as well as in the Sankey diagram in Figure 2.4. The efficiencies which relate this are called the net indicated efficiency (η_{net}) and the gas exchange efficiency ($\eta_{\text{gas exchange}}$) and they are defined in Equations (2.8) and (2.9). The net indicated mean effective pressure (imep_{net}) in Equation (2.8) is determined similarly to the ($\text{imep}_{\text{gross}}$), however, by integrating over all four strokes.

$$\text{pmep} = \text{imep}_{\text{gross}} - \text{imep}_{\text{net}} \tag{2.7}$$

$$\eta_{\text{net}} = \frac{\text{imep}_{\text{net}}}{\text{fuelmep}} = 1 - \frac{\big(\text{exmep} + \text{htmep} + \text{clmep} + \text{pmep}\big)}{\text{fuelmep}} \tag{2.8}$$

$$\eta_{\text{gas exchange}} = \frac{\text{imep}_{\text{net}}}{\text{imep}_{\text{gross}}} = \frac{\text{imep}_{\text{gross}} - \text{pmep}}{\text{imep}_{\text{gross}}} = 1 - \frac{\text{pmep}}{\text{imep}_{\text{gross}}} \tag{2.9}$$

In an engine there are several rotating parts which are moving against each other and thus create friction. This type of friction is work lost as heat and the relative amount can be substantial. However, as the engine load increases the ratio between friction mean effective pressure (fmep) and fuelmep generally reduces, and thus the mechanical efficiency (η_{mech}) increases. The mechanical efficiency is defined in Equation (2.10) where bmep stands for brake mean effective pressure and is the resulting final work delivered to the crank-shaft.

$$\eta_{\text{mech}} = \frac{\text{bmep}}{\text{imep}_{\text{net}}} = \frac{\text{imep}_{\text{net}} - \text{fmep}}{\text{imep}_{\text{net}}} = 1 - \frac{\text{fmep}}{\text{imep}_{\text{net}}} \tag{2.10}$$

Consequently, the brake efficiency (η_{brake}) can be defined as the ratio between bmep and fuelmep or in other words the energy which is left after all the losses have been subtracted, see Equation (2.11).

$$\eta_{\text{brake}} = \frac{\text{bmep}}{\text{fuelmep}} = 1 - \frac{\big(\text{exmep} + \text{htmep} + \text{clmep} + \text{pmep} + \text{fmep}\big)}{\text{fuelmep}} \tag{2.11}$$

Moreover, the brake efficiency is the product of the three part efficiencies: gross indicated, gas exchange and mechanical as shown in Equation (2.12).

$$\eta_{\text{brake}} = \eta_{\text{gross}} \cdot \eta_{\text{gas exchange}} \cdot \eta_{\text{mech}} \tag{2.12}$$

Consequently, the high gross indicated efficiency, which is typically found with PPC, needs to be achieved in combination with high gas exchange and mechanical efficiencies, in order to obtain a high brake efficiency. Recent research has shown that this is not done easily [9, 34, 37]. To illustrate the issue, Figure 2.5 shows an example of how the losses could be distributed when comparing CDC with PPC. In this example, due to a high level of dilution for the PPC case, a low global temperature is obtained and hence a lower heat transfer loss. However, not all this lower heat transfer loss is converted into boundary work. Instead a relatively large part is just transferred into exhaust loss. Furthermore, because of the dilution, the exhaust gas has a lower temperature which leads to lower gas exchange efficiency for the PPC concept. Consequently, the brake efficiency is on the same level comparing the two concepts. Although, higher friction losses may arise in the fuel injection system due to the lower lubricity of gasoline (or alcohols), or to higher maximum in-cylinder pressures, the fmep is arguably more dependent on the engine hardware design than on the combustion concept. Thus, to investigate the possibility to transfer the high

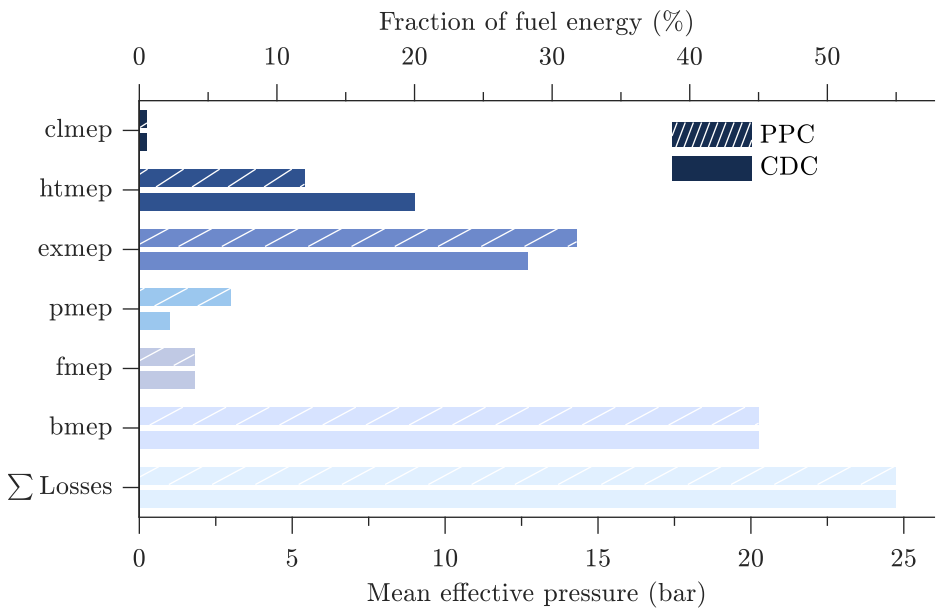

Figure 2.5: Illustrative example of the distribution of losses comparing CDC to PPC. These values are fictive but represent the results from [9, 34, 37].

indicated efficiencies found for PPC to high brake efficiencies, the reduction of the gas exchange loss is likely the most effective. For instance, would it be possible to achieve a higher gas exchange efficiency by using a different turbocharger, or by making changes to the EGR configuration. Chapter 4 attempts to answer these questions.

Chapter 3

Models and Validation

In order to successfully model and simulate a multi cylinder heavy-duty compression ignition engine system, I have used a number of engine and combustion models. The aim of this chapter is to give a short introduction to each of these models as well as provide validation results wherever it is appropriate.

3.1 Gas Dynamic Multi Cylinder Engine Model

The modeling framework GT-suite was used to simulate the gas flow and heat transfer in pipes, ducts and bends, as well as model turbocharger dynamics [54]. A 1-D gas dynamic multi cylinder engine (MCE) model, representing a multi cylinder heavy-duty Scania D13 engine, was built and validated using experimental data obtained on a similar engine in our laboratory. This model was used in Papers I-V. The specifications of the engine is presented in Table 3.1 and Figure 3.1 shows a schematic layout of the model. This engine has six cylinders in an in-line configuration, a bore of 130 mm, a stroke of 160 mm and a compression ratio of 17.3:1. The engine was modeled with a low pressure (LP) exhaust gas recirculation (EGR) route and a high pressure (HP) EGR route. The LP EGR route included a bypass path which made it possible to increase the inlet temperature to the compressor and consequently the intake manifold temperature. The air system comprised a single-stage turbocharger with a variable geometry turbine (VGT) and a waste gate (WG) as well as a charge air cooler (CA-C). In addition, the charge air cooler had a bypass path so that the intake manifold temperature could be controlled. The pipe lengths and diameters were measured on the engine. The intake and exhaust valve lift profiles as well as the valve flow coefficients were measured and provided by Scania. The friction mean effective pressure (fmep)

Table 3.1: Specifications for the 1-D gas dynamic multi cylinder engine model, representing a heavy-duty Scania D13 diesel engine.

Item	Value
Displacement Volume	12.74 L (in-line 6)
Bore × Stroke	130 mm × 160 mm
Connecting rod length	255 mm
Compression ratio	17.3:1
Number of valves	4 per cylinder
Inlet valve close (IVC)	−160°ca aTDC @ 0.1 mm lift
Exhaust valve open (EVO)	145°ca aTDC @ 0.1 mm lift
EGR system	Low and high pressure route with cooler and by-pass valve
Air system	Single-stage turbocharger with variable geometry turbine and waste-gate and charge air cooler with by-pass valve

was modeled based on a correlation described in [55]. This correlation is presented in Equation (3.1) and consists of a simple equation where the friction mean effective pressure is a function of the net mean effective pressure (imep_{net}), the stroke (s), the engine speed (n), and the maximum in-cylinder pressure (p_{max}).

$$\begin{aligned} \text{fmep} &= c \cdot 0.0104 \cdot \text{imep}_{\text{net}} + 0.3 \cdot \text{s} \cdot \text{n} + 1.0955 \cdot 10^{-3} \cdot p_{\text{max}} \\ c &= \begin{cases} 1, & \text{at } \text{imep}_{\text{net}} \leq 50\,\% \text{ of full load} \\ 2, & \text{otherwise} \end{cases} \end{aligned} \tag{3.1}$$

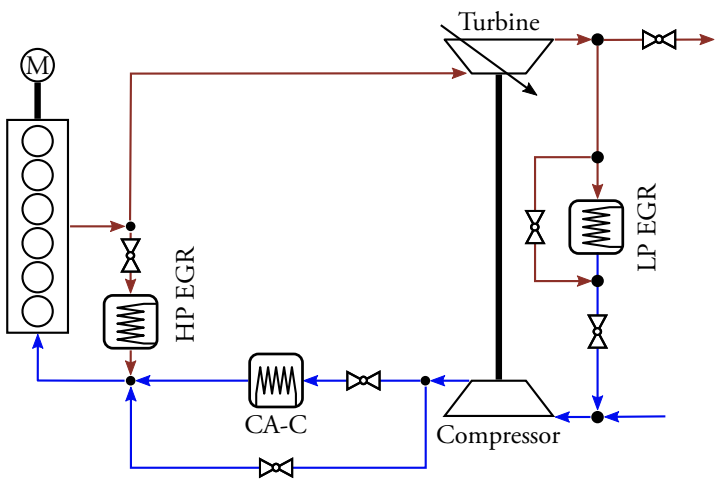

Figure 3.1: Schematic layout of the 1-D gas dynamic multi cylinder engine model which comprises a heavy-duty Scania D13 diesel engine.

The heat transfer was modeled in two separate ways. In Papers I and II, the model known as the "Flow" model in GT-Suite was used [56]. Subsequently, in-cylinder heat transfer measurements on the same type of engine showed that the model by Hohenberg provided an improved prediction of the heat transfer and thus this model was used in Papers III-V [57, 58].

A set of proportional-integral controllers were used to control the intake manifold pressure and temperature, EGR level, and exhaust back pressure. The intake manifold pressure was regulated by actuating the turbine's rack position, while the intake manifold temperature was regulated by actuating the bypass valves surrounding the EGR and charge air coolers. Furthermore, the EGR valve was actuated in order to regulate the EGR level. The engine exhaust valve, that is the back pressure valve, was actuated to regulate the exhaust back pressure in order to simulate a back pressure from an exhaust after-treatment system.

The experimental data which was used to validate the model is presented in Table A1. The experimental in-cylinder pressure traces were converted into fuel burn rates and then imposed in the simulations. The built-in tool in GT-suite called the three pressure analysis, was used for this conversion. In addition, a verification was made against two other standard methods, however, all three showed similar results[1]. The fuel which was used during these experiments was a mixture between Swedish service station gasoline (with a research octane number (RON) of 95) and n-heptane. The resulting RON of this blend was circa 76. Details for this fuel is presented in Table 3.2. Moreover, detailed information about this experimental apparatus, including the set-up, as well as the measurement and control systems can be found in Refs. [59–62]. Figure 3.2 shows the error between measured and simulated values for a selection of key parameters. These parameters are the gross imep ($\text{imep}_{\text{gross}}$), net imep ($\text{imep}_{\text{net}}$), EGR, normalized air-fuel ratio (λ), exhaust manifold temperature (T_{em}), and exhaust temperature (T_{exh}) defined in Equations (3.3) to (3.6). In these equations, V_d is the

[1]With standard method I mean converting in-cylinder pressure into a rate of heat release according to Equation (3.2) and then apply a slight shift (the size of which is determined by matching the simulated and measured cylinder pressure traces) of the whole curve as the rate of heat release slightly lags the burn rate.

$$\frac{\mathrm{d}Q}{\mathrm{d}\theta} = \frac{\gamma(\theta)}{\gamma(\theta)-1} p(\theta) \frac{\mathrm{d}V}{\mathrm{d}\theta} + \frac{1}{\gamma(\theta)-1} V(\theta) \frac{\mathrm{d}p}{\mathrm{d}\theta} + h_t(\theta) A(\theta)(T(\theta) - T_{\text{wall}}) \qquad (3.2)$$

The difference between the methods lay in the way the ratio of specific heats (γ) were calculated during the compression stroke. Method one uses the global temperature (T) as calculated from the ideal gas equation of state to determine the gas properties from the NASA tables, while the second method uses the stochastic reactor model, presented subsequently, to predict the gas properties based on a compression which matched the experimental. The ratio of specific heats during the combustion and expansion are determined analogously to method one, except that the composition is assumed to change linearly from reactants to products during the duration of combustion.

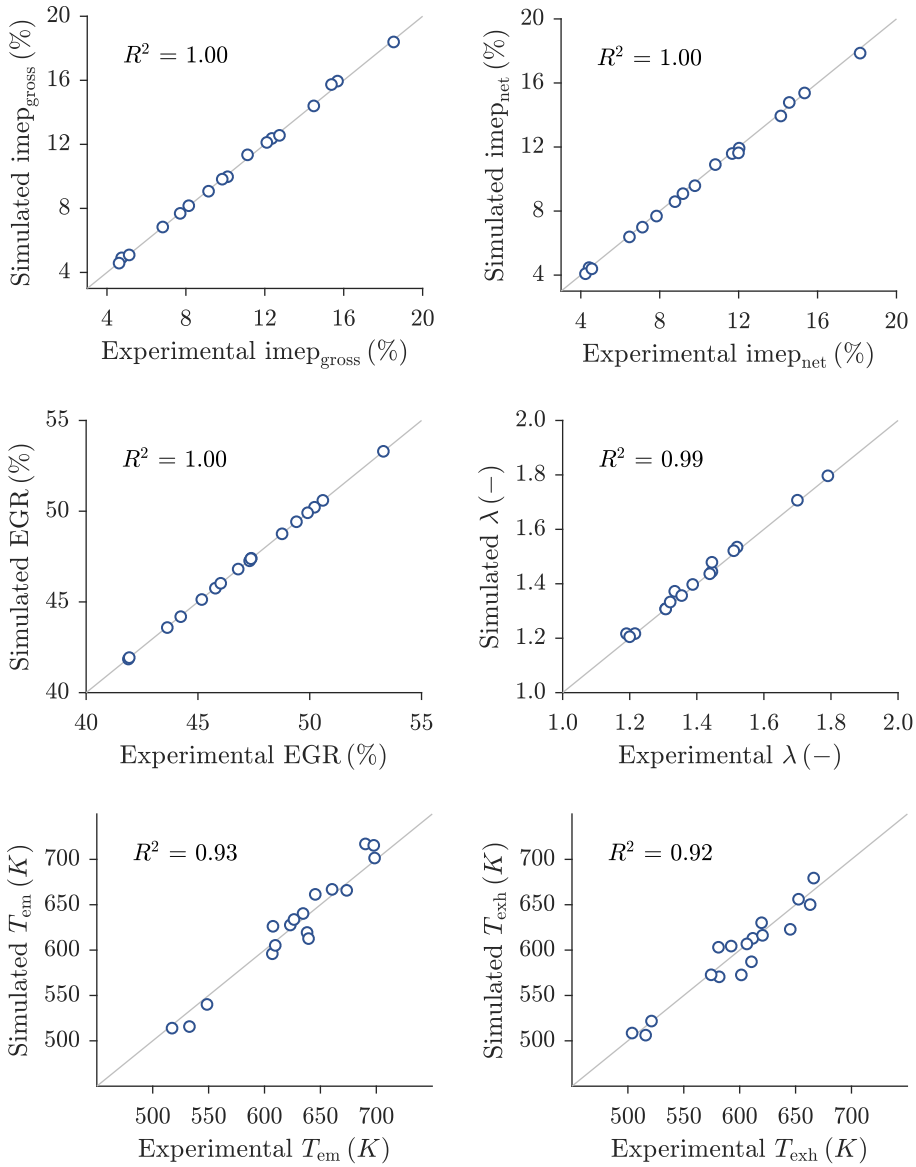

Figure 3.2: Validation results for the 1-D gas dynamic multi cylinder engine model. Model predicted versus experimentally measured for the parameters: $\text{imep}_{\text{gross}}$, imep_{net}, EGR, λ, T_{em}, and T_{exh}. In addition, all sub figures show the coefficient of determination R^2.

cylinder displacement volume, θ is the crank angle degree, p and V are the in-cylinder pressure and volume as a function of θ, $\dot{m}_{\text{EGR}}$ and $\dot{m}_{\text{air}}$ are the mass flow of recirculated exhaust gas and incoming air respectively, and subscript $(_{\text{s}})$ is a notation which

stands for stoichiometric. The exhaust manifold temperature was taken before the turbine, while the exhaust temperature was taken after the turbine.

Table 3.2: Properties of methanol and the gasoline used in the experiments in Tables A1 and A2.

Fuel	Methanol	Gasoline
Formula	CH_3OH	0.8 $CH_{1.87}O_{0.05}$ + 0.2 C_7H_{16}
Octane number	109	∼76
H/C	4	∼2.26
O/C	1	∼0.04
Lower heating value (MJ/kg)	19.9	43.7
Stoichiometric air-fuel-ratio	6.5	15.7
Heat of vaporization (kJ/kg)	1104	344
Density (kg/m^3)	792	737

$$\text{imep}_{\text{gross}} = \frac{1}{V_d} \int_{-\pi}^{\pi} p(\theta) \frac{\mathrm{d}V}{\mathrm{d}\theta} \mathrm{d}\theta \tag{3.3}$$

$$\text{imep}_{\text{net}} = \frac{1}{V_d} \int_{-2\pi}^{2\pi} p(\theta) \frac{\mathrm{d}V}{\mathrm{d}\theta} \mathrm{d}\theta \tag{3.4}$$

$$\text{EGR} = \frac{\dot{m}_{\text{EGR}}}{\dot{m}_{\text{air}} + \dot{m}_{\text{EGR}}} \tag{3.5}$$

$$\lambda = \frac{\dfrac{\dot{m}_{\text{air}}}{\dot{m}_{\text{fuel}}}}{\left(\dfrac{\dot{m}_{\text{air}}}{\dot{m}_{\text{fuel}}}\right)_{\text{s}}} \tag{3.6}$$

Furthermore, all sub-figures in Figure 3.2 shows the coefficient of determination (R^2) which is a measure of how well the model can predict the experimental data. An R^2 value of one means that there is complete correlation, while a value of zero means that there is no correlation at all. The coefficient of determination is defined in Equation (3.7) where SS_{res} is the residual sum of squares, SS_{tot} is the total sum of squares, $y = [y_1, \ldots, y_n]^T$ is the measured data set, and $\hat{y} = [\hat{y}_1, \ldots, \hat{y}_n]^T$ is the predicted data set.

$$R^2 = 1 - \frac{SS_{\text{res}}}{SS_{\text{tot}}} = 1 - \frac{\sum_i (y_i - \hat{y}_i)^2}{\sum_i (y_i - \bar{y})^2} \tag{3.7}$$

3.2 Gas Dynamic Single Cylinder Engine Model

A second 1-D gas dynamic engine model was built and used in order to simulate experiments performed in a different test cell in our laboratory. This model was built in GT-Suite, similarly to the multi cylinder engine model, and also represents a heavy-duty Scania D13 engine. However, this engine was operated in a single cylinder engine (SCE) configuration, that is only one cylinder was active with combustion. The specifications of this engine are presented in Table 3.3 and Figure 3.3 shows a schematic layout of the engine. Compressed air was delivered to the test cell by an external compressor which means that no exhaust gas turbocharger was used. The pressure of the air could be reduced by a valve and a heater was used to increase the temperature before the air was mixed with EGR. The exhaust gas was circulated in a high pressure EGR route configuration and an EGR cooler was used to cool the exhaust gas if needed.

The experimental data samples 1 to 72, in Table A2, were used to validate the model. In all these experiments, methanol was used as fuel, see Table 3.2. Further information about this experimental set-up and the measurement system that was used can be found in the methodology section of Ref. [63]. For the single-cylinder engine

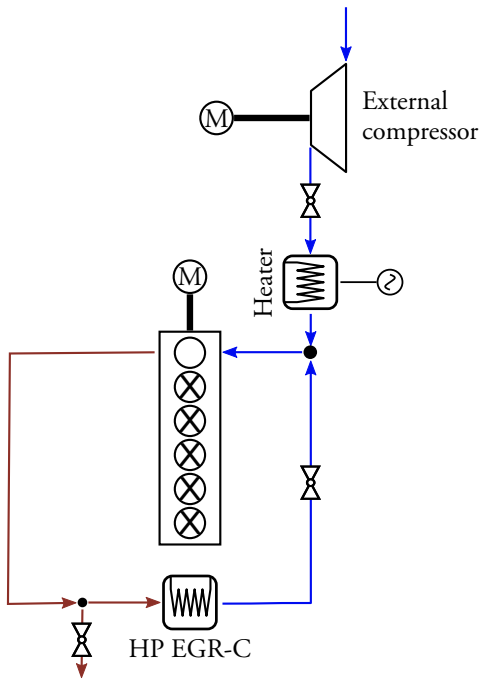

Figure 3.3: Schematic layout of the 1-D gas dynamic single-cylinder engine model which comprises a heavy-duty Scania D13 diesel research engine with one cylinder active.

Table 3.3: Specifications for the 1-D gas dynamic single-cylinder engine model, representing a heavy-duty Scania D13 diesel research engine with one cylinder active.

Item	Value
Displacement Volume	2.12 L
Bore × Stroke	130 mm × 160 mm
Connecting rod length	255 mm
Compression ratio	15:1, 17.3:1, 27:1
Number of valves	4
Inlet valve close (IVC)	–160°ca aTDC @ 0.1 mm lift
Exhaust valve open (EVO)	145°ca aTDC @ 0.1 mm lift
EGR system	HP EGR route with cooler
Air system	External compressor and air heater

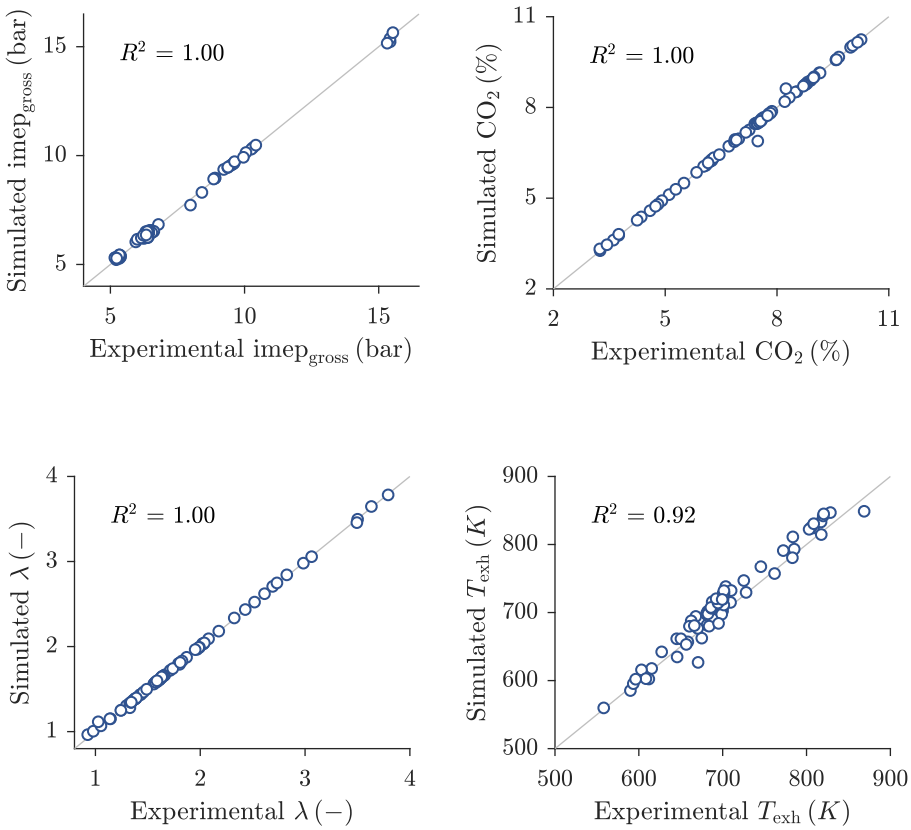

Figure 3.4: Validation results for the single-cylinder engine model. Model predicted versus experimentally measured for the parameters: $\text{imep}_{\text{gross}}$, exhaust CO_2 emissions, λ, and T_{exh}.

model, Figure 3.4 shows the validation results as the error between model predicted and measured for the parameters $\text{imep}_{\text{gross}}$, exhaust CO_2 emissions, λ, and T_{em}.

3.3 Stochastic Reactor Model

The gas dynamic engine models (both SCE and MCE) discussed previously, are capable of predicting the gas dynamic phenomena outside the engine cylinders. To model the in-cylinder events, that is injection of fuel, vaporization, mixing, combustion, heat transfer and emissions formation, I have used a stochastic reactor model (SRM). The stochastic reactor model is a 0-D model from a commercial software package[2], LOGEresearch [67]. The main advantage of this model, and reason for choosing it for this work, is the combination of low computational time, possibility to use detailed kinetic models in order to predict emissions, as well as the capability of modeling mixture and temperature inhomogeneities and turbulence. These advantages were suitable in this work which has focused on optimizations consisting of large amounts of simulations together with a need for a high level of predictability.

In the stochastic reactor model, the engine combustion cylinder is discretized using a number of particles. Every particle has its own composition and temperature and they all have a representative equal mass. The composition and temperature are treated as random variables which vary within the cylinder. These scalars represent the in-cylinder mixture according to a probability density function (PDF). The PDF is initialized using a seed at the start of one simulation. Finally, the model is 0-D because the particles do not contain information of their spatial location inside the cylinder.

Two different models were used for simulating the interactions between the particles, i.e. the mixing and exchange of heat. The modified coalescence/dispersal (C/D) model was used in Paper VI [68]. At the time for Papers III-V the Euclidean minimum spanning tree model had been implemented in the stochastic reactor model [69]. The Euclidean minimum spanning tree model gives a more realistic description of the mixing process for multiple fuel injections than the modified C/D model, because it considers the locality in the scalar space. This means that only particles which are neighbors in the scalar space are allowed to mix, whereas the modified C/D model, on the other hand would allow unrealistic mixing between cold fuel particles and lean air particles [69]. Furthermore, the current implementation considers the mixture fraction (usually denoted Z) for constructing the spanning tree. The intensity at which the particles mix is governed by a turbulent mixing time. The mixing time (τ) is defined as the ratio between a turbulent length scale and the mean velocity

[2]It should be noted that there exist other similar implementations and software packages based on this approach. For instance [64–66].

of the gas and thus has the dimension time. Low values of the mixing time, means high intensity mixing.

The details of the stochastic reactor model, the implementation as well as the successful application for direct injection engines have been described thoroughly in several papers in the past [69–75]. Additionally, and as described by these authors, to use the stochastic reactor model in a predictive manner the main challenge is that the mixing time needs to be provided in advance of the simulation. Several approaches have been suggested to overcome this challenge. For the papers that use the stochastic reactor model in this thesis, I have used two different approaches to determine the mixing time. In Paper VI the technique described in [70] was used. In this approach the mixing time is determined based on three different phases during the closed cycle. A constant, and relatively high, initial value on τ is kept during the compression stroke until the start of injection. At the start of injection, a low value on τ is set because the turbulence level inside the cylinder increases and thus a high intensity level of mixing can be seen. From the end of injection and until the exhaust valves open the mixing time increases exponentially, i.e. the turbulent intensity decays. For Papers III-V, a more recently implemented correlation was used [69]. This correlation was originally proposed by Kozuch and is based on a turbulent kinetic energy - turbulent dissipation ($k-\epsilon$) approach [76]. The correlation is shown in Equations (3.8) and (3.9) and includes the effects of charge density, dissipation, squish flow, fuel injection and swirl on the turbulent mixing time. In this equation C_{den}, C_{diss}, C_{sq}, C_{inj}, C_{swirl}, C_τ are constants, l is a length scale which is proportional to the cylinder volume, c_m is the mean piston velocity, and n is the engine speed. The initial condition for the kinetic energy at inlet valve closing (ivc) is approximated using Equation (3.10) where d_{cyl} is the cylinder bore, η_{vol} is the volumetric efficiency, d_{iv} is the intake valve diameter, and h_{iv} is the maximum lift of the intake valve. The two different approaches, denoted as "Parameterized" and "$k-\epsilon$", for determining the turbulent mixing time are exemplified in Figure 3.5.

$$\frac{\mathrm{d}k}{\mathrm{d}\theta} = \left(\underbrace{-C_{\text{den}} \frac{2}{3} \frac{k}{V} \frac{\mathrm{d}V}{\mathrm{d}t}}_{\text{density}} - \epsilon + \underbrace{\left[C_{\text{sq}} \frac{k_{\text{sq}}^{3/2}}{l} \right]_{\theta>0}}_{\text{squish}} + \underbrace{C_{\text{inj}} \frac{\mathrm{d}k_{\text{inj}}}{\mathrm{d}t}}_{\text{injection}} + \underbrace{C_{\text{sw}} \frac{c_m^3}{l}}_{\text{swirl}} \right) \frac{1}{6\text{n}} \tag{3.8}$$

$$\epsilon = \underbrace{C_{\text{diss}} \frac{k^{3/2}}{l}}_{\text{dissipation}}$$

$$\tau = C_\tau \frac{k}{\epsilon} \tag{3.9}$$

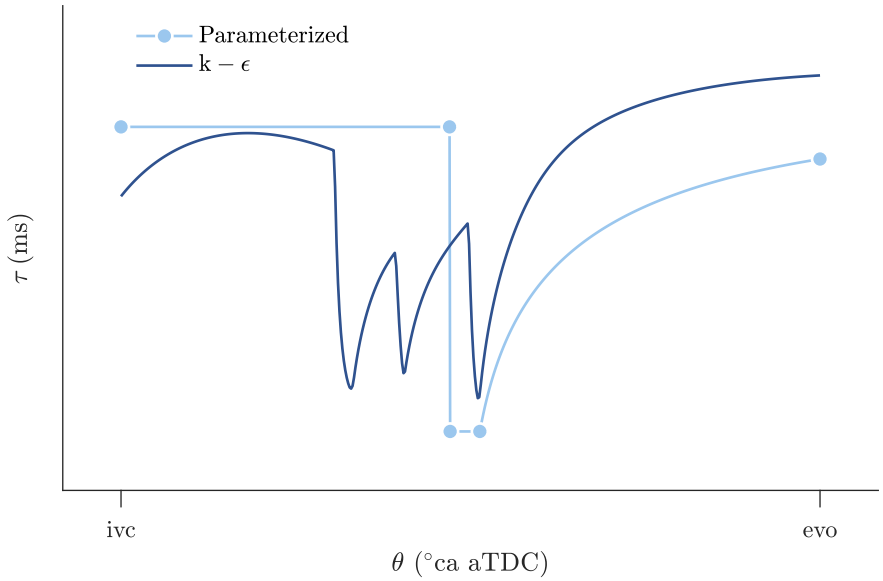

Figure 3.5: Exemplification of the two different approaches, denoted as "Parameterized" and "$k-\epsilon$", which were used to determine the turbulent mixing time. In the parameterized case the mixing time is set to a constant value during the compression stroke. The single fuel injection event is depicted by a decrease in mixing time, and after this injection the mixing time decays exponentially. In the $k-\epsilon$ case the mixing time is initiated according to Equation (3.10) and then decays due to compression. The increase in turbulence is depicted for this triple injection case, and also the mixing time decay after each injection. After the last fuel injection the mixing time increases.

$$k_{\text{ivc}} = \frac{1}{8}\left(\frac{c_m d_{\text{cyl}}^2 \eta_{\text{vol}}}{d_{\text{iv}} h_{\text{iv}}}\right)^2 \tag{3.10}$$

The constants C_{den}, C_{diss}, C_{sq}, C_{inj}, C_{swirl}, C_τ, in Equations (3.8) and (3.9) were calibrated using one 10^{th} of the experimental cases from both Tables A1 and A2. The final constant values are presented in Table 3.4 and compared to the ones used in Ref. [69]. As noted by the authors of Ref. [69], the values of these constants will be highly dependent on the particular engine geometry and injection system. In contrast to the light-duty engine which they used, a heavy-duty engine was used in this work hence it is not surprising that the constant values differ. For instance, it is expected that the amount of turbulence induced in a heavy-duty engine by fuel injection is

Table 3.4: The final values used in Equation (3.8).

C_i	C_{den}	C_{diss}	C_{sq}	C_{inj}	C_{sw}	C_τ
This Work	1.0	2.0	1.0	15.0	30.0	1.0
Ref. [69]	1.0	5.0	1.0	5.0	20.0	2.0

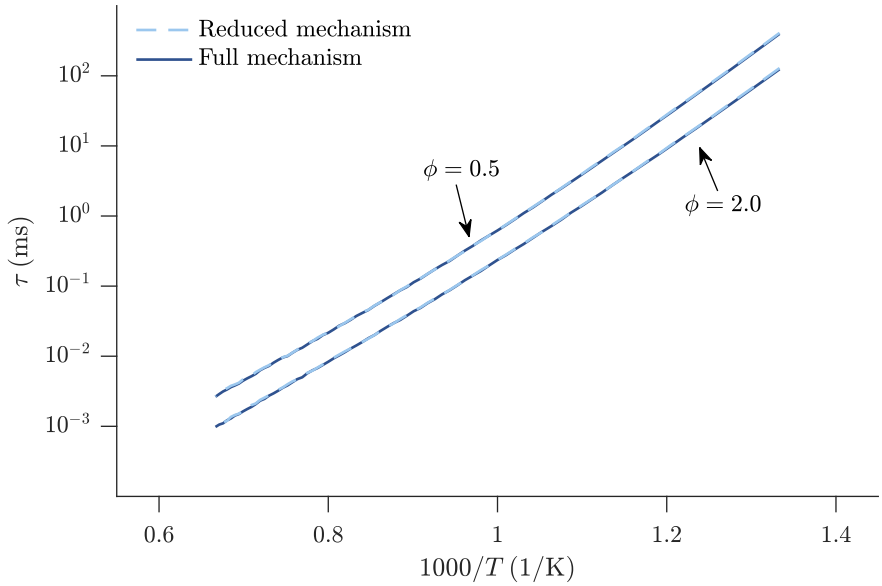

Figure 3.6: Ignition delay time, simulated in a constant volume homogeneous reactor at an initial pressure of 100 bar, as a function of temperature and equivalence ratio, comparing the reduced form and the full AramcoMech 2.0 kinetic mechanism. The reduced mechanism was used in the stochastic reactor model to simulate methanol combustion.

significantly higher, thus leading to a higher value of C_{inj}. Finally, the rest of the experiments in Tables A1 and A2 were simulated using the calibrated constants.

Two different chemical kinetic mechanisms, one for each fuel in Tables A1 and A2, were used. Methanol was modeled with the AramcoMech 2.0 mechanism [77]. While this mechanism contains species ranging from C_1 to C_4, methanol is a C_1 species and hence the mechanism could be reduced while maintaining the same accuracy. To verify this, the ignition delay times were simulated in a homogeneous reactor with constant volume at a pressure of 100 bar. The results, for the reduced and full mechanisms, are shown in Figure 3.6. It can be seen that the reduced mechanism is able to match the full kinetic mechanism very well and thus it could be used in the stochastic reactor model to simulate methanol combustion. The reduced mechanism contained 22 species and 202 reactions. The gasoline-like fuel was modeled as a surrogate consisting of ethanol, iso-octane, and n-heptane which matched the octane number and H/C and O/C ratios from Table 3.2. For this surrogate the chemical kinetic model from [78] was used in its full form consisting of 81 species and 691 reactions. For NO_x formation, the extended Zel'dovich mechanism was used together with reaction pathways for NO_2 formation [79]. Finally, the approach described in [80] was used to generate fuel injection rate profiles in Papers III-V, while the signal from the injection needle was used for Paper VI.

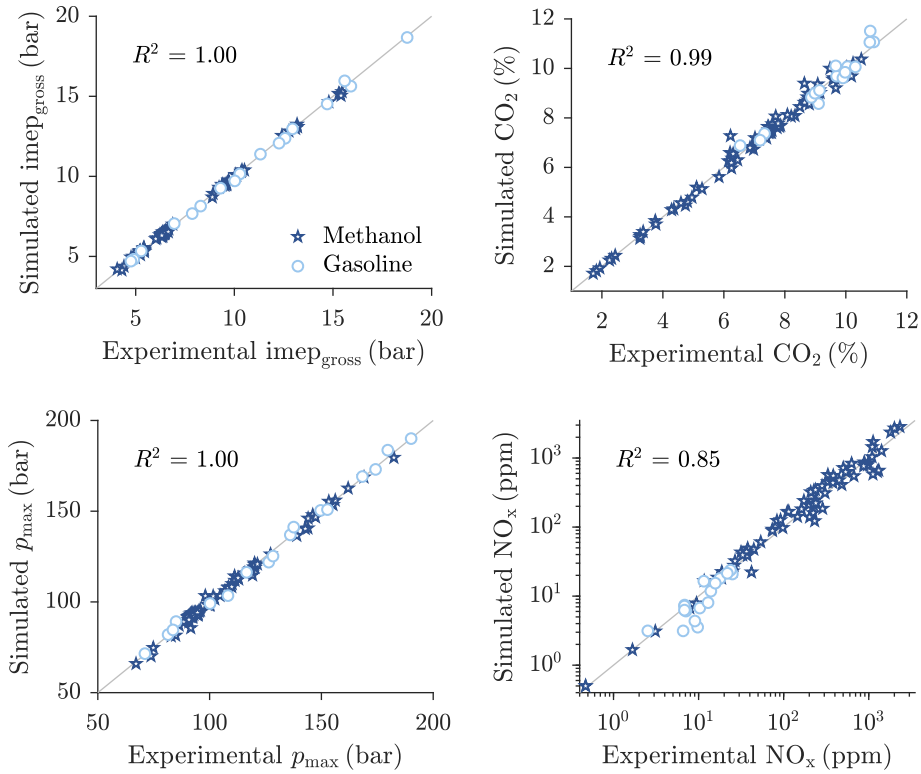

Figure 3.7: Validation results for the stochastic reactor model. Model predicted versus experimentally measured for the parameters: $\text{imep}_{\text{gross}}$, exhaust CO_2 emissions, p_{max}, and exhaust NO_x emissions.

The validation results for the stochastic reactor model are presented in Figures 3.7 to 3.9. Figure 3.7 shows the error between model predicted and experimentally measured for the following parameters: $\text{imep}_{\text{gross}}$, CO_2, p_{max}, and exhaust NO_x emissions for both methanol and gasoline. A good match between the predicted and measured values could be obtained. Additionally, Figures 3.8 and 3.9 show the in-cylinder pressure as a function of crank angle degree for a wide spread of the samples.

3.4 Full Engine Cycle Simulation

The stochastic reactor model and multi cylinder engine gas dynamic model were finally coupled as depicted in Figure 3.10, to obtain a predictive full cycle engine model. This model was used in Papers III-V. Matlab© was used to write and read text files, pre process and post process data. Every simulation started with an estimation of the boundary conditions (BC) for the stochastic reactor model. Three parallel closed-

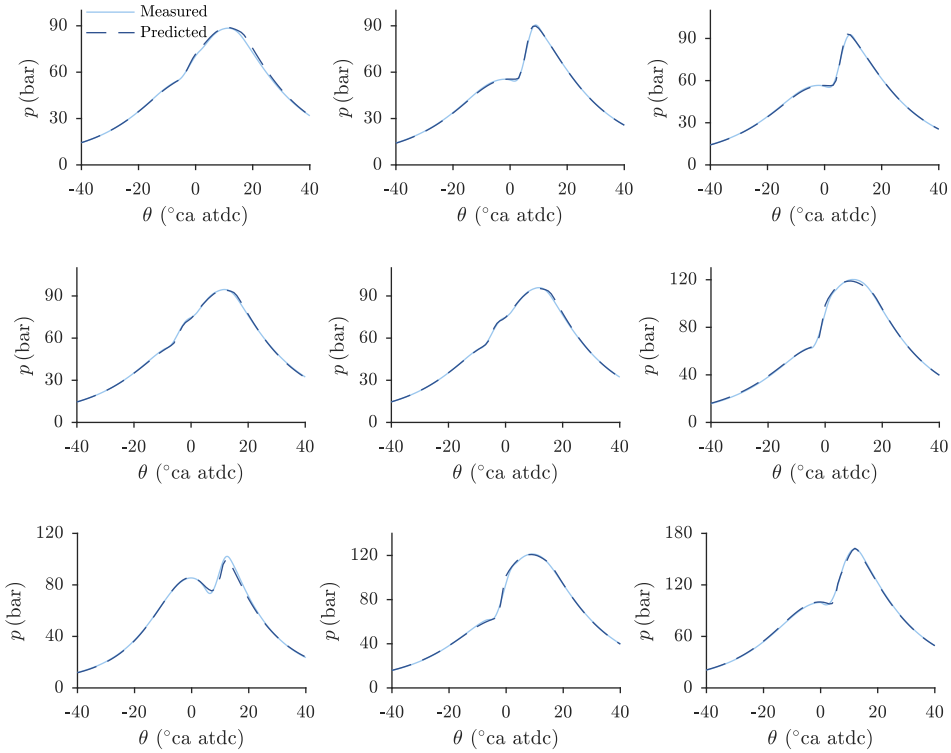

Figure 3.8: Stochastic reactor model predicted versus measured in-cylinder pressure profiles for methanol. These cases correspond to cases (left to right, top to bottom) 70, 42, 44, 67, 65, 59, 33, 62, and 17 from Table A2. Light blue solid lines represent the experiments and dark blue dashed lines the simulations.

cycle simulations were run with the stochastic reactor model, in order to capture the stochastic phenomena resulting from different initial PDF seeds. The averaged burn rate profile was then passed to the gas dynamic model. The MCE model was then run, with the burn rate profile kept constant, until steady-state was reached. If the convergence criteria were met, the simulation was finished, otherwise another iteration started by updating the boundary conditions. In order to fulfill the convergence criteria, the relative difference in between iterations for the in-cylinder maximum pressure ($p_{\max}$) and temperature ($T_{\max}$) were not allowed to exceed 1.0 % while the difference in brake efficiency (η_{brake}) was not allowed to exceed 0.5 %. Consequently, at least two iterations were needed. These specific values were chosen as representative of the experimental variance which the SRM and GT-Suite models were validated against.

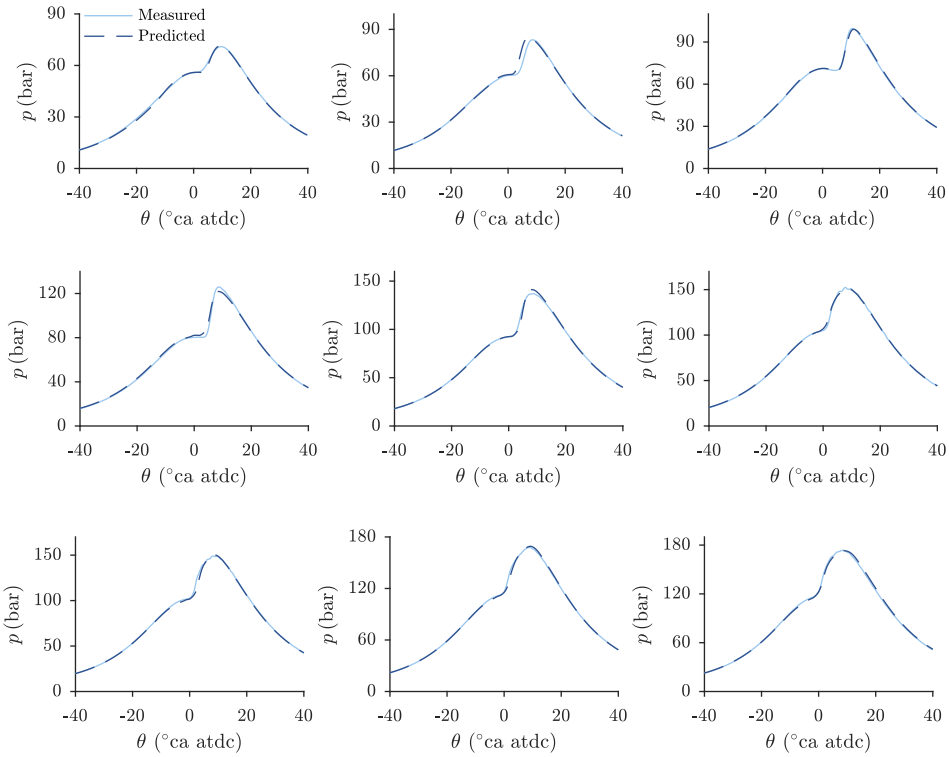

Figure 3.9: Stochastic reactor model predicted versus measured in-cylinder pressure profiles for gasoline. These cases correspond to cases (left to right, top to bottom) 8, 13, 2, 3, 11, 16, 5, 6, and 17 from Table A1. Light blue solid lines represent the experiments and dark blue dashed lines the simulations.

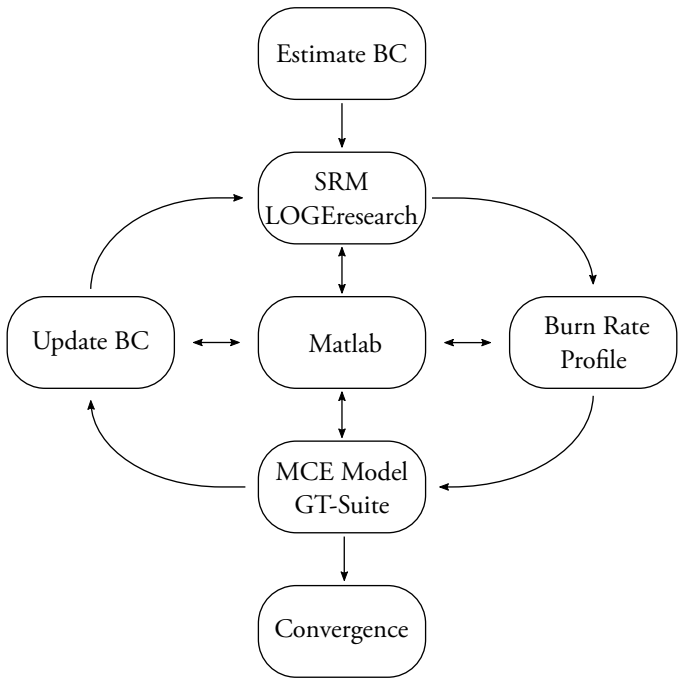

Figure 3.10: The coupling between the combustion model (SRM) and the 1-D gas dynamic multi cylinder engine model.

Chapter 4

Gas Exchange Analysis

This chapter will cover results and discussion on the gas exchange performance of an engine applying the partially premixed combustion (PPC) concept. As described in Chapter 2, it has so far been difficult to transfer the high gross indicated efficiencies shown for PPC to comparably high brake efficiencies. The main issue has been a low gas exchange efficiency. This chapter attempts to analyze the reasons for this poor gas exchange performance, as well as show examples on how the gas exchange efficiency could be improved. The chapter is divided into three different sections. In the first section, the gas exchange efficiency is analyzed with regards to a number of relevant engine parameters. The second section focuses on the choice of turbocharger and presents a comparison of four different turbocharger configurations. In the third section, a comparison between different exhaust gas recirculation (EGR) configurations is shown.

4.1 Influence of Engine Parameters on Gas Exchange Efficiency

Before analyzing a complete engine and turbocharger system it is useful to review the influence of some of the engine parameters which affect the gas exchange efficiency the most. The gas exchange efficiency ($\eta_{\text{gas exchange}}$) is defined in Equation (4.1) where (imep_{net}) and ($\text{imep}_{\text{gross}}$) are the net and gross indicated mean effective pressures defined in Equations (3.3) and (3.4), (pmep) is the pump mean effective pressure defined in Equation (2.7), and ($p_{0,\text{em}}$) and ($p_{0,\text{im}}$) are the total exhaust and intake manifold pressures. For a constant gross indicated mean effective pressure, the gas exchange efficiency is directly proportional to the difference between intake and exhaust man-

ifold pressure. I will therefore proceed with a simple analysis to investigate how this difference is affected.

$$\eta_{\text{gas exchange}} = \frac{\text{imep}_{\text{net}}}{\text{imep}_{\text{gross}}} = 1 - \frac{\text{pmep}}{\text{imep}_{\text{gross}}} \propto 1 + \frac{p_{0,\text{im}} - p_{0,\text{em}}}{\text{imep}_{\text{gross}}} \tag{4.1}$$

Figure 4.1 shows the schematic layout for an engine with a single stage turbocharger. For this turbocharger, the power required by the compressor (P_c) to generate a specific intake manifold pressure (i.e. boost) must equal the power generated by the turbine (P_t), times any mechanical inefficiencies ($\eta_{\text{tc, mech}}$) caused by friction and heat losses. This is formulated in Equation (4.2).

$$P_\text{c} = \eta_{\text{tc, mech}} P_\text{t} \tag{4.2}$$

For this simple turbocharger, the following steady flow energy equation, on a unit mass basis, can be applied: $q = \Delta h_0 + w$, in which q is heat rejected to the environment, Δh_0 is the change in total enthalpy, and w is the work produced [81]. If we assume that friction and heat losses are negligible (i.e. we have an adiabatic turbocharger without any friction irreversibilities) then the steady flow energy equation can be reduced to $w = \Delta h_0 = \bar{c}_p \Delta T_0$ where $\bar{c}_p$ is the mean specific heat capacity at constant pressure, and ΔT_0 is the change in total temperature. The power is then defined as the work (w) multiplied with the mass flow ($\dot{m}$) through either the compressor or turbine.

The power generated by the turbine, can therefore be defined as shown in Equation (4.3), where $\dot{m}_\text{em}$ is the engine mass flow through the exhaust manifold, $\bar{c}_{p,\text{t}}$

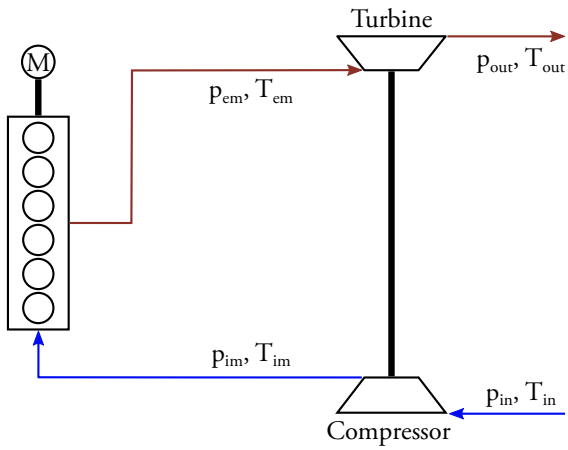

Figure 4.1: Simple schematic layout of a six-cylinder engine and its corresponding single stage turbocharger.

is the mean specific heat of the exhaust gas, and $T_{0,\text{em}}$ and $T_{0,\text{out}}$ are the total exhaust manifold and outlet gas temperatures respectively.

$$P_t = \dot{m}_{\text{em}} \bar{c}_{p,\text{t}} \left(T_{0,\text{em}} - T_{0,\text{out}} \right) \tag{4.3}$$

Analogously, Equation (4.4) shows the power consumed by the compressor where $\bar{c}_{p,\text{c}}$ is the mean specific heat of the inlet gas, $T_{0,\text{im}}$ and $T_{0,\text{in}}$ are the total intake manifold and inlet gas temperatures respectively.

$$P_c = \dot{m}_{\text{im}} \bar{c}_{p,\text{c}} \left(T_{0,\text{im}} - T_{0,\text{in}} \right) \tag{4.4}$$

The isentropic efficiencies of the turbine ($\eta_{\text{is,t}}$) and of the compressor ($\eta_{\text{is,c}}$) relates the amount of isentropic-to-real work and are defined in Equations (4.5) and (4.6), where $p_{0,\text{in}}$ and $p_{0,\text{out}}$ are the total inlet and outlet pressures respectively and $\bar{\gamma}_\text{t}$ and $\bar{\gamma}_\text{c}$ are the ratio of specific heats for the turbine and compressor. So far, I have assumed that the specific heat capacity of the gas in the compressor and turbine, is the same for the inlet and outlet as well as constant. These gas properties are dependent on the composition and temperature of the gas, and to a small extent on the pressure, and since the temperature changes from inlet to outlet, this assumption is a simplification. However, as the purpose of this analysis is to show the general trends, it is arguably sufficient.

$$\eta_{\text{is,t}} = \frac{h_{0,\text{em}} - h_{0,\text{out}}}{h_{0,\text{em}} - h_{0,\text{out,is}}} = \frac{\bar{c}_{p,\text{t}}(T_{0,\text{em}} - T_{0,\text{out}})}{\bar{c}_{p,\text{t}}(T_{0,\text{em}} - T_{0,\text{out,is}})} = \frac{1 - \dfrac{T_{0,\text{out}}}{T_{0,\text{em}}}}{1 - \left(\dfrac{p_{0,\text{out}}}{p_{0,\text{em}}} \right)^{\frac{\bar{\gamma}_\text{t} - 1}{\bar{\gamma}_\text{t}}}} \tag{4.5}$$

$$\eta_{\text{is,c}} = \frac{h_{0,\text{im,is}} - h_{0,\text{in}}}{h_{0,\text{im}} - h_{0,\text{in}}} = \frac{\bar{c}_{p,\text{c}}(T_{0,\text{im,is}} - T_{0,\text{in}})}{\bar{c}_{p,\text{c}}(T_{0,\text{im}} - T_{0,\text{in}})} = \frac{\left(\dfrac{p_{0,\text{im}}}{p_{0,\text{in}}} \right)^{\frac{\bar{\gamma}_\text{c} - 1}{\bar{\gamma}_\text{c}}} - 1}{\dfrac{T_{0,\text{im}}}{T_{0,\text{in}}} - 1} \tag{4.6}$$

Finally, Equations (4.2) to (4.6) can be combined to yield Equation (4.8) which relates $p_{0,\text{em}}$ to $p_{0,\text{im}}$, η_{tc}, and $T_{0,\text{em}}$. In order to arrive to this equation, I have used the fact that the total turbocharger efficiency (η_{tc}) is equal to the product of the turbine, compressor and mechanical efficiencies as shown in Equation (4.7).

$$\eta_{\text{tc}} = \eta_{\text{is,t}} \cdot \eta_{\text{is,c}} \cdot \eta_{\text{tc, mech}} \tag{4.7}$$

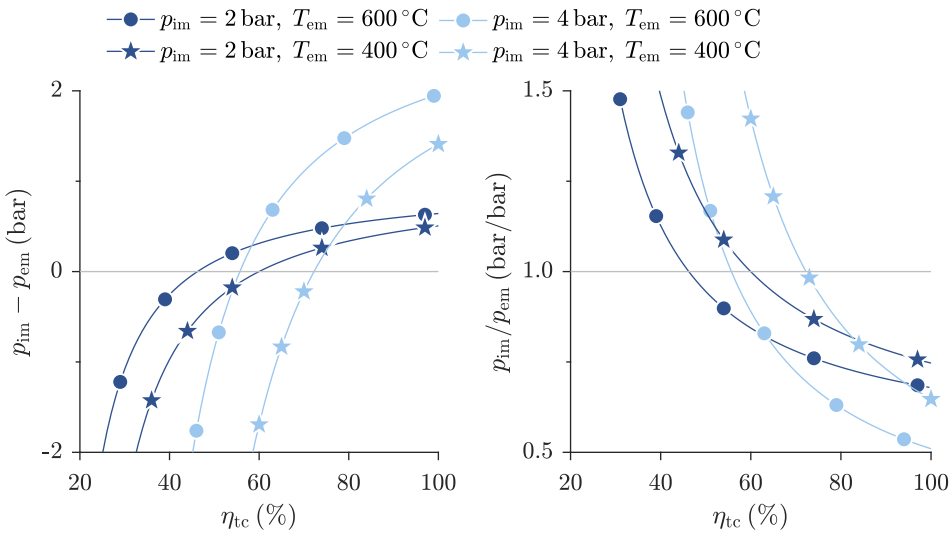

Figure 4.2: Difference (left) and ratio (right) between intake manifold pressure (p_{im}) and exhaust manifold pressure (p_{em}) as a function of turbocharger efficiency.

$$\left(\frac{p_{0,\mathrm{em}}}{p_{0,\mathrm{out}}}\right)^{\frac{\bar{\gamma}_t}{\bar{\gamma}_t - 1}} = 1 - \frac{\dot{m}_{\mathrm{im}} \bar{c}_{p,c} T_{0,\mathrm{in}}}{\dot{m}_{\mathrm{em}} \bar{c}_{p,t} \eta_{\mathrm{is,tc}} T_{0,\mathrm{em}}} \left[\left(\frac{p_{0,\mathrm{im}}}{p_{0,\mathrm{in}}}\right)^{\frac{\bar{\gamma}_c - 1}{\bar{\gamma}_c}} - 1 \right] \tag{4.8}$$

Equation (4.8) can now be used to investigate the influence of turbocharger efficiency, intake manifold pressure and exhaust manifold temperature. The results are presented in Figure 4.2 which shows the difference and ratio between intake and exhaust manifold pressure as a function of turbocharger efficiency. The constant values which were used in this calculation can be seen in Table 4.1.

From Equation (4.1) we saw that the gas exchange efficiency increased with higher values of $p_{0,\mathrm{im}} - p_{0,\mathrm{em}}$, for a given value of $\mathrm{imep}_{\mathrm{gross}}$. This can be achieved with a higher turbocharger efficiency or higher exhaust temperature. Furthermore, it is interesting to notice how a higher turbocharger efficiency is needed in order to achieve $p_{0,\mathrm{im}} > p_{0,\mathrm{em}}$ at a higher boost pressure, that is by requiring a higher boost pressure, either a higher back pressure or higher turbocharger efficiency is needed. Also, it should be noted that there is a strong non-linearity going from $p_{0,\mathrm{em}} > p_{0,\mathrm{im}}$ to

Table 4.1: The constants used to calculate the results in Figure 4.2.

Item	$\bar{c}_{p,\mathrm{t}}$	$\bar{c}_{p,\mathrm{c}}$	$\bar{\gamma}_{\mathrm{t}}$	$\bar{\gamma}_{\mathrm{c}}$	$T_{0,\mathrm{in}}$	$p_{0,\mathrm{in}}$	$\dot{m}_{\mathrm{em}}/\dot{m}_{\mathrm{im}}$
Value	1115 J/(kg K)	1005 J/(kg K)	1.33	1.40	330 K	1 bar	1.021 kg/kg

$p_{0,\mathrm{im}} > p_{0,\mathrm{em}}$. In summary, this simple analysis suggests that for an engine concept which utilizes a high degree of dilution (either by air or EGR), a higher turbocharger efficiency is required to compensate for the higher intake pressure which is needed to deliver high boost and the lower exhaust temperature which results from diluting the charge. With this in mind we can move on to analyze various ways to achieve a higher turbocharger efficiency and in turn increasing the potential for a higher gas exchange efficiency with PPC.

4.2 Evaluation of Turbochargers for Partially Premixed Combustion

The choice of turbocharger configuration has a fundamental influence on the obtainable turbocharger efficiency. Furthermore, the turbocharger efficiency depends on the engine operating condition (i.e. speed and load). To investigate and quantify this for an engine using the PPC concept, the numerical study in Paper I was conducted which evaluated four different turbocharger configurations. The multi cylinder engine (MCE) model which was presented in Section 3.1 was used to simulate the engine operating conditions presented in Table 4.2. These operating conditions had been found experimentally to generate high gross indicated efficiencies. The high

Table 4.2: The engine operating conditions used to evaluate the four different turbocharger configurations. Engine speed (n), gross IMEP ($\mathrm{imep_{gross}}$), EGR rate, lambda (λ), intake manifold temperature (T_{im}), EGR cooler gas outlet temperature (T_{EGR}), start of injection (θ_{soi}), and number of injection events (n_{inj}).

n (rpm)	$\mathrm{imep_{gross}}$ (bar)	EGR (%)	λ	T_{im} (K)	T_{EGR} (K)	θ_{soi} (°ca aTDC)	n_{inj}
800	5	49	1.94	293	291	-30.4	2
800	13	44	1.51	293	291	-9.4	1
800	19	45	1.22	293	291	-7.6	1
800	Max.	45	1.20	293	291	opt.	1
1300	5	49	1.94	293	291	-30.4	2
1300	13	44	1.51	293	291	-9.4	1
1300	19	45	1.22	293	291	-7.6	1
1300	Max.	44	1.20	293	291	opt.	1
1600	5	50	1.79	293	291	-24.2	1
1600	13	46	1.36	293	291	-12.4	1
1600	19	47	1.22	293	291	-7.6	1
1600	Max.	45	1.20	293	291	opt.	1
1900	5	50	1.79	293	291	-23.8	1
1900	13	46	1.36	293	291	-12.4	1
1900	19	47	1.22	293	291	-7.6	1
1900	Max.	45	1.20	293	291	opt.	1

Table 4.3: The specifications of the four different turbochargers. The diameters (d) of the turbine and compressor impellers are normalized with respect to TC2's turbine diameter.

	HP turbine	HP compressor	LP turbine	LP compressor
TC0	η_{is} = 78 %	η_{is} = 78 %	-	-
TC1	VGT + WG, d = 0.95 (-)	d = 1.05 (-)	-	-
TC2	VGT + WG, d = 1.00 (-)	d = 1.15 (-)	-	-
TC3	VGT + WG, d = 1.00 (-)	d = 1.31 (-)	WG, d = 1.18 (-)	d = 1.44 (-)

degree of dilution can be noted by the EGR level which is between 44 % to 50 %. The rate of heat release profiles were taken from engine experiments when the same engine was operated with a gasoline fuel with an approximate research octane number (RON) of 76. A practical issue, from a modeling point of view, was that the experiments did not cover the engine's complete range of load and speed and thus there were not rate of heat release profiles for all operating conditions. This was solved by noting that the rate of heat release, as a function of crank angle degree, did not change particularly when varying the engine speed [82]. As a result it was possible to use the experimental rate of heat release profiles, obtained at 1300 rpm for the 800 rpm cases and correspondingly the 1600 rpm's rate of heat release profiles could be used for the 1900 rpm cases.

The specifications of the four different turbochargers (TC0, TC1, TC2, and TC3) are presented in Table 4.3. The first turbocharger (TC0) was a shaft-less, ideal turbocharger with a free floating turbine and a prescribed isentropic efficiency of 61 % (assuming 100 % mechanical efficiency). This turbocharger was used as a benchmark when comparing the performance of the other turbochargers. The second and third turbochargers were both single-stage (i.e. one compressor and one turbine). In order to achieve a more variable exhaust manifold pressure, a variable geometry turbine (VGT) was used for both these configurations and a waste-gate (WG) was modeled. The turbine and compressor for TC1 and TC2 were provided by the turbocharger manufacturer BorgWarner. BorgWarner helped us choose a combination of compressor and turbine from their diesel engine product line. As can be seen in Table 4.3, the compressor and turbine wheels of TC2 were slightly larger than those of TC1. Furthermore the ratio between the compressor and turbine wheel diameters was slightly different. The advantage of using an off-the-shelf turbocharger is that we can compare the results to a conventional diesel engine. Furthermore, there would be no need to redesign existing turbochargers in order to apply the PPC concept. However, as will become clear later, this comes with a penalty in the highest brake efficiency that can be obtained. So called turbocharger performance maps are used in order to simulate the performance of a turbocharger in GT-Suite. These maps were provided by BorgWarner for both compressors and turbines. Because the turbines were variable-geometry turbines, the performance changes with the opening position and thus mul-

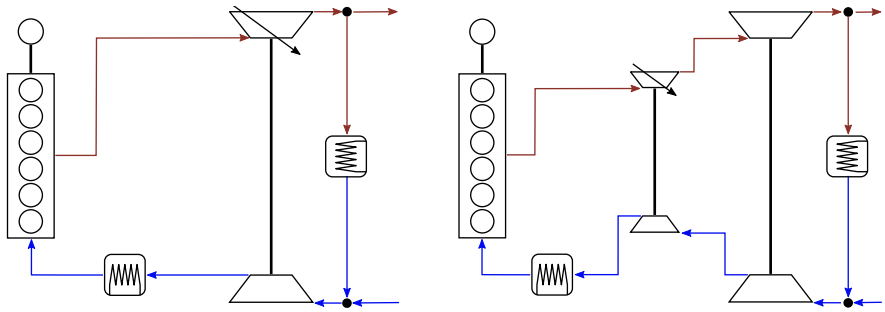

a) Single-stage turbocharger with VGT **b)** Two-stage turbocharger with VGT on the HP stage

Figure 4.3: Schematic layout of a single-stage (a) and two-stage (b) turbocharger configuration as used in this work.

tiple maps were used (six for TC1 and eight for TC2). The third configuration was a two-stage turbocharger, where the low pressure (LP) and high pressure (HP) stages operated in series, and where the HP stage included a VGT. The principle difference between a single-stage and two-stage turbocharger is shown in Figure 4.3. TC3 was constructed and modeled based on the performance maps of TC2. That meant that the reduced mass flow ($\dot{m}_{\text{red}}$) in these maps was scaled, thus changing the effective flow area. It should be noted that this scaling is in reality not that trivial [83]. For instance, the isentropic efficiency of the compressor and turbine increases slightly with wheel diameter, see Equation (4.9), where η is the efficiency and β is an empirical constant between 0.1 and 0.625. But because the differences, for the scalings that we are considering, were between 0 % and 3 % (depending on which β was chosen), we chose to not scale the efficiency of the performance maps for this study. Furthermore, the scaling rule for determining the scaled diameter based on the mass flow multiplier is described in [83]. This was used in Table 4.3 to calculate the resulting diameters for the HP and LP stages of TC3 and it will be used throughout this chapter, see Equation (4.10). The friction and heat transfer losses for the turbocharger can be significant, especially at low engine speed and load [84, 85]. However, as we did not have any data for these losses they were neglected, that is the mechanical efficiency was set to 100 % and no correction was made to the performance maps for heat transfer.

$$\eta_{\text{scaled}} = 1 - \frac{1 - \eta_{\text{baseline}}}{\left(\frac{d_{\text{scaled}}}{d_{\text{baseline}}}\right)^{\beta}} \tag{4.9}$$

$$d_{\text{scaled}} = \sqrt{\frac{\dot{m}_{\text{red, scale}}}{\dot{m}_{\text{red, baseline}}} d_{\text{baseline}}^2} \tag{4.10}$$

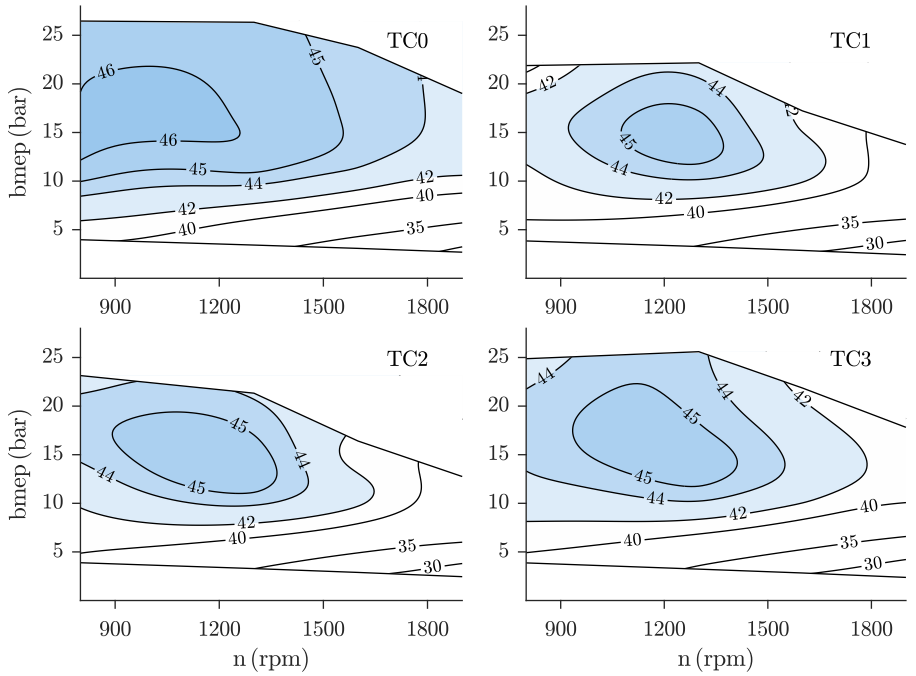

Figure 4.4: Engine brake efficiency (%) of the complete speed-load range and comparing TC0, TC1, TC2, and TC3. The contours are created based on scattered data from the 16 operating conditions using an interpolation technique.

For a two-stage turbocharger, which operates in series, it is common to add an inter-cooler between the first and second compressor stages. This is done to reduce the amount of work which is needed in the second compressor stage and thus increase the gas exchange efficiency. An inter-cooler was, however, not used in this work, and as a result it should be acknowledged that it could affect the final results for this turbocharger configuration. A practical issue of using an inter-cooler, which is worth mentioning, is the fact that it adds significant cost and a slight increase of volume and weight to the engine.

The simulated engine brake efficiency is presented in Figure 4.4 for all turbocharger configurations. The maximum brake efficiency for TC0, TC1, TC2, and TC3 was 46.0 %, 45.1 %, 45.1 %, and 45.2 % while the arithmetic mean was 42.1 %, 39.3 %, 39.7 %, and 40.2 % respectively. None of the real turbochargers were thus able to provide either higher maximum or average efficiency than the shaft-less with free floating turbine. For the real turbochargers, the region of highest efficiency is located around a gross imep of 15 bar and an engine speed of 1250 rpm. Comparing the two single-stage turbochargers, TC1 and TC2, a slightly higher brake efficiency was obtained in the lower engine speed region with TC2.

Only a slight improvement in brake efficiency was obtained by choosing a two-stage turbocharger, although it should be remembered that the use of an inter-cooler would likely increase the overall efficiency. However, a significantly higher engine load could be reached because the boosting was done in two steps instead of one. Partly this is because the amount of energy which is needed to compress a gas, does not increase linearly with the pressure ratio. For instance it can be seen in Figure 4.2 that to increase the pressure ratio over the compressor with a factor of two, more than double the amount of energy is required (because a higher turbocharger efficiency is needed). This is further complicated by the fact that above a certain pressure ratio (the island of peak efficiency), the isentropic efficiency of the compressor decreases rapidly, and offsets the potential rise in pressure ratio. This can be seen in Figure 4.5, which shows compressor characteristics for every compressor. The compressor characteristics com-

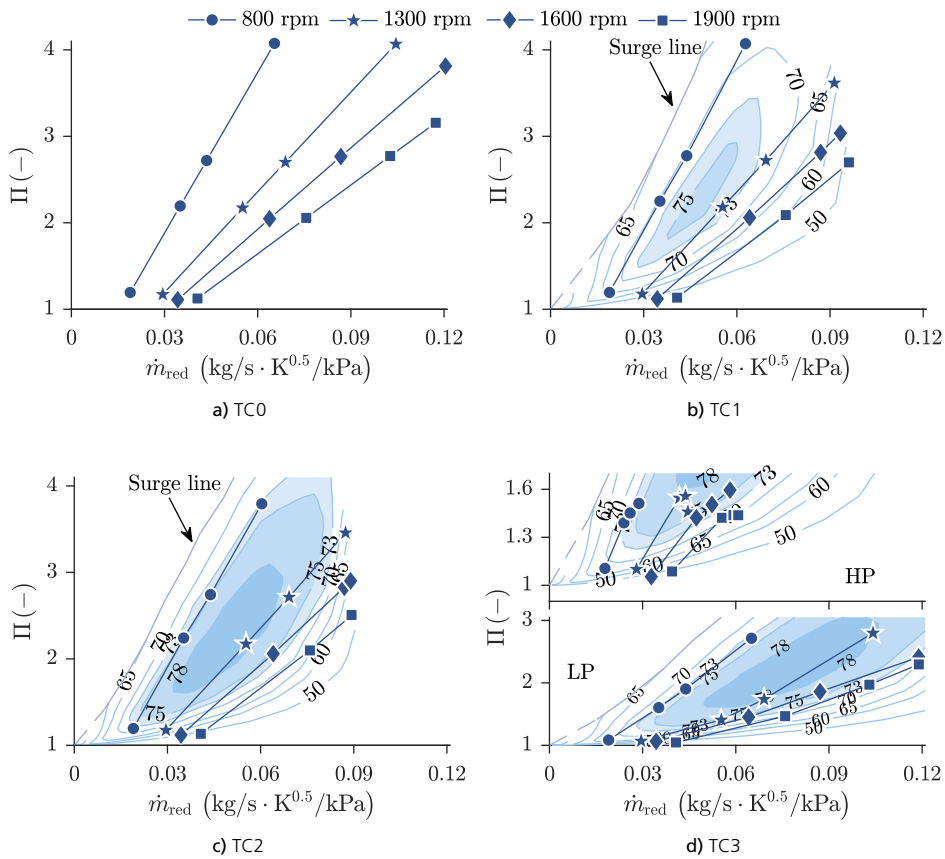

Figure 4.5: Compressor characteristics of TC0, TC1, TC2, and TC3. The operating conditions are superimposed on the map where a straight line represents a constant engine speed but with increasing engine load as the pressure ratio increases. The surge line corresponds to the low flow limit. Outside this line lies a region of unstable flow. The contours represent isentropic efficiency (%) of the compressor.

prise the operating conditions superimposed on the compressor map which consists of the isentropic efficiency (the contour islands) as a function of pressure ratio (Π) and reduced mass flow ($\dot{m}_{\text{red}}$) which are defined in Equations (4.11) and (4.12). In these equations p_{im} is the static outlet pressure of the compressor, $p_{0,\text{in}}$ is the total inlet pressure of the compressor, $\dot{m}$ is the actual mass flow through the compressor, $T_{0,\text{in}}$ is the total inlet temperature of the compressor, γ_{ref} is a reference ratio of specific heats, R_{ref} is the reference gas constant and γ and R are the actual ratio of specific heats and gas constant at the inlet of the compressor.

$$\Pi = \frac{p_{\text{im}}}{p_{0,\text{in}}} \tag{4.11}$$

$$\dot{m}_{\text{red}} = \dot{m} \frac{\sqrt{T_{0,\text{in}}}}{p_{0,\text{in}}} \sqrt{\frac{\gamma_{\text{ref}} R_{\text{ref}}}{\gamma R}} \tag{4.12}$$

From Figure 4.5 we can furthermore observe that for a constant engine speed (n), the operating conditions form a straight line. The reason is that the engine mass flow is then a linear function of the intake manifold density (ρ_{im}), thus proportional to the intake manifold pressure, as shown by Equation (4.13) where η_{vol} is the volumetric efficiency, V_d is the displacement volume, and n is the engine speed (cf. [86, p. 54]).

$$\dot{m}_{\text{engine}} = \eta_{\text{vol}} \cdot \rho_{\text{im}} \cdot V_d \cdot \text{n} \cdot \frac{1}{2} \propto \frac{p_{\text{im}}}{T_{\text{im}}} \tag{4.13}$$

The four lines of different engine speed, in Figure 4.5, are located in a wide spread in the compressor map. This means that only a few operating conditions can be run with the highest compressor efficiency. For the two-stage compressor the situation is slightly better as the boost pressure can be reached by dividing the compression into two steps and thereby achieve a higher compressor efficiency. This is verified in Figure 4.6a which shows the average compressor efficiency for all configurations. The highest compressor efficiency was obtained with TC0 and then followed by TC3, TC2, and TC1. On the other hand, a higher turbine efficiency could be achieved with TC1 than with TC3 and TC2, see Figure 4.6b. As a consequence the difference in combined turbocharger efficiency was relatively small comparing TC1, TC2, and TC3, see Figure 4.6d. Although as mentioned previously, it was indeed possible to achieve a substantially higher load with TC3. Finally the average gas exchange efficiency can be seen in Figure 4.6c.

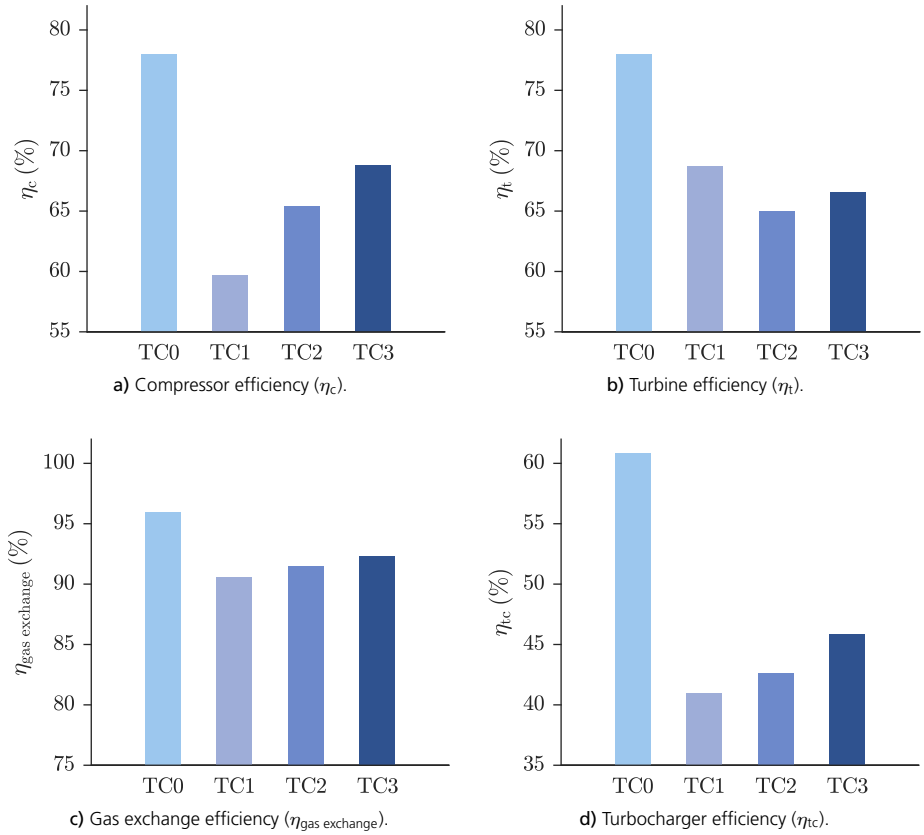

Figure 4.6: Compressor efficiency, turbine efficiency, gas exchange efficiency, and turbocharger efficiency for TC0, TC1, TC2, and TC3, respectively.

4.2.1 The effect of intake manifold temperature

For the results presented so far the intake manifold temperature (T_{im}) was set equal to what was used in the experiments to obtain the rate of heat release profiles. However, that meant that it was around 293 K which is very low. Water condensation is governed by the dew point temperature which in turn depends on gas temperature, pressure, and composition. The dew point temperature reduces with lower pressure and with increasing EGR level (due to higher water content). As these simulations were done using a long route EGR configuration (which in this case meant low pressures), as well as EGR levels around 45 % to 55 %, it was likely that the temperature in the inlet of the compressor as well as in both the EGR and charge air coolers were below the dew point. This is an issue because serious damage would be inflicted to the compressor impeller and both EGR and charge air coolers due to corrosion and fouling caused by the water condensation [40]. On the other hand, it has been found

that lowering the intake manifold temperature by only 35 K can raise the gross indicated efficiency by 4.4 % due to higher ratio of specific heats and less in-cylinder heat transfer loss [38]. In order to investigate this influence, the operating conditions in Table 4.2 were once again simulated but with a higher intake manifold temperature. To simulate a realistic intake manifold temperature, water condensation was prevented in both the charge air cooler (CA-C) and in the EGR cooler (EGR-C). Additionally a safety margin of 20 K was applied. This is formulated in Equation (4.14). By using this equation, I assumed that the engine's charge air cooler was using air as its cooling medium and as such, could reach a lowest outlet gas temperature of 313 K. Correspondingly, I assumed that the EGR cooler was using the engine cooling water as its cooling medium and therefore could achieve a lowest outlet gas temperature of 363 K.

$$\begin{aligned} \text{EGR-C:} \quad T_{\text{out}} &= \begin{cases} T_{\text{dew}} + 20\,\text{K}, & \text{if } T_{\text{dew}} + 20\,\text{K} > 363\,\text{K} \\ 363\,\text{K}, & \text{otherwise} \end{cases} \\ \text{CA-C:} \quad T_{\text{out}} &= \begin{cases} T_{\text{dew}} + 20\,\text{K}, & \text{if } T_{\text{dew}} + 20\,\text{K} > 313\,\text{K} \\ 313\,\text{K}, & \text{otherwise} \end{cases} \end{aligned} \tag{4.14}$$

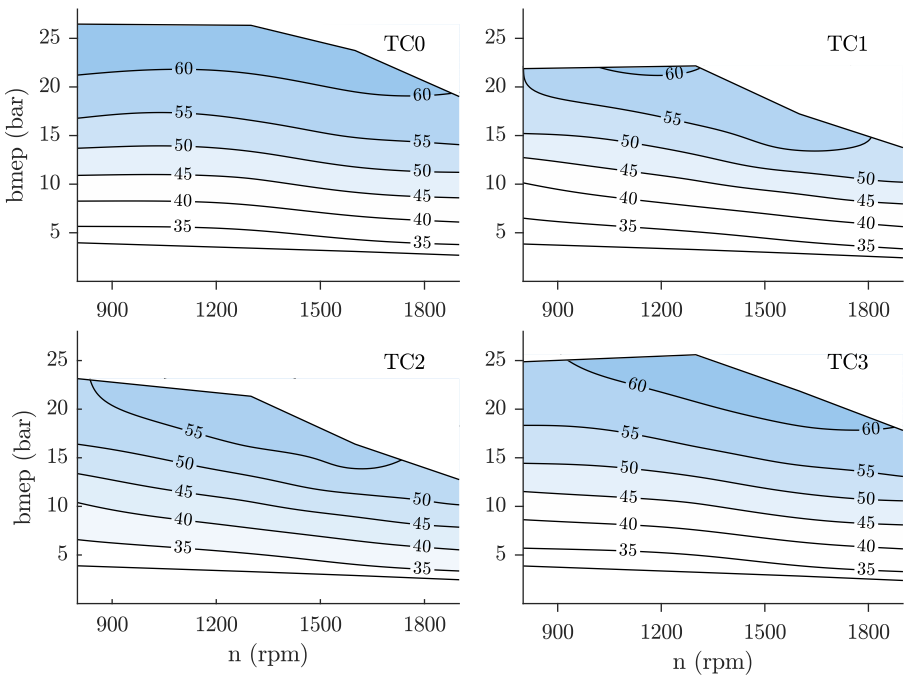

Figure 4.7: Difference in intake manifold temperature (K), between low and high intake manifold temperature, of the complete speed-load range and comparing TC0, TC1, TC2, and TC3. The contours are created based on scattered data from the 16 operating conditions using an interpolation technique.

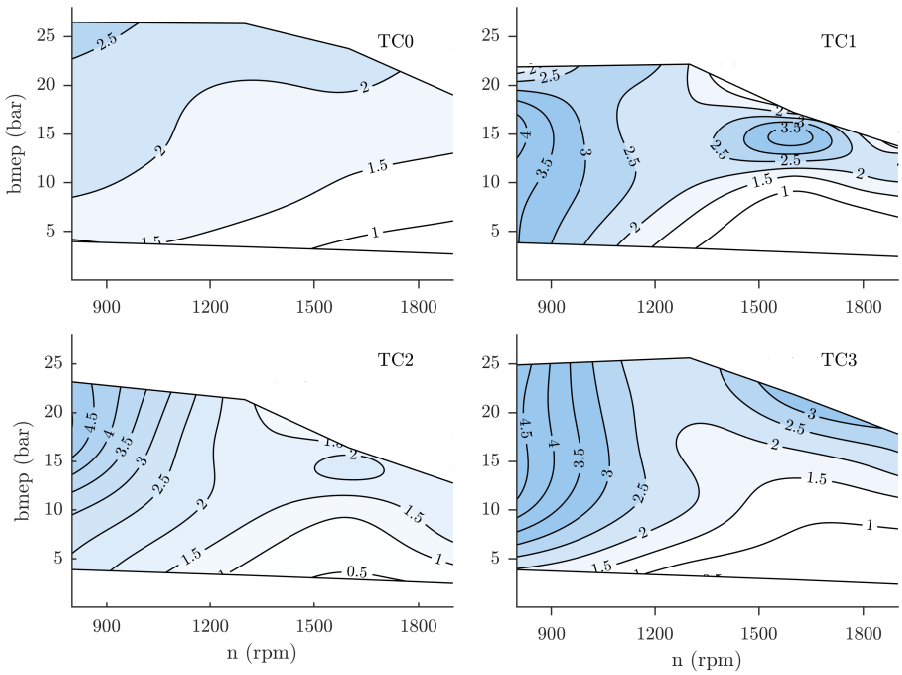

Figure 4.8: Difference in engine brake efficiency (%), between low and high intake manifold temperature, of the complete speed-load range and comparing TC0, TC1, TC2, and TC3. The contours are created based on scattered data from the 16 operating conditions using an interpolation technique.

Figure 4.7 shows the difference in intake manifold temperature for all operating points. As the difference in all cases is above 20 K (which was the imposed safety margin), we can conclude that the intake manifold temperature in the previous results was in fact below the dew point. Furthermore, this difference increases with load because the pressure in the charge air cooler gets higher.

The difference in brake efficiency between low and high intake manifold temperatures is then presented in Figure 4.8. For all operating points, the brake efficiency is higher with a lower intake manifold temperature. However, the largest difference is found for the lowest and highest engine speeds and at the highest engine load. Additionally, although not shown here, the highest achievable load was reduced substantially when going to the higher temperatures. The reason is that when increasing the intake manifold temperature, the intake manifold pressure needs to increase as well, in order to reach the same λ and EGR level (i.e. the same engine mass flow). As a result the compressor needs more power to generate a higher boost pressure which means that the turbine needs to generate a high power and therefore needs to operate with a higher engine back pressure. For a lower boost pressure this can be done relatively efficiently, however, at the highest load the compressor and turbine are already operating at their

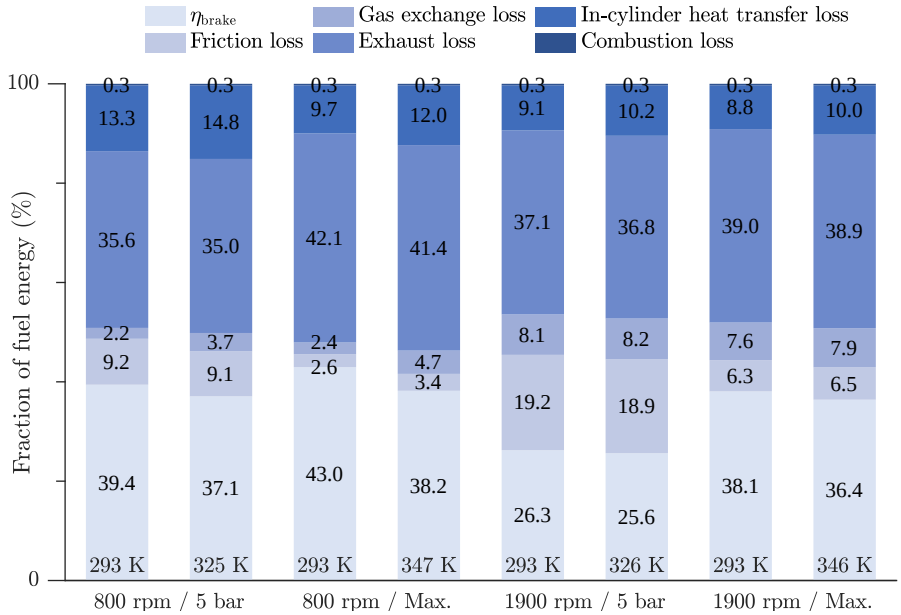

Figure 4.9: Energy balance for TC2 for the lowest and highest engine loads at 800 rpm and 1900 rpm and comparing low and high intake manifold temperatures. All fields represent losses except the field for brake efficiency (η_{brake}). Heat transfer loss refers to in-cylinder heat transfer losses.

limits. Furthermore, an increase in pressure ratio for the compressor above the peak efficiency island, without a corresponding increase in reduced mass flow (see Equation (4.12)) leads to a lower compressor efficiency. At the lowest speed the compressor is operating close to the surge line and just a small increase in pressure ratio causes a large decline in the compressor efficiency.

The differences in brake efficiency were investigated further by dividing the injected fuel energy into useful brake energy and the different loss terms (i.e. combustion loss, in-cylinder heat transfer loss, exhaust loss, gas exchange loss, and friction loss). This is presented in an energy balance diagram and shown in Figure 4.9. The energy balance was constructed for TC2 for the lowest and highest engine loads at 800 rpm and 1900 rpm and comparing low and high intake manifold temperatures. It can be seen that a lower intake manifold temperature led to a reduction of the in-cylinder heat transfer in all cases. However, all of this reduction could not be converted into useful work, instead some of it ended up as enthalpy in the exhaust (i.e. the exhaust loss term was higher). Moreover, at 800 rpm the gas exchange loss was almost twice as high for the cases with higher intake manifold temperature whereas at 1600 rpm this difference is negligible. In conclusion, a lower intake manifold temperature increases both gross indicated and gas exchange efficiency.

4.2.2 The effect of EGR

The use of high EGR levels is beneficial for reducing NO_x emissions and also, to some extent, facilitates PPC by prolonging the ignition dwell. However, as was shown in Figure 4.2, from a theoretical point of view, a high degree of dilution will most likely deteriorate the gas exchange efficiency. To quantify this reduction, the following sensitivity study was conducted. Constant air-fuel-ratio was targeted and the EGR level was varied between 0 % to 50 %. This is an important distinction, as an alternative way would be to keep the same engine mass flow, thus reducing λ as EGR is increased. TC0 was considered in order to decouple the thermodynamic effect of EGR from the effect of a different turbocharger efficiency. The effect of different turbocharger efficiency was instead considered by sequentially setting the turbocharger efficiency of TC0 to 61 % and then to 49 %. Furthermore, both low and high intake manifold temperatures were considered (see Equation (4.14)). The maximum engine load at 800 rpm and 1900 rpm were the operating conditions chosen because the largest difference in brake efficiency was found for them.

The brake efficiency as a function of EGR is presented in Figures 4.10a to 4.10d. Additionally the gross indicated efficiency (η_{gross}) is included into these figures for better understanding of the trends. First, we can notice that the gross indicated efficiency increases with EGR for all cases. The reason is that the in-cylinder heat losses are lower because of the dilution which reduces the global in-cylinder temperature. Although the gross indicated efficiency increases in all cases, it does so more for the cases with low intake temperature and for the cases with higher engine speed due to less in-cylinder heat transfer, which is in accordance with the discussion above (see Figure 4.9). It should be noted that the same rate of heat release profile was used here as the EGR level was varied (although it was different for the different engine speeds). Typically it would not be easy to achieve that in an engine, but on the other hand it serves well here because the thermodynamic effect of EGR can be decoupled from the effect of a different rate of heat release profile. Considering the brake efficiency, it can be noted that there is an optimum EGR level which yields the highest brake efficiency. However, this point is different for the different cases. For instance, in Figure 4.10a, the turbocharger efficiency is 61 % and a low intake manifold temperature is used. We can see that for this case, the optimum EGR level is as high as 40 %. However, by either reducing the turbocharger efficiency (Figure 4.10c) or increasing the intake manifold temperature (Figure 4.10b), the optimum EGR level shifts to a lower value. At a turbocharger efficiency of 49 % and for a high intake manifold temperature (Figure 4.10d), the optimum EGR level is only 5 % for the lower engine speed. The reason why a higher EGR level does not produce a higher brake efficiency although it yields a higher gross indicated efficiency can be explained as follows. When the EGR level is increased, a higher boost pressure is needed. This results in a lower gas exchange

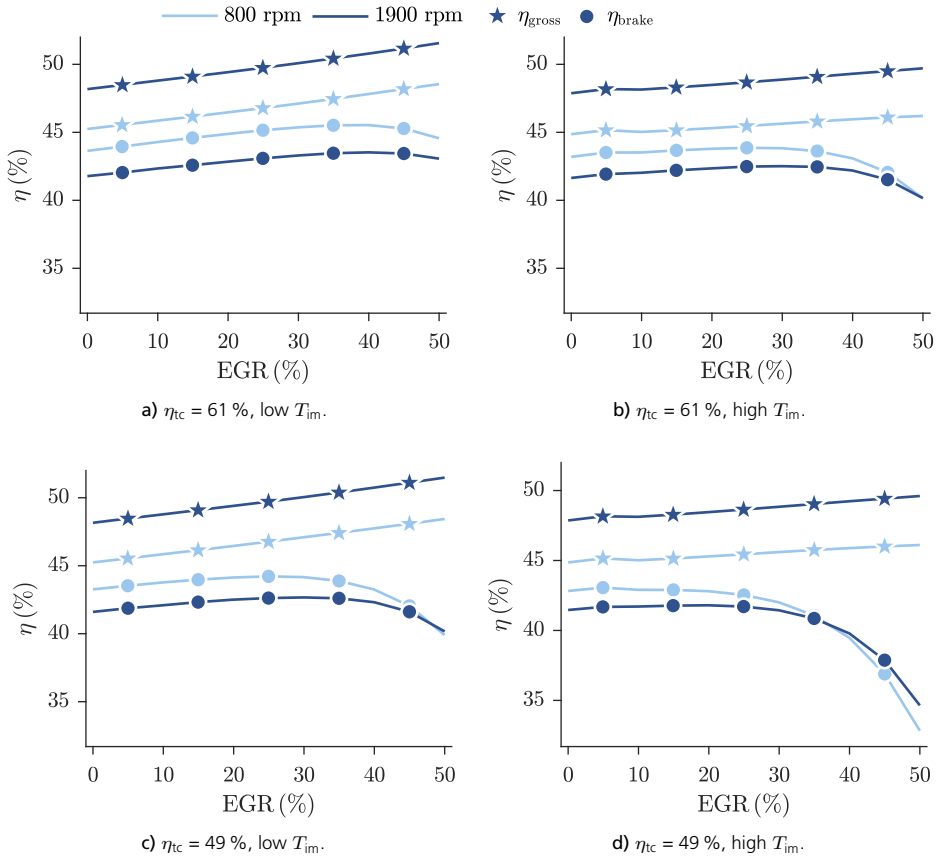

Figure 4.10: Brake and gross indicated efficiency as a function of EGR level. Four different cases are shown where the difference is in the specified turbocharger efficiency and whether a low or high intake manifold temperature is applied.

efficiency, however, this reduction of gas exchange efficiency is at first offset by the increase in gross indicated efficiency but then, at a certain point, the reduction in gas exchange efficiency is simply larger and thus a drop in brake efficiency occurs. Consequently there exist a trade-off between a higher gross indicated efficiency and a lower gas exchange efficiency which depends on the level of dilution and operating point.

4.2.3 Mismatch of Turbine and Compressor Wheel Diameter

It was mentioned in the beginning of this section that the single-stage turbochargers, TC1 and TC2, were taken from the diesel engine product line of BorgWarner. In contrast to conventional diesel combustion, the PPC concept utilizes a high degree of dilution, and hence there will be higher mass flows over the compressor and turbine.

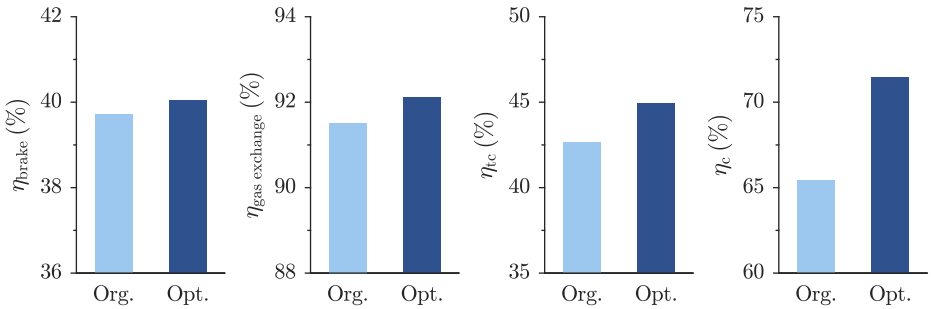

Figure 4.11: Simulated brake, gas exchange, turbocharger, and compressor efficiency for the engine, comparing the original and optimized TC2.

A turbocharger, designed specifically for the PPC concept, could potentially reach a higher average turbocharger efficiency, and thus a higher engine brake efficiency. This was tested by optimizing the size of the performance maps of TC2 on the operating conditions from Table 4.2. As was explained earlier, this was done by multiplying the reduced mass flow from the performance map by a constant. The average brake, gas exchange, turbine, and compressor efficiencies for the original and optimized TC2 are shown in Figure 4.11. A higher value for all these parameters, except for the turbine efficiency, were obtained with the optimized turbocharger. What is more interesting, is the obtained optimal sizes of the compressor and turbine wheels, which can be seen in Table 4.4. The optimized compressor wheel diameter was 8.9 % larger, while the diameter of the turbine wheel was 3.8 % smaller. Thus the ratio between the compressor and turbine wheel diameters increased from 1.150 to 1.301. Not only is this an interesting result, but it reveals that a turbocharger, designed for a diesel engine, cannot fulfill its potential when the PPC concept is applied. It is also, likely, the reason why TC2 performed better than TC1 which had a ratio of 1.10 between the compressor and turbine wheel diameters. Furthermore, this behavior can partly be explained by considering the equation for reduced mass flow through either the compressor $\left(\dot{m}_{\text{red, c}}\right)$ or turbine $\left(\dot{m}_{\text{red, t}}\right)$, see Equation (4.15). The reduced mass flow controls the effective flow area of the turbine and compressor.

Table 4.4: Normalized diameters of the compressor and turbine wheels, comparing the original TC2 and the optimized. The diameters are normalized with respect to the diameter of TC2's turbine wheel. The last column shows the ratio between the compressor and turbine wheels.

	Turbine	Compressor	Compressor / Turbine
Original TC2	1.000	1.150	1.150
Optimized TC2	0.962	1.252	1.301

$$\begin{aligned} \text{Compressor reduced mass flow:} \quad & \dot{m}_{\text{red, c}} = \dot{m}_{\text{c}} \frac{\sqrt{T_{0,\text{in}}}}{p_{0,\text{in}}} \sqrt{\frac{\gamma_{\text{em,ref}} R_{\text{em,ref}}}{\gamma_{\text{em}} R_{\text{em}}}} \\ \text{Turbine reduced mass flow:} \quad & \dot{m}_{\text{red, t}} = \dot{m}_{\text{t}} \frac{\sqrt{T_{0,\text{em}}}}{p_{0,\text{em}}} \sqrt{\frac{\gamma_{\text{in,ref}} R_{\text{in,ref}}}{\gamma_{\text{in}} R_{\text{in}}}} \end{aligned} \tag{4.15}$$

If we assume that the inlet temperature and pressure are fixed to the ambient, the reduced mass flow over the compressor does not change with the operating conditions. Therefore the flow capacity of the compressor is proportional to the real mass flow through the compressor. The reduced mass flow over the turbine, on the other hand, depends, not only on turbine mass flow, but on the exhaust manifold temperature and pressure as they change with the operating conditions or with the turbocharger efficiency. For the PPC concept, which relies on a large degree of dilution, this means that the exhaust temperature will be comparably lower and to compensate for the lower enthalpy that a lower temperature yields, a higher exhaust manifold pressure is needed. This gives a much lower reduced mass flow than for the compressor and thus a lower effective flow area which means that the optimum diameter of the turbine will be smaller than the diameter of the compressor [87]. To verify this reasoning, Figure 4.12 shows the reduced mass flow for the turbine and compressor as a function of EGR. These results were taken from the simulations with varying EGR level which were presented earlier. It is evident that the reduced mass flow of the compressor increases with higher engine mass flow, in fact, it would have increased linearly with EGR if the volumetric efficiency[1] (η_{vol}) did not also increase slightly with EGR. The reduced mass flow of the turbine, on the other hand decreases with EGR. Finally, Figure 4.12b shows that with a lower turbine efficiency, this decline is even more pronounced because the exhaust manifold pressure must be higher.

This discussion has so far concentrated on the reduced mass flow and thus the effective inlet flow area. However, to be able to match the turbine to the compressor, they have to be designed for the same shaft speed. The design of a new turbocharger most often starts with the design of the compressor. The optimal turbocharger speed is then set and the design of the turbine must adhere to this speed. Furthermore, the speed of the compressor will decrease with increasing values on the compressor wheel diameter if the same specific speed should be obtained. Consequently, if a larger compressor is needed, which is likely for the PPC concept as the previous discussion concluded, the optimal speed of the compressor will be lower and thus the turbine needs also operate with a lower speed. In the design of the turbine, the measure known as the blade speed ratio (BSR) is key and needs to be considered. It is the ratio between

[1] I am here considering all gases in the manifold and not just the air, which is in contrast to the conventional definition of volumetric efficiency.

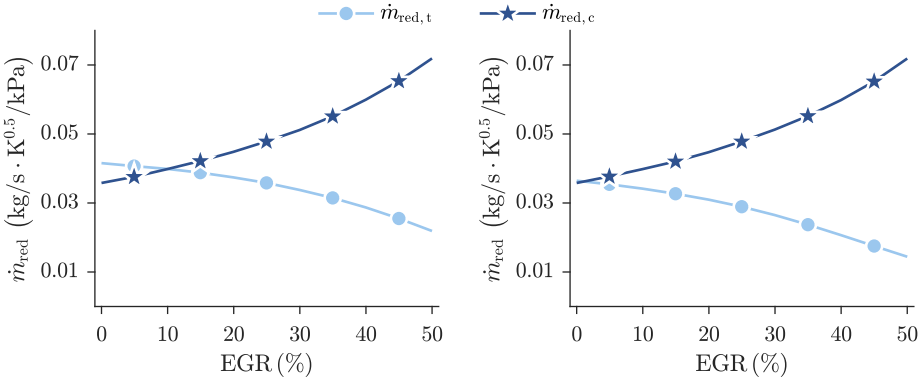

a) η_{tc} = 61 %, low T_{im}.

b) η_{tc} = 49 %, low T_{im}.

Figure 4.12: Reduced mass flow for the compressor $(\dot{m}_{\mathrm{red,\,c}})$ and turbine $(\dot{m}_{\mathrm{red,\,t}})$ as a function of EGR.

the turbine tip speed and the outlet speed that would be obtained from an isentropic expansion (c_{is}). The BSR is defined in Equation (4.16), where ω is the turbocharger rotational speed, r_{t} is the turbine tip radius and $T_{0,\mathrm{em}}$ is the total temperature at the turbine inlet.

$$\mathrm{BSR} = \frac{U_{2,\mathrm{t}}}{c_{\mathrm{is}}} = \frac{\omega r_{\mathrm{t}}}{\sqrt{2c_{p,\mathrm{t}}T_{0,\mathrm{em}}\left(1-\Pi_{\mathrm{t}}^{\frac{1-\gamma_{\mathrm{t}}}{\gamma_{\mathrm{t}}}}\right)}} \tag{4.16}$$

For a radial in-flow turbine, the theoretical highest efficiency is obtained for a BSR between 0.6 and 0.8 [87, p. 153, 88, p. 86, 89, p. 273]. Moreover, the turbine efficiency decreases rapidly on both sides of the optimal BSR. Following the conclusion from earlier, that the turbine should have a lower effective flow area, hence it should have a smaller inlet diameter, we can see that both a lower turbocharger speed and turbine diameter will lead to a reduction in BSR. Figure 4.13 shows the turbine efficiency, turbine blade speed ratio and turbocharger speed, comparing the original and optimized TC2. The average turbocharger speed is lower because the compressor is larger. A lower speed and a small turbine lead to a lower BSR and finally to a lower average turbine efficiency. The lower turbine efficiency stands in contrast to the average compressor efficiency, which increased with the optimal TC2 (see Figure 4.11). The optimized TC2 had a ratio of 1.301 between compressor and turbine wheel diameters. The performance equilibrium between compressor and turbine is presented in Equation (4.17) where d_{c} and d_{t} are the compressor and turbine wheel diameters

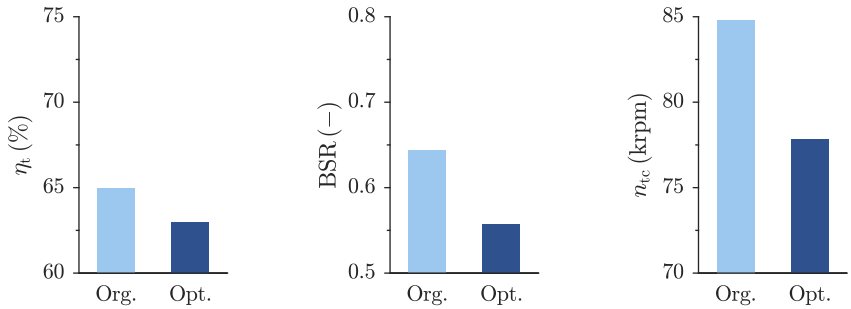

Figure 4.13: Turbine efficiency, turbine blade speed ratio (BSR), and turbocharger speed (n_{tc}) for the engine, comparing the original and optimized TC2.

respectively and σ is the slip factor of the compressor which depends on the number of blades and any potential back sweep of the blades [88, p. 85].

$$\frac{d_c}{d_t} = \frac{1}{\text{BSR}}\sqrt{\frac{\eta_t}{2\sigma}} \tag{4.17}$$

In this equation it is assumed that the inlet velocity of the compressor is completely axial. For simplicity we can assume that the slip factor is unity, then the BSR of the turbine is 0.47 for a turbine efficiency of 75 % and for a $d_c/d_t = 1.301$. One way to design a turbine with a lower optimal BSR is for instance to use a mixed in-flow turbine or an axial turbine for which the optimal BSR is lower, although probably not as low as 0.47 [90, 91].

4.3 Application of Dual Loop EGR

We have seen that the gas exchange efficiency is very much affected by the turbocharger efficiency and degree of dilution. If a certain degree of dilution is needed, for example to reduce NO_x and soot emissions, and a specific turbocharger is used, these variables are all fixed. However, as was seen in Figure 4.5, the compressor was not working at its highest efficiency in more than a couple of operating points, thus there exists a potential to increase the average turbocharger efficiency and by that, increasing the average brake efficiency. The reason why the compressor did not operate with highest possible efficiency was that the compressor mass flow is proportional to the engine mass flow which in turn is proportional to the engine speed and boost pressure (i.e. engine load). As a result, the compressor mass flow changes with engine operating conditions. In this section, I will present some of the results from Paper II in which we investigated if it is possible to control the mass flow through the compressor by

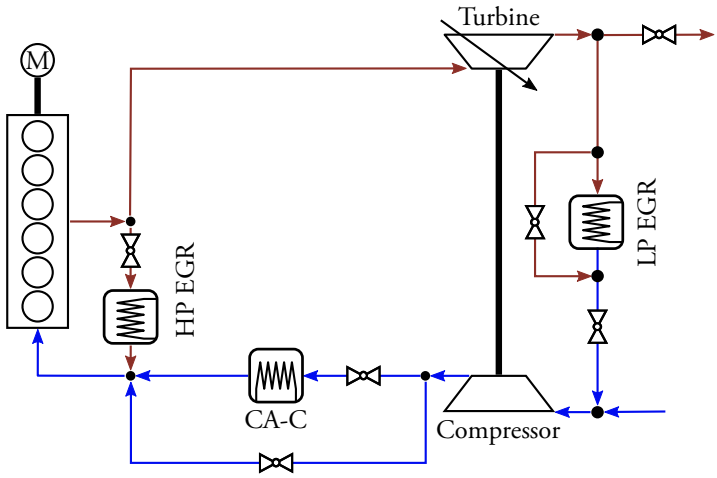

Figure 4.14: Schematic layout of the engine with two different EGR routes (HP and LP).

using two different EGR routes. In this case one high pressure (HP) EGR route and one low pressure (LP) EGR route were used.

The two EGR routes are shown schematically in Figure 4.14 and it can be seen that the HP route receives exhaust gas before the turbine (where the pressure is high), whereas the LP route receives the exhaust after the turbine, where the pressure is low. The hypothesis is that at low engine speeds, more mass flow would ideally be needed in order to push the compressor operating point to the right in the compressor map where there is a higher efficiency. This can be done by letting more of the exhaust gas flow through the LP route. On the other hand, at high engine speeds there is a surplus of mass flow flowing through the compressor. Thus, at high engine speeds it would be ideal to let some of this gas bypass the turbocharger completely, that is lead some of the flow through the HP route. This has been tested before, however, without any relevant success, see for instance Refs. [92–94]. A possible explanation for why it did not work in those cases is that the authors were using a fixed size turbocharger, i.e. they were performing experiments on an existing engine which was designed to operate with only HP or LP EGR. Ideally, both the compressor and turbine should be designed to be used in a combined HP and LP EGR route arrangement. Additionally, the more EGR that is used, the more the compressor mass flow can be adjusted. The very high levels of EGR, used with PPC, makes this concept optimal for testing if the dual route EGR configuration can result in a higher average brake efficiency.

The combined HP and LP EGR route configuration was compared against running the engine with only HP EGR and then also with only LP EGR. For each of these three cases the same multi cylinder engine model was used to simulate the engine performance on the operating conditions as shown in Table 4.2. As discussed pre-

Table 4.5: Normalized diameter of the three different turbochargers' compressor and turbine wheels used in the comparison of EGR configurations. The diameters are normalized with respect to the diameter of TC2's turbine wheel from Table 4.3. The last column shows the ratio between the compressor and turbine wheels.

	Turbine	Compressor	Compressor / Turbine
LP EGR	0.962	1.252	1.301
HP EGR	0.707	0.920	1.301
HP and LP EGR	0.883	1.060	1.200

viously, the performance of each EGR configuration will depend largely on the size of the turbocharger. Therefore, the turbocharger was resized for every EGR configuration to yield the highest average brake efficiency. This optimization of the size of the compressor and turbine was done by scaling the performance maps for TC2 from Table 4.3 in accordance with the discussion in Section 4.2. An equal weight was put on every operating point when determining the maximum brake efficiency. The resulting diameters (compared to the original TC2) for the turbine and compressor are shown in Table 4.5. It is interesting to note that the ratio of compressor to turbine wheel diameters, is lower for the combined HP and LP EGR route configuration, and

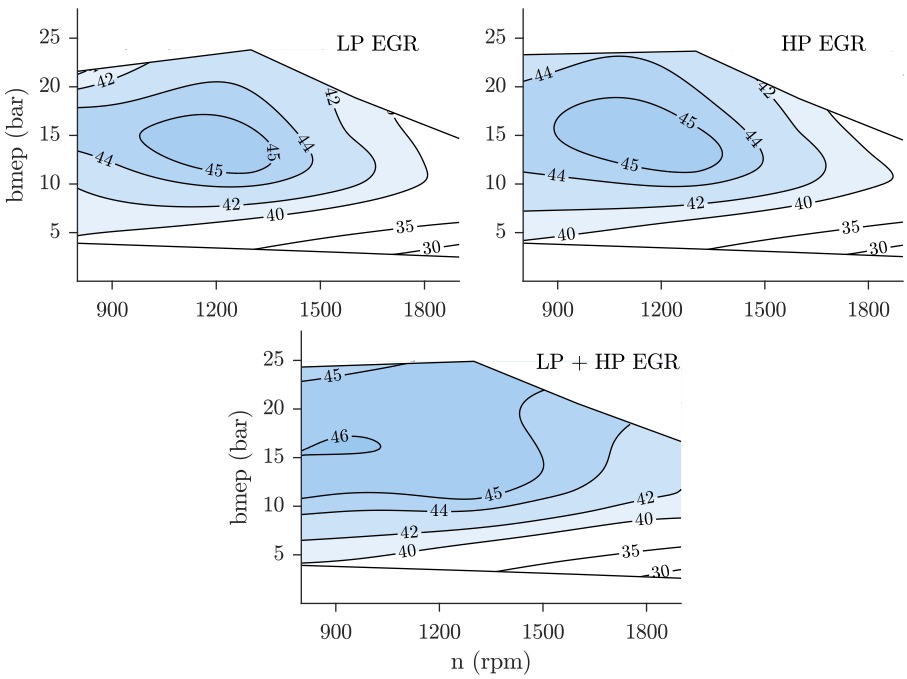

Figure 4.15: Engine brake efficiency (%) of the complete speed-load range for the LP EGR, HP EGR, and LP and HP EGR route configurations. The contours are created based on scattered data from the 16 operating conditions using an interpolation technique.

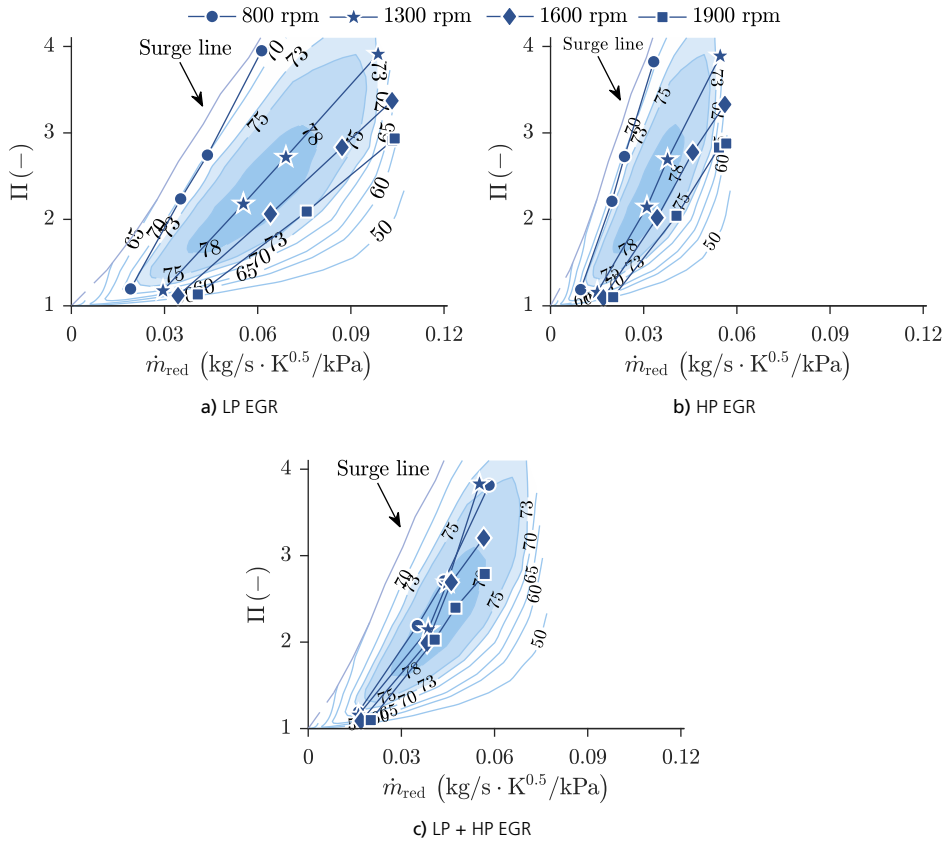

Figure 4.16: Compressor characteristics for the LP EGR, HP EGR, and LP and HP EGR route configurations. The operating conditions are superimposed on the map where a straight line represents a constant engine speed but with increasing engine load as the pressure ratio increases. The surge line corresponds to the low flow limit. Outside this line lies a region of unstable flow. The contours represent isentropic efficiency (%) of the compressor.

therefore (following the discussion from Section 4.2.3) suggests that it would be easier to obtain a high turbine efficiency with a radial turbine.

The resulting brake efficiency as a function of engine speed and bmep is shown in Figure 4.15 for all three EGR route configurations. The brake efficiency is higher for all operating points with combined HP and LP EGR route configuration. Furthermore, a higher bmep was obtained with the LP and HP EGR route configuration, especially in the low engine speed region. Figure 4.16 shows the compressor characteristics for all three EGR route configurations. From this figure it is evident that it was possible to control the mass flow through the HP EGR route to achieve a higher compressor efficiency. This is verified in Figure 4.17a which shows the average compressor efficiency for all three EGR route configurations. The average compressor efficiency is 5 %pt. higher for the combined LP and HP EGR route configuration. Addition-

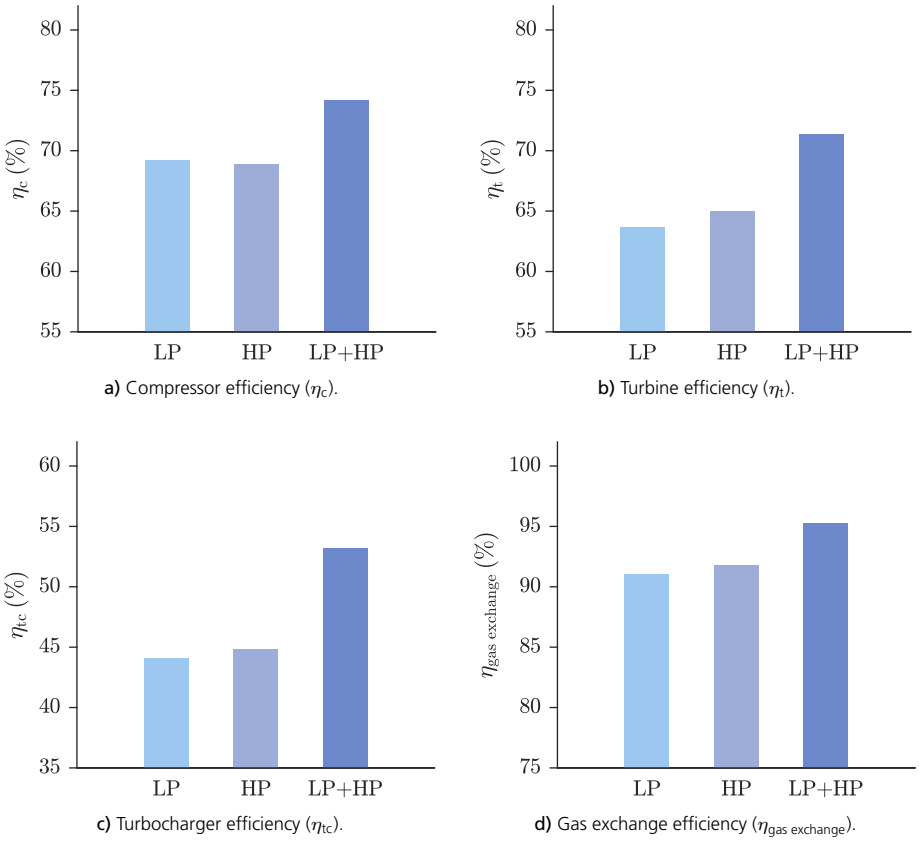

a) Compressor efficiency (η_c).

b) Turbine efficiency (η_t).

c) Turbocharger efficiency (η_{tc}).

d) Gas exchange efficiency ($\eta_{gas\ exchange}$).

Figure 4.17: Gas exchange efficiency, turbine efficiency, compressor efficiency, and turbocharger efficiency for the LP EGR, HP EGR, and LP and HP EGR route configurations.

ally Figure 4.17b shows the average turbine efficiency which was also 5 %pt. higher for combined route configuration. Figures 4.17c and 4.17d finally show the average total turbocharger efficiency and the gas exchange efficiency and it can be seen that an improvement by 9 %pt. and 4 %pt. respectively could be achieved by using the combined EGR route configuration. Paper II also included a sensitivity analysis on the intake manifold temperature, corresponding to the one in Section 4.2.1, and the results showed that, in that case, the combined LP and HP EGR route configurations could achieve an even larger improvement than mentioned here above.

4.4 Summary

This chapter set out to analyze important factors which affect the gas exchange efficiency, as well as different ways to increase it, for a PPC engine. The theoretical

effect of dilution was first investigated. It was seen that, both a low exhaust manifold temperature and a high intake manifold pressure, increase the demand for a high turbocharger efficiency, in order to achieve a positive pressure differential over the engine.

Next, the engine brake efficiency was simulated with four different turbocharger configurations. These turbochargers were a free floating turbocharger (TC0) with a prescribed isentropic efficiency which was used as a baseline, two single stage turbochargers (TC1 and TC2) - which both included a variable geometry turbine and waste-gate, and finally a two-stage turbocharger (TC3) with a variable geometry turbine but without an inter-cooler. The peak brake efficiencies for TC0, TC1, TC2, and TC3, were 46.0 %, 45.1 %, 45.1 %, and 45.2 %, while the arithmetic mean was 42.1 %, 39.3 %, 39.7 %, and 40.2 %, respectively. None of the real turbochargers were thus able to provide either higher maximum or average efficiency, than the shaft-less with free floating turbine. Furthermore, it was shown that the turbine and compressor were mismatched. Due to the high level of dilution, which led to a low exhaust temperature, the reduced mass flow over the compressor was significantly larger, than the reduced mass flow over the turbine. Consequently, a larger compressor wheel together with a smaller turbine wheel would have been more suitable.

Although it was possible to achieve a reasonably high average brake efficiency with a high degree of dilution, especially high levels of EGR, it was evident that this dilution is detrimental for achieving a high gas exchange efficiency. A sweep in EGR level showed that there exists an optimal level of EGR for which the highest brake efficiency was achieved. However, this optimal level was shifted towards lower EGR levels when the turbocharger efficiency was lower, or when the intake manifold temperature was higher.

The gas outlet temperature of the EGR and charge air coolers should be kept above the dew point, in order to prevent fouling and corrosion in the compressor, as well as in the coolers themselves. However, an increase in this temperature was shown to be detrimental for both the gross indicated efficiency, and the gas exchange efficiency, which consequently led to a decrease in brake efficiency.

Finally, the application of a dual loop EGR configuration, in which the mass flow of exhaust gas through the turbine is controlled, yielded a substantial increase in average gas exchange efficiency. The reason was that with the dual loop configuration, more of the operating points could be run with a high compressor efficiency.

Chapter 5

Re-Optimization of the Engine Settings to achieve Maximum Engine Brake Efficiency

The previous chapter showed that applying a high level of dilution leads to an increase in gross indicated efficiency. However, if too high levels of dilution are used, the penalty in gas exchange loss can offset the increase in gross indicated efficiency, and thus lead to a decrease in overall brake efficiency. Ultimately, it is the brake efficiency that should be maximized in order to minimize the fuel consumption of the engine. On the other hand, the use of dilution is what yields low local emissions of NO_x and soot with the partially premixed combustion (PPC) concept. The balance between efficiency and emissions is not trivial, and to say how much dilution should be used requires detailed analysis of the engine system over its whole operating range. In this chapter, which is based on the content in Papers III-V, I will attempt to shed light onto this problem, that is: for a specific engine system, how should engine parameters such as level of exhaust gas recirculation (EGR), intake manifold temperature, intake manifold pressure, fuel injection pressure, and injection strategy, be chosen in order to maximize the brake efficiency, while constraining NO_x and soot. In addition, I will investigate the effect of two properties which are arguably fundamental to the engine system, namely the choice of fuel and engine compression ratio. For this purpose I have conducted a simulation-based study with four main cases including three different fuels and two different compression ratios.

Table 5.1: Case setup for the study with the fuel properties and the compression ratio used.

Case	1	2	3	4
Fuel	Methanol	Methanol	Gasoline	Gasoline
Octane number	109	109	76	97
Lower heating value (MJ/kg)	19.9	19.9	44.1	42.9
Stoichiometric air-fuel-ratio	6.5	6.5	14.77	14.16
Compression ratio	17.3	21.6	17.3	17.3

While the specifics are presented in Table 5.1, the cases can be summarized as:

1. Methanol with standard compression ratio
2. Methanol with optimized compression ratio
3. Gasoline with RON = 76 and standard compression ratio
4. Gasoline with RON = 97 and standard compression ratio

I will motivate the choice of these particular cases next. First of all, it is likely that the highest brake efficiencies that can be achieved, as well as the resulting combustion characteristics, depend on which fuel is being used. The choice of fuel for PPC was discussed previously in Chapters 1 and 2 and there I referred to researchers who say that the optimal fuel for PPC is a gasoline with a research octane number (RON) in the range of 65 to 80. This type of fuel is advocated because of its ability to, on the one hand achieve stable combustion at low engine loads, and on the other hand avoid excessive maximum pressure rise rate at high engine loads[1]. Consequently by using a fuel of this type, it would be possible to cover the whole engine load range. However, it is questionable if the combustion with this type of fuel can be defined as PPC. The reason is that a fuel which has a RON of 65 to 80 does simply not have enough auto-ignition resistance to yield a separation between the end of fuel injection and start of combustion at high loads. On the other hand it is not certain that PPC will be optimal when the brake efficiency is targeted. Or in other words: it might be the case that PPC yields the highest brake efficiency at low load, but conventional diesel combustion is preferable at high load. To investigate this, I chose two different gasoline fuels for this study: one with a RON of 76 and one with a RON of 97, which are named case 3 and 4 (see Table 5.1). Naturally, because a real gasoline fuel consists of several species and is difficult to model exactly, these two gasoline fuels were modeled as surrogates consisting of iso-octane, n-heptane and ethanol. The blending rules from [95] were used to determine the fraction of each species in order to match the RON .

[1]In this context stable combustion means combustion without misfire and excessive cycle to cycle variations.

Dilution with exhaust gas recirculation is, as was described in Chapter 2, very effective for reducing NO_x emissions and achieving low temperature combustion and hence PPC. However, for a fuel with propensity for soot formation, as is gasoline, dilution with EGR also yields an increase of soot and PM emissions[2]. In contrast, fuels with high oxygen content has shown to produce significantly lower levels of soot, thus it is possible that by using such a fuel a higher degree of freedom can be obtained when optimizing the engine settings [50–52]. Fuels with high oxygen content are for instance methanol and ethanol. Moreover, both methanol and ethanol are liquid and of sufficient energy density for vehicle applications. I chose methanol for this work as it is the simplest fuel that can be produced from renewable sources and which is liquid at atmospheric conditions, as well as it has the largest oxygen content [22].

As with any other fuel there are advantages and disadvantages with using methanol in an engine application, especially in a direct injection, compression ignition, engine. A big advantage is that methanol can be produced in large scale from renewable sources which would increase its sustainability and help decrease the net CO_2 emissions for the transport sector[3]. The low lower heating value of methanol is, however, a disadvantage as it means that a larger (roughly two times as big) fuel tank needs to be installed on the vehicle in order to achieve a similar driving range as with gasoline. Furthermore, changes to the fuel injection systems are needed to prevent long term wear. None of these things were considered in this study, however, they have to be paid attention to if methanol is going to be used for commercial vehicles.

Methanol has a RON of 109 and as a result needs a significantly higher temperature to auto-ignite under engine conditions than for instance diesel and even the gasoline fuels that were mentioned above [96]. This can be regarded as both an issue or a possibility but if we regard it as a problem for the meantime, we can solve it by using a higher engine compression ratio. Figure 5.1 shows, on the left hand side, the in-cylinder pressure as a function of temperature for the compression stroke of the closed cycle. The final temperature and pressure of this compression depend on the inlet pressure and temperature as well as the compression ratio. As can be seen, a higher inlet temperature as well as a higher compression ratio leads to a higher final temperature. Additionally, this figure shows the ignition delay time (in ms) as a function of initial pressure and temperature, plotted as iso-contours. A shorter ignition delay time means that it will take a shorter time from the start of injection (SOI) to the start of combustion (SOC). The shortest ignition delay time is achieved for the highest initial temperature and highest compression ratio. Moreover, Figure 5.1 shows, on the right hand side, the ignition delay time for different λ. A higher λ leads to a

[2]It should be mentioned, despite not being very practical, that levels of EGR on the order of 70 % could actually cause soot and PM to decline [10].

[3]It is true that methanol can be produced from renewable sources at large scale, however, it should be noted that most of the current production is based on coal and natural gas.

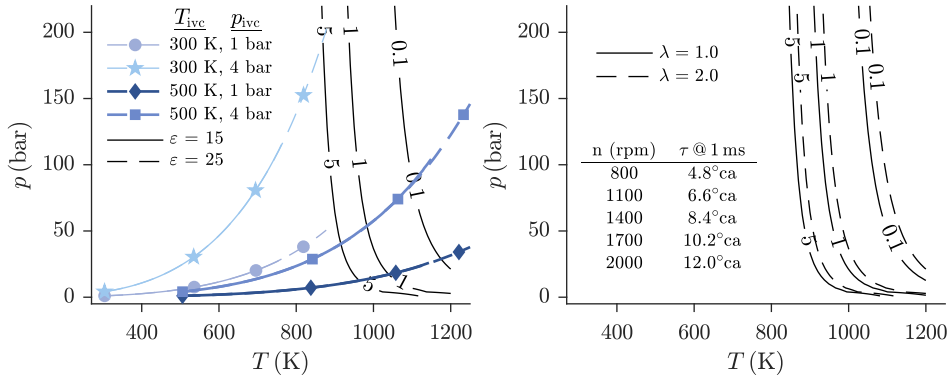

Figure 5.1: To the left: Pressure as a function of temperature for the compression stroke with different inlet conditions and two compression ratios (ε). Contours with constant ignition delay time (ms), for methanol, are superimposed. For these ignition delay times, the EGR was equal to 25 % and λ was equal to 2. To the right: Contours of ignition delay (τ) at 0.1 ms, 1 ms, and 5 ms as a function of initial temperature and initial pressure and two different λ.

longer ignition delay time. Additionally this figure shows the duration in crank angle degrees for various speeds, corresponding to an ignition delay time of 1 ms, which can be used when transferring this information to engine conditions.

The data in Figure 5.1 can be used in order to get an idea of the required inlet temperature for a certain compression ratio. This is presented in Figure 5.2 which shows the ignition delay time, as constant iso-contours, as a function of inlet temperature and compression ratio. For instance, if we take 1100 rpm as the engine speed, then for an ignition delay of 6.6°ca (which corresponds to 1 ms) the needed inlet temperature at a compression ratio of 15 is 420 K. In contrast, the required inlet temperature at a

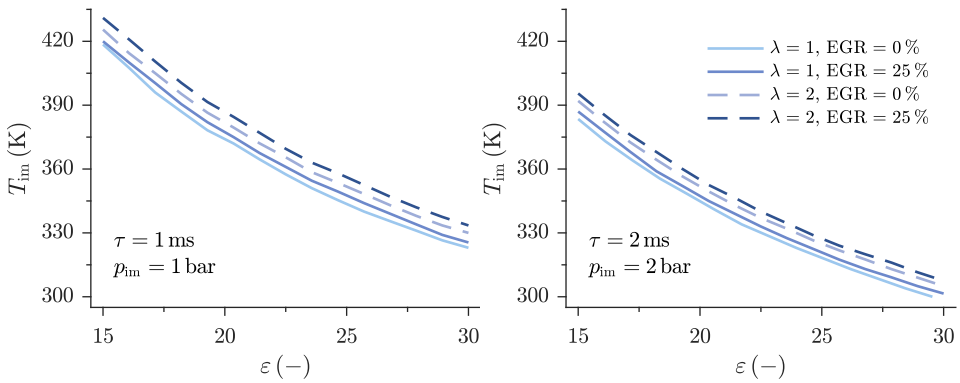

Figure 5.2: Constant ignition delay time (τ), for methanol, as a function of inlet temperature (T_{im}) and compression ratio (ε) at different inlet pressure (p_{im}), air-fuel ratio (λ) and EGR.

compression ratio of 30, and an ignition delay of 13.2°ca, is only 310 K. This example shows the significant effect of compression ratio on the required inlet temperature. The previous chapter showed that a low intake manifold temperature would be beneficial from both a gross and brake efficiency perspective. Additionally, the theoretical efficiency for heat release processes, which include both constant volume and constant pressure, can be found in, for instance, the book by Heywood [86, p. 172].

$$\begin{aligned} \eta &= 1 - \frac{1}{\varepsilon^{\gamma-1}} \left(\frac{\alpha\beta^{\gamma} - 1}{\alpha\gamma(\beta - 1) + \alpha - 1} \right) \\ \beta &= 1, \quad \text{(for constant volume heat release)} \\ \alpha &= 1, \quad \text{(for constant pressure heat release)} \end{aligned} \tag{5.1}$$

This equation, Equation (5.1), indicates that the efficiency increases with higher compression ratio (ε), which suggest that an infinitely high compression ratio would be preferable. However, a reason why this is not the case, and why the theoretical equation for efficiency is generally not applicable, is because it does not consider the in-cylinder heat transfer and lack of instantaneous combustion. Specifically, Equation (5.1) depicts that the efficiency approaches 100 % with higher compression ratio due to the increase in the ratio between the highest and lowest cycle temperatures. However, for constant inlet conditions (i.e p_{im}, T_{im}, and EGR, as well as the same rate of combustion) in-cylinder heat transfer would increase with compression ratio because of a higher global temperature. In addition, the maximum in-cylinder pressure and NO_x emissions would increase, and therefore require a retarded combustion phasing [97]. In conclusion, it is generally found that with higher compression ratios, the gross efficiency increases up to a certain point and then starts to decline. However, this point is not trivial to determine. For instance, a change of the inlet conditions and rate of combustion could be used to compensate for the higher heat transfer and maximum pressure. Furthermore, the optimal compression ratio will be different depending on the operating point considered. Thus, the chosen compression ratio will be the best compromise. Because the compression ratio is such a fundamental property of the engine, I chose to include two different cases in this study when considering methanol. As a benchmark, the standard compression ratio was used for the first case and for the second case, the compression ratio was optimized to achieve the highest brake efficiency.

5.1 Operating Points

Chapter 4 showed that the gas exchange performance of the engine varies with both engine speed and load. Moreover, the resulting combustion will be significantly af-

fected by the targeted engine load, and to a minor extent by the engine speed. Consequently, the choice of operating points is very important in order to be able to draw general conclusions from the results of a study of this kind. On the other hand, it is beneficial to keep the number of cases to a minimum to avoid additional simulation cost. Furthermore, the operating points should cover a relevant range of engine speed and load. With this in mind, the operating points for this study were taken from the 12 mode non-idle European stationary cycle (ESC) supplemental emission test (SET) points [98]. These operating points are shown in Figure 5.3, where the letters (A, B, C) indicate different engine speeds, see Equation (5.2) where n is the engine speed and n_{min} and n_{max} are the minimum and maximum engine speeds which were considered for this particular engine.

$$\begin{aligned} n_{\text{A}} &= n_{\text{min}} + 0.25\,(n_{\text{max}} - n_{\text{min}}) \\ n_{\text{B}} &= n_{\text{min}} + 0.50\,(n_{\text{max}} - n_{\text{min}}) \\ n_{\text{C}} &= n_{\text{min}} + 0.75\,(n_{\text{max}} - n_{\text{min}}) \\ n_{\text{min}} &= 800\,\text{rpm}, \quad n_{\text{max}} = 2000\,\text{rpm} \end{aligned} \tag{5.2}$$

The engine load in the European stationary cycle is taken as 25 %, 50 %, 75 %, and 100 %. These percentages can be converted into a mean effective pressure, namely fuelmep which is defined in Equation (5.3) where $\dot{m}_{\text{fuel}}$ is the mass of the fuel that is injected every cycle, Q_{LHV} is the lower heating value of the fuel and V_d is the engine displacement volume. The fuelmep corresponding to 100 % was set to 60 bar and was considered representative for the engine. This conversion can be seen on the left

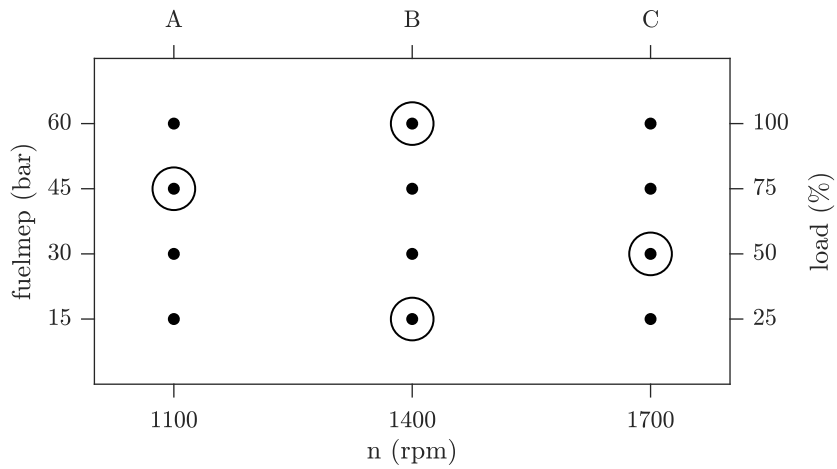

Figure 5.3: Operating points from the 12 mode non-idle European stationary cycle. The selected points for this study are encircled.

y-axis in Figure 5.3. The selected points for this study are encircled in Figure 5.3 and four in total, i.e. A75, B25, B100, and C50.

$$\text{fuelmep} = \frac{\dot{m}_{\text{fuel}} \cdot Q_{\text{LHV}}}{V_d} \tag{5.3}$$

The multi cylinder engine (MCE) model with the optimized turbocharger (TC2) from Table 4.4, which was presented in Section 3.1, was used for this study together with the stochastic reactor model (SRM) described in Section 3.3. The coupling described in Section 3.4 was used to perform full engine cycle simulations.

5.2 Optimization Strategy

In order to find the maximum brake efficiency for any of the cases described above at any of the four operating points, I considered the optimization problem defined in Equations (5.4) to (5.6).

$$\begin{gathered} \boldsymbol{u} = \left[\text{EGR}\ \ T_{\text{im}}\ \ p_{\text{im}}\ \ p_{\text{inj}}\ \ \theta^1_{\text{soi}}\ \ \theta^2_{\text{soi}}\ \ \theta^3_{\text{soi}}\ \ r^1_{\text{inj}}\ \ r^2_{\text{inj}}\ \ r^3_{\text{inj}}\right]^T \\ r^3_{\text{inj}} = 1 - (r^1_{\text{inj}} + r^2_{\text{inj}}) \end{gathered} \tag{5.4}$$

$$\begin{gathered} \boldsymbol{y} = \left[\eta_{\text{brake}}\ \ p_{\text{max}}\ \ p'_{\text{max}}\ \ T_{\text{dew}}\ \ s\text{NO}_{\text{x}}\ \ \lambda\right]^T \\ \boldsymbol{y} = f(\boldsymbol{u}) \end{gathered} \tag{5.5}$$

$$\begin{aligned} \underset{\boldsymbol{u}}{\text{maximize}} \quad & \eta_{\text{brake}} \\ \text{subject to} \quad & p_{\text{max}} < 225\,\text{bar}, \\ & p'_{\text{max}} < 15\,\text{bar/°ca}, \\ & s\text{NO}_{\text{x}} < 1.0\,\text{g/(kW h)}, \\ & T_{\text{im}} > T_{\text{dew}} + 20\,\text{K}, \\ & \lambda > 1.3\ \text{(gasoline)} \end{aligned} \tag{5.6}$$

In these equations, the search space, denoted $\boldsymbol{u}$, is a vector which holds the independent variables. $\boldsymbol{u}$ includes the EGR level (EGR), the intake manifold temperature (T_{im}), the intake manifold pressure (p_{im}), the fuel injection pressure (p_{inj}), three different start of injection timings (θ^1_{soi}, θ^2_{soi}, θ^3_{soi}), and the fraction of fuel that is injected

in each of the first two injection events (r^1_{inj}, r^2_{inj}). The fraction of fuel injected in the third injection event is easily realized to be one minus the sum of the rest. The cost function, denoted $\boldsymbol{y}$, is also a vector and includes the objective, i.e. the brake efficiency (η_{brake}), and the constraints. Constraints were set on maximum in-cylinder pressure (p_{max}), maximum in-cylinder pressure rise rate (p'_{max}), brake specific NO_x emissions (sNO_x), intake manifold temperature (T_{im}), and soot emissions. The intake temperature was limited to be 20 K over the dew point, analogous to Section 4.2.1, in order to prevent condensation in the intake manifold, EGR and charge air coolers as well as the compressor, see Equation (4.14).

Although methanol does not produce soot emissions, gasoline does. Therefore it was of interest to set a constraint on soot emissions in the optimizations. However, the chemical kinetic model that was used for the gasoline fuels did not include species and reactions to model soot emissions. Instead the soot emissions had to be limited implicitly by requiring a minimum lambda (λ). From multiple studies it has been shown that soot emissions, from combustion with similar gasoline fuels, decline with higher air-fuel ratio [59, 99]. In order to choose a suitable minimum lambda, the study in [100] was considered. There the authors, in their PPC recipe, propose to limit soot emissions below a filtered smoke number (FSN) of 2.0. They argue that soot emissions below this limit are easily removed with a particulate filter. Looking further into the results in Refs. [59, 99], it can be seen that FSN < 2.0 can likely be achieved by using $\lambda > 1.3$ and therefore this was chosen.

The optimal compression ratio in case 2 was found by including the compression ratio (ε) in $\boldsymbol{u}$. For the other cases, the optimizations could be performed for one operating point at a time. However, as the compression ratio can only take one value, the optimization of case 2 had to be done for all operating points simultaneously. In addition, the optimal compression ratio was set to be the one which maximized the average brake efficiency. However, because an engine does not normally operate an equal amount of time in every operating point, an arithmetic mean would not have been suitable. Instead the same weights ($\boldsymbol{w}$) which are used in the European stationary cycle were applied. That meant that the average brake efficiency was calculated as shown by Equation (5.7).

$$\eta_{\text{brake}} = \boldsymbol{w}^T \boldsymbol{\eta}_{\text{brake}} \quad \text{for} \quad \boldsymbol{w} = [0.17, 0.35, 0.31, 0.17]^T \tag{5.7}$$

The difference between local and global optima is important to consider when solving any optimization problem. A local optimum is the set of variables which maximizes (or minimizes) the cost function locally, whereas a global optimum is the set of independent variables which maximizes the cost function for the whole domain. The optimization problem in Equation (5.6) includes up to ten independent variables and

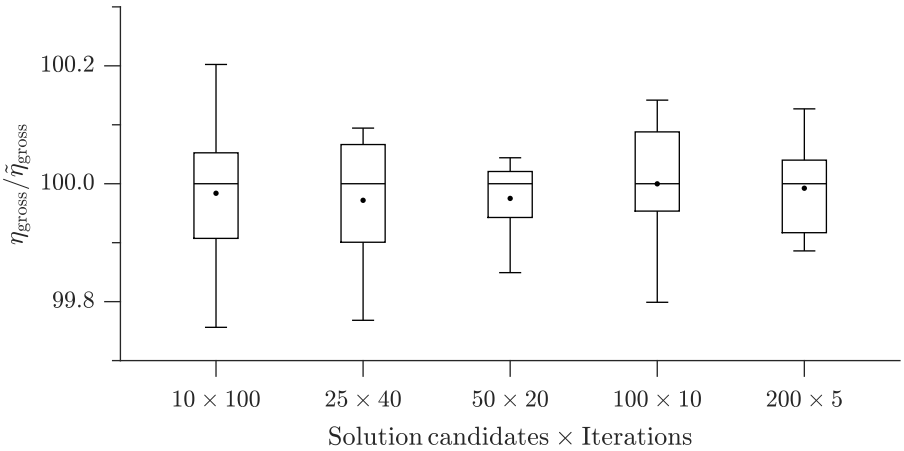

Figure 5.4: The influence of the combination of solution candidates and iterations on particle swarm optimization algorithm results taken as the normalized gross indicated efficiency, $\eta_{\text{gross}}/\tilde{\eta}_{\text{gross}}$. Where $\tilde{\eta}_{\text{gross}}$ denotes the efficiency median for each combination. For each box, the central mark is the mean and the central line is the median, the box extends vertically between the 25th and 75th percentiles, the whiskers extend to the most extreme data that are not considered outliers. No data was considered to be outliers.

as a result many so called "local optimization algorithms" would have a difficulty in finding the global optima. In contrast, the optimization algorithm that I chose for this study comes from a family of optimization algorithms called population-based stochastic techniques. It is called the particle swarm optimization (PSO) algorithm and uses a meta heuristic approach for finding the global optima when the optimization problem includes many independent variables[4] [101]. The advantage of this particular algorithm is that it can relatively quickly go through a large search space. However, there is no guarantee that the optimal solution is found. The implementation was done in Matlab©. The particle swarm optimization algorithm uses a set of solution candidates and moves them around the search space, $\boldsymbol{u}$, through iterations, using a simple relation, to find the global optimal solution of the cost function $\boldsymbol{y}$.

The number of solution candidates and the number of iterations are not easy to decide. The level of convergence will to some extent set the number of iterations, but it is difficult to define convergence with this type of algorithm. As a consequence, a fixed number of iterations is often used. For a given problem, it is common practice to increase the number of solution candidates as the number of independent variables increases, however, depending on the problem the optimal number of solution candidates varies[5]. To decide the optimal combination of solution candidates and iterations, I conducted a small study in which the PSO was applied on a sub problem and com-

[4]It should be acknowledged that there exist a number of other optimization algorithms from the same family, as well as other types of algorithms. No in-depth analysis into which algorithm would be best for this type of work was however performed.

[5]In this context optimal means the balance between convergence and simulation time.

pared different combinations. The objective of Equation (5.6) was changed to the gross indicated efficiency because that facilitated the use of only the SRM, without the added simulation time which running the SRM together with the multi cylinder engine model would have required. Furthermore, the optimizations were repeated 10 times per case. Figure 5.4 shows the results. The tested combinations of (solution candidates × iterations) were 10 × 100, 25 × 40, 50 × 20, 100 × 10, and 200 × 5. The difference between these cases is not large, however, the case with 50 solution candidates and 20 iterations shows the smallest variance and was therefore chosen for all further optimizations that will be presented.

5.3 Optimization Results

Table 5.2 shows the resulting values for the objective and constraints after the optimizations. Additionally, Table 5.3 shows the final values for the input variables from Equation (5.4). In these tables the four different cases are denoted as: M1 for methanol with $\varepsilon = 17.3$, M2 for methanol with $\varepsilon = 21.6$, G1 for gasoline with RON $= 76$, and G2 for gasoline with RON $= 97$. First, we can observe that the constraints were met for all the operating points and cases. The specific values of the engine settings, i.e. the independent variables, which the optimizer found deserve some discussion. First of all it can be noted that the optimal compression ratio for methanol, case 2, was 21.6 which is significantly higher than the standard compression ratio of 17.3.

By choosing a higher compression ratio it could be assumed that the required intake manifold temperature (T_{im}) would be reduced as discussed earlier in this chapter. This was in fact the case which can be seen in Figure 5.5 which shows the intake manifold temperature for all operating points and cases. The gasoline with the lowest RON had the lowest T_{im}. The case with methanol and the standard compression ratio required

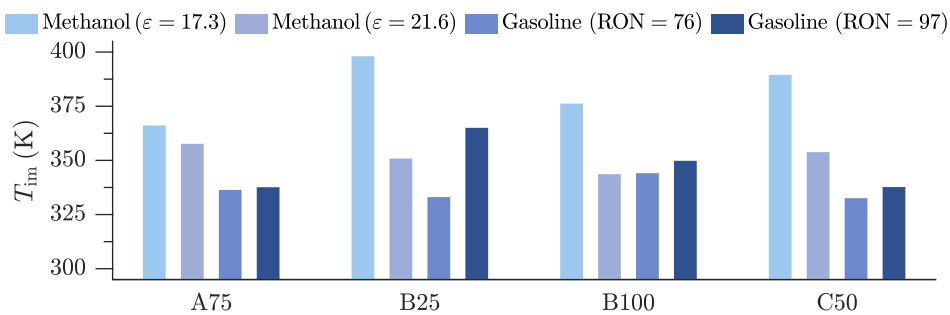

Figure 5.5: Intake manifold temperature for all operating points, comparing methanol (with $\varepsilon = 17.3$ and $\varepsilon = 21.6$) and gasoline (with RON $= 76$ and RON $= 97$).

Table 5.2: Final values of $\boldsymbol{y}$ from Equation (5.5) after optimization of objective (η_{brake}) and constraints from Equation (5.6), for all operating points (A75, B25, B100, C50) and all four cases i.e. methanol with $\varepsilon = 17.3$ (M1), methanol with $\varepsilon = 21.6$ (M2), gasoline with RON $= 76$ (G1) and gasoline with RON $= 97$ (G2).

	A75				B25				B100				C50			
	M1	M2	G1	G2	M1	M2	G1	G2	M1	M2	G1	G2	M1	M2	G1	G2
η_{brake} (%)	47.5	48.2	45.4	45.5	40.7	43.1	39.4	39.1	44.5	45.0	41.6	42.1	45.2	47.1	42.0	42.3
p_{max} (bar)	224	217	225	219	115	135	107	118	225	225	224	225	192	215	160	169
p'_{max} (bar/°ca)	13.7	10.4	13.4	12.4	7.5	14.0	15.0	14.7	7.7	7.0	6.5	6.9	13.8	13.8	14.0	15.0
sNO_x (g/(kW h))	0.87	0.78	0.89	0.89	0.02	0.02	0.79	0.74	0.30	0.32	0.93	0.89	0.66	1.00	0.78	0.96
$T_{\text{im}} - T_{\text{dew}}$ (K)	53	37	20	20	95	65	28	56	56	20	24	28	135	81	20	25
λ (-)	1.66	1.26	1.30	1.34	2.29	2.56	1.49	1.72	1.45	1.15	1.39	1.33	2.10	1.97	1.41	1.53

Table 5.3: Final values of $\boldsymbol{u}$ from Equation (5.5) after optimization of objective (η_{brake}) and constraints from Equation (5.6), for all operating points (A75, B25, B100, C50) and all four cases i.e. methanol with $\varepsilon = 17.3$ (M1), methanol with $\varepsilon = 21.6$ (M2), gasoline with RON $= 76$ (G1) and gasoline with RON $= 97$ (G2).

	A75				B25				B100				C50			
	M1	M2	G1	G2	M1	M2	G1	G2	M1	M2	G1	G2	M1	M2	G1	G2
ε (-)	17.3	21.6	17.3	17.3	17.3	21.6	17.3	17.3	17.3	21.6	17.3	17.3	17.3	21.6	17.3	17.3
EGR (%)	15	22	31	31	22	10	38	41	16	21	25	27	0	0	31	31
T_{im} (K)	366	358	336	338	398	351	333	365	376	344	344	350	389	354	333	338
p_{im} (bar)	3.13	2.55	2.85	2.93	1.70	1.48	1.21	1.57	3.85	3.06	3.86	3.82	2.40	2.07	2.08	2.28
p_{inj} (bar)	1110	1170	1840	2180	1620	1720	1920	1600	870	490	1780	2110	1660	1330	2140	2470
θ^1_{soi} (°ca aTDC)	-48	-55	-34	-34	-70	-53	-47	-37	-64	-66	-40	-44	-65	-65	-11	-28
θ^2_{soi} (°ca aTDC)	-30	-29	-8	-4	-47	-49	-26	-17	-	-	-6	-5	-42	-42	-	-2
θ^3_{soi} (°ca aTDC)	-23	-13	-	-	-	-3	-1	4	-	-	-	-	-16	-15	-	-
r^1_{inj} (–)	0.51	0.61	0.02	0.14	0.26	0.14	0.57	0.80	1.00	1.00	0.03	0.05	0.90	0.63	1.00	0.41
r^2_{inj} (–)	0.49	0.22	0.98	0.86	0.74	0.81	0.18	0.08	0.00	0.00	0.97	0.95	0.02	0.27	0.00	0.59
r^3_{inj} (–)	0.00	0.18	0.00	0.00	0.00	0.05	0.25	0.12	0.00	0.00	0.00	0.00	0.08	0.11	0.00	0.00

the highest T_{im} which varied between 365 K to 400 K depending on the operating point. The resulting T_{im} for the gasoline with the higher RON and the methanol case with higher compression ratio were in between these two cases.

Provided that the intake manifold temperature is sufficiently above the dew point, and that the most favorable combustion can be achieved, the optimal intake manifold temperature is likely to be as low as possible. In contrast, the intake manifold pressure (p_{im}) has a larger effect on the optimization results. Together with the fuel injection parameters, the intake manifold pressure determines the gross indicated efficiency that can be obtained. Furthermore, as was shown in the previous chapter, p_{im} has the largest influence on the gas exchange efficiency (cf. Section 4.2.2). At the same time the constraints on NO_x, λ, and p_{max} need to be fulfilled, i.e. a sufficient amount of dilution is required. Figure 5.6 shows the resulting p_{im} for all cases and operating points. For the two cases with methanol, the p_{im} was lower with the higher compression ratio. The reason is that, for the same level of λ and EGR, a lower intake manifold pressure is needed for the case with higher compression ratio. This is because the same mass flow can be obtained due to a lower intake manifold temperature. Moreover, this is indeed preferable in order to meet the constraint on p_{max} because the resulting p_{max} will be higher for a higher compression ratio (provided that the same combustion phasing is obtained). Moving on to the two cases with gasoline fuels there is not a very large difference in p_{im}, other than for the B25 operating point where the gasoline with the higher RON shows a higher p_{im}.

As was discussed earlier, EGR is very effective when it comes to reducing NO_x emissions. Thus, it is intuitive to think that the optimization algorithm would tend to increase the EGR until the NO_x emission are within the constraint of 1.0 g/(kW h) and only further if it would mean an increase in brake efficiency. However, more analysis is needed in order to answer this for all cases and operating points, i.e. was EGR used to increase brake efficiency or only as a mean to meet the NO_x constraint. Meanwhile, the level of EGR is presented in Figure 5.7 for all cases and operating

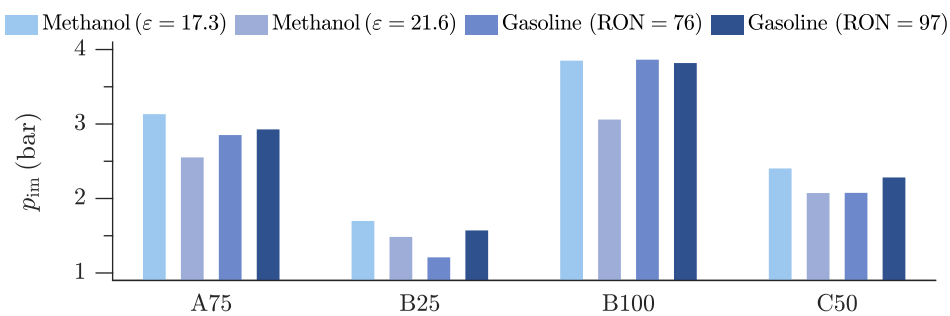

Figure 5.6: Intake manifold pressure for all operating points, comparing methanol (with $\varepsilon = 17.3$ and $\varepsilon = 21.6$) and gasoline (with RON = 76 and RON = 97).

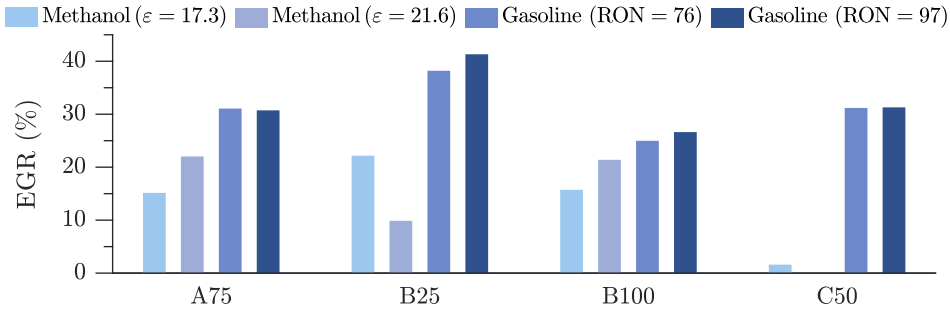

Figure 5.7: EGR for all operating points, comparing methanol (with $\varepsilon = 17.3$ and $\varepsilon = 21.6$) and gasoline (with RON = 76 and RON = 97).

points. It is easily noticed that the amount of EGR for both the cases with gasoline fuels are at a higher level than for the cases with methanol. In fact, for the operating point with the highest engine speed (C50), no EGR is needed with methanol.

With less EGR for the cases with methanol, it is natural that the λ would be higher. This was also the result as shown in Figure 5.8, for all operating points, except for the case with higher compression ratio at the points with higher load: A75 and B100. Moreover, this means that the ratio of specific heats (γ) would generally be higher for these cases and at the same time yield enough dilution to reach a low global in-cylinder temperature in order to reduce heat transfer. The reason why λ is lower with the higher compression ratio is simply because of the constraint on maximum in-cylinder pressure.

Having presented the results for these parameters (i.e. T_{im}, p_{im}, EGR, λ), it is logical to analyze the gas exchange efficiency. It is presented in Figure 5.9 where it can be seen that the highest gas exchange efficiency was obtained for the case with methanol and the highest compression ratio. The reason why this case has the highest gas exchange efficiency is because of a combination of low T_{im} and low degree of dilution which

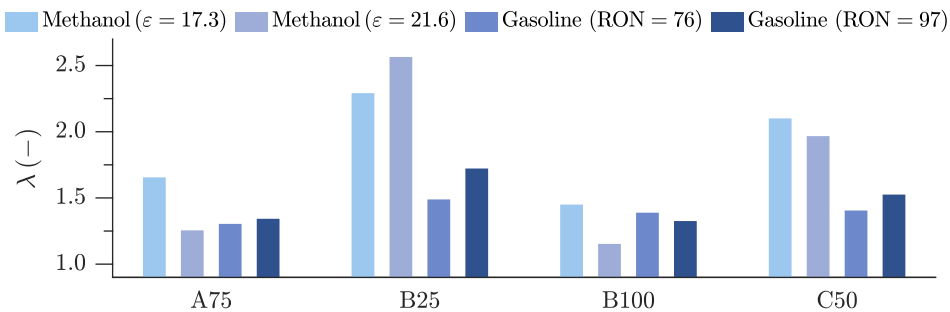

Figure 5.8: λ for all operating points, comparing methanol (with $\varepsilon = 17.3$ and $\varepsilon = 21.6$) and gasoline (with RON = 76 and RON = 97).

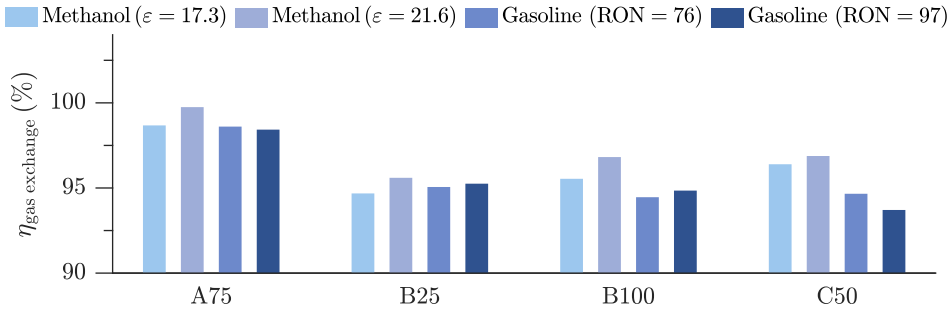

Figure 5.9: Brake efficiency for all operating points, comparing methanol (with $\varepsilon = 17.3$ and $\varepsilon = 21.6$) and gasoline (with RON = 76 and RON = 97).

results in a lower pressure ratio for the compressor. In contrast, the cases with gasoline required a significant amount of EGR. The case with methanol and low compression ratio did not require more EGR, however, as the required T_{im} and p_{im} were higher, the resulting gas exchange efficiency is lower.

Figure 5.10 shows the optimized engine brake efficiency. The maximum brake efficiency is obtained for the A75 operating point for all cases. Furthermore, the arithmetic mean brake efficiency is 44.5 %, 45.9 %, 42.1 %, and 42.2 % for the four cases respectively. Thus the case with methanol and high compression ratio generated the highest brake efficiency. Interestingly, there is not a significant difference between the gasoline fuels, despite a fairly large difference in RON value. The difference in brake efficiency is larger between the cases with methanol and the gasoline fuels, than what can be explained by the difference in gas exchange efficiency. Moreover, the friction losses were comparable between the cases (although obviously varying depending on operating point). Consequently, there must be a difference in the gross indicated efficiency. This is indeed true, which can be seen in Figure 5.11. The average gross indicated efficiency was 52.0 %, 53.0 %, 49.7 %, and 49.9 %. Additionally, the high-

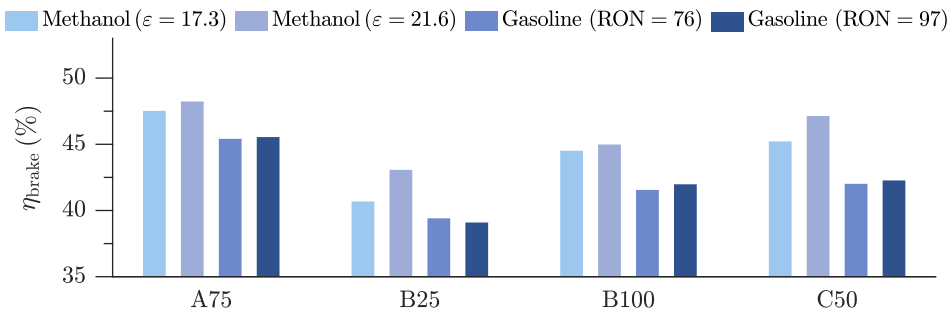

Figure 5.10: Brake efficiency for all operating points, comparing methanol (with $\varepsilon = 17.3$ and $\varepsilon = 21.6$) and gasoline (with RON = 76 and RON = 97).

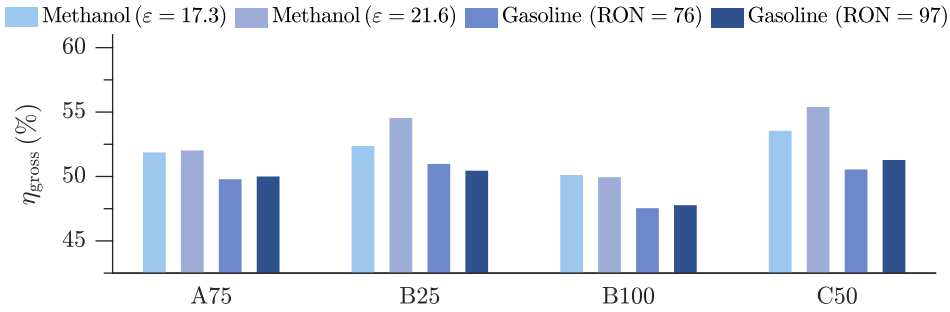

Figure 5.11: Gross efficiency for all operating points, comparing methanol (with $\varepsilon = 17.3$ and $\varepsilon = 21.6$) and gasoline (with RON = 76 and RON = 97).

est gross indicated efficiency was 55.4 % and obtained for the case with methanol and high compression ratio. This value seems very high, however, a gross indicated efficiency of 52.8 % was measured for an operating point with lower engine speed, and without any optimization [53]. Consistent with the obtained brake efficiencies, the difference in gross indicated efficiency is small between the two cases with gasoline. In contrast, the difference between the two cases with methanol is larger. Especially, for the operating points with lower engine load i.e. B25 and C50. Here, the advantage of using a higher compression ratio is significant. At the operating points with higher engine load, the difference is smaller and in fact for the B100 operating point, the gross indicated efficiency is higher for the case with lower compression ratio. The explanation can be found in that the constraint on p_{max}, leads to a lower p_{im} (rather than a further retarded combustion phasing), and hence a lower λ, which results in a lower ratio of specific heats for the higher compression ratio case.

The chemically bound energy in the fuel which does not become gross indicated work, i.e. $100\,\% - \eta_{\text{gross}}$, can be split into three separate categories. First, there will be a part of the fuel that will not combust completely, i.e. be emitted to the exhaust. This

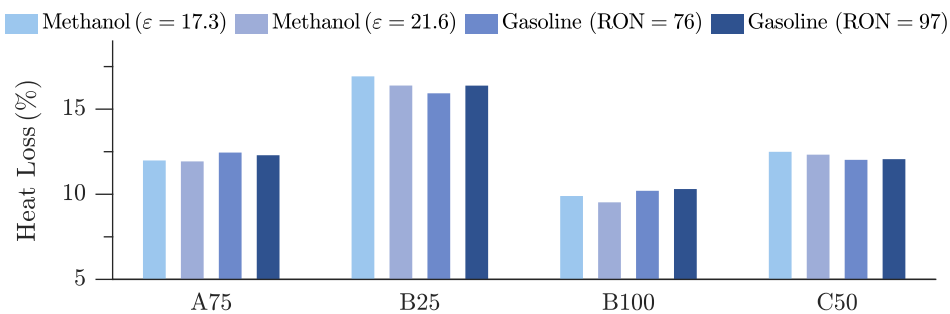

Figure 5.12: In-cylinder heat transfer loss for all operating points, comparing methanol (with $\varepsilon = 17.3$ and $\varepsilon = 21.6$) and gasoline (with RON = 76 and RON = 97).

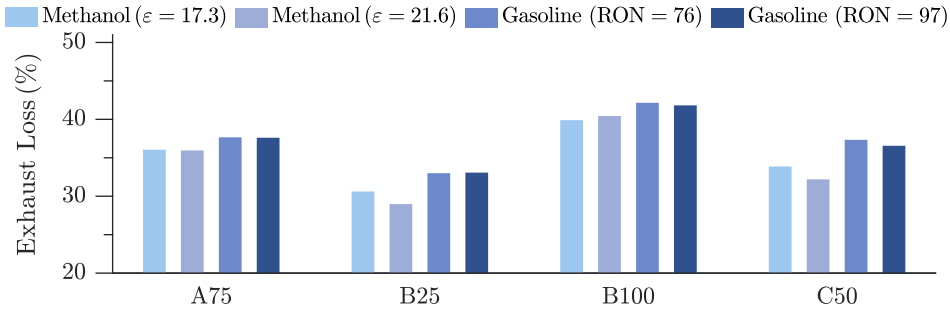

Figure 5.13: Exhaust loss for all operating points, comparing methanol (with $\varepsilon = 17.3$ and $\varepsilon = 21.6$) and gasoline (with RON = 76 and RON = 97).

is what is commonly called the combustion loss and will be on the order of 0 % to 2 % for the type of combustion considered here. In fact, for the cases and operating points simulated here, the combustion loss was very small (on the order of 0.2 %) and overall equivalent, comparing case to case, and thus will not be discussed further. The second and third categories are in-cylinder heat transfer loss and exhaust loss. The in-cylinder heat transfer loss is the heat lost to the cylinder walls during the closed cycle. This loss, as a percentage of fuel energy, is presented in Figure 5.12 for all cases and operating points. Despite accounting for a large part of the total losses, the difference comparing the cases in heat loss is small and cannot explain the whole difference in gross indicated efficiency. Furthermore there is no trend, comparing the four cases, as there was in for instance the gross indicated or brake efficiency. To explain this and the overall difference in gross efficiency we need to look at the last category of in-cylinder losses, namely the exhaust loss.

The exhaust loss includes the energy which was not used to produce work or transferred as heat to the cylinder walls, but instead exits the cylinder into the exhaust manifold[6]. The percentage of fuel energy that this loss attributed to, for the cases and operating points simulated here, is presented in Figure 5.13. The exhaust loss is higher for the cases with gasoline compared to the cases with methanol. Furthermore, by comparing Figure 5.11, which showed the gross indicated efficiency, to Figure 5.13, we can see that they show the same trend. Thus, most of the difference in gross indicated efficiency can be explained by the difference in exhaust loss. The exhaust loss is related to the amount of work that is needed to compress the gas during the compression stroke and how much energy that is available during the expansion stroke. The work needed for the compression stroke for an isentropic thermodynamic process is $w = c_v(T_1 - T_2)$, where w is the work, c_v is the specific heat capacity at constant volume, T_1 is the temperature at the start of compression and T_2 is the temperature

[6]From the perspective of the cylinder this energy is a loss, but it should be noted that the whole of this energy is not completely wasted, as part of it is used to drive the turbine.

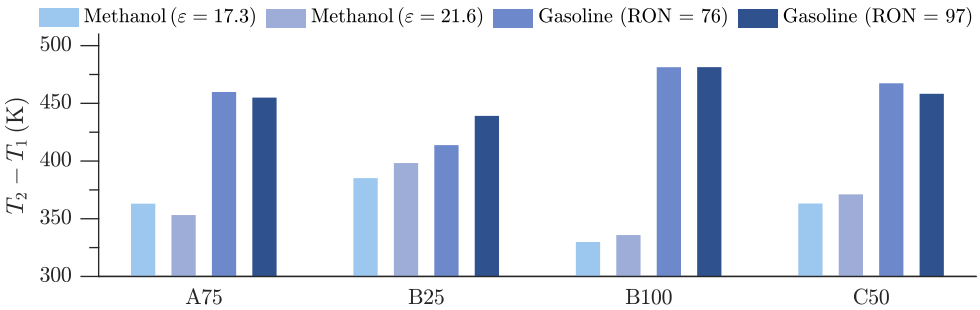

Figure 5.14: The difference in temperature between the end and start of the compression stroke for all operating points, comparing methanol (with $\varepsilon = 17.3$ and $\varepsilon = 21.6$) and gasoline (with RON $= 76$ and RON $= 97$).

at the end of the compression [86, p. 169]. Thus, for a fixed inlet temperature, the required work will reduce with a lower T_2 or a lower c_v. That means that if there are ways to reduce T_2 or c_v, the compression work can also be reduced. The c_v can be reduced by increasing the amount of air in relation to EGR, and external cooling can be applied to reduce T_2. For the latter, the most obvious means is the fuel injection itself[7]. The reason is that when the fuel is injected it has a lower temperature than the gas inside the cylinder and as a result, the in-cylinder temperature decreases. How much this reduction will amount to depends on the heat of vaporization of the fuel. For methanol, the heat of vaporization is 1104 kJ/kg, while it is only around 345 kJ/kg for the gasoline fuels considered here. In addition, twice the mass of fuel is injected in the case of methanol. As a result, the theoretical reduction in compression work from cooling by fuel injection is significantly greater with methanol. The difference between the average global temperature at start of compression and end of compression ($T_2 - T_1$) can be used to quantify the effect of cooling from fuel injection. Figure 5.14 shows this difference for all cases and all operating points. It is clear that the temperature increase, due to compression, is significantly lower for the methanol cases which suggest that also the compression work is in fact lower.

Although it is beneficial if the compression work can be reduced, it will be inconsequential if the work produced during the expansion is not maintained. The expansion work in itself can be increased with a higher average ratio of specific heats. The average ratio of specific heats will be largely influenced by the inlet conditions, that is the relative amount of air and EGR and the intake manifold temperature and pressure. The average ratio of specific heats for the closed part of the cycle is shown in Figure 5.15. For the case with methanol and high compression ratio we can observe the following.

[7]It should be observed that the in-cylinder temperature reduces during the compression stroke due to heat transfer to the cylinder walls. This reduction depends on the actual in-cylinder temperature and hence T_1. However, for the cases considered here the difference is comparably small and therefore neglected.

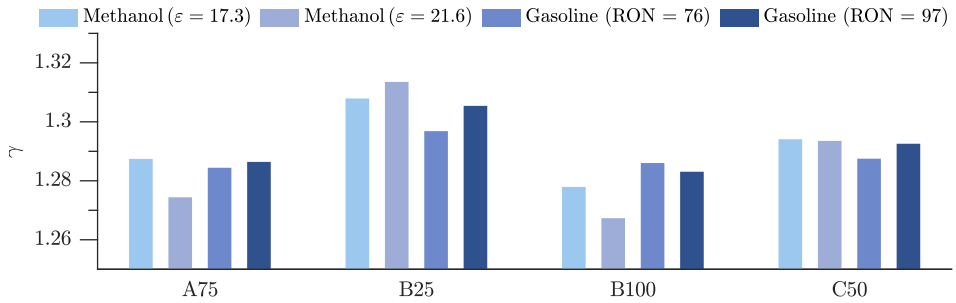

Figure 5.15: The average ratio of specific heats (γ) during the closed part of the cycle for all operating points, comparing methanol (with $\varepsilon = 17.3$ and $\varepsilon = 21.6$) and gasoline (with RON $= 76$ and RON $= 97$).

For operating point B25, the combination of low intake temperature and EGR level, but a high λ, yields a high γ. In contrast, a low γ is obtained in the high load operating point because the high compression ratio led to a low intake manifold pressure and hence a low λ.

The expansion work is furthermore influenced by the rate of heat release, because a short combustion duration, and a combustion phasing close to top dead center (TDC), will lead to a longer effective expansion duration. Figures 5.16 to 5.19 show the rate of heat release and corresponding in-cylinder pressure for all operating points and cases. It can be noted that the rate of heat release profiles for the two gasoline fuels are similar and that the same is true when comparing the two different cases with methanol. In contrast there is a large difference comparing methanol to gasoline. This is further exemplified by calculating the timings (θ_x), in crank angle degree, for the start of combustion (θ_{10}), combustion phasing (θ_{50}), and end of combustion (θ_{90}). The definition of these timings are shown in Equation (5.8). The x is the fraction of the fuel energy that has been converted into heat. Solving for θ_x, then gives these timings.

$$x = \frac{\int_{\text{ivc}}^{\theta_x} \frac{\mathrm{d}Q}{\mathrm{d}\theta}\,\mathrm{d}\theta}{\int_{\text{ivc}}^{\text{evo}} \frac{\mathrm{d}Q}{\mathrm{d}\theta}\,\mathrm{d}\theta} \cdot 100 \tag{5.8}$$

The calculated combustion timings, θ_{10}, θ_{50}, and θ_{90} are presented in Table 5.4. First, we can note that the start of combustion occurs overall a couple of crank angle degrees later for the cases with methanol, compared to the cases with gasoline. This is also true for the combustion phasing, except for the highest engine load (B100) where the θ_{50} for the methanol cases is located earlier than for the gasoline cases. From a theoretical point of view, a start of combustion as close to TDC (and a short combustion duration) as possible is beneficial because it leads to a longer effective expansion,

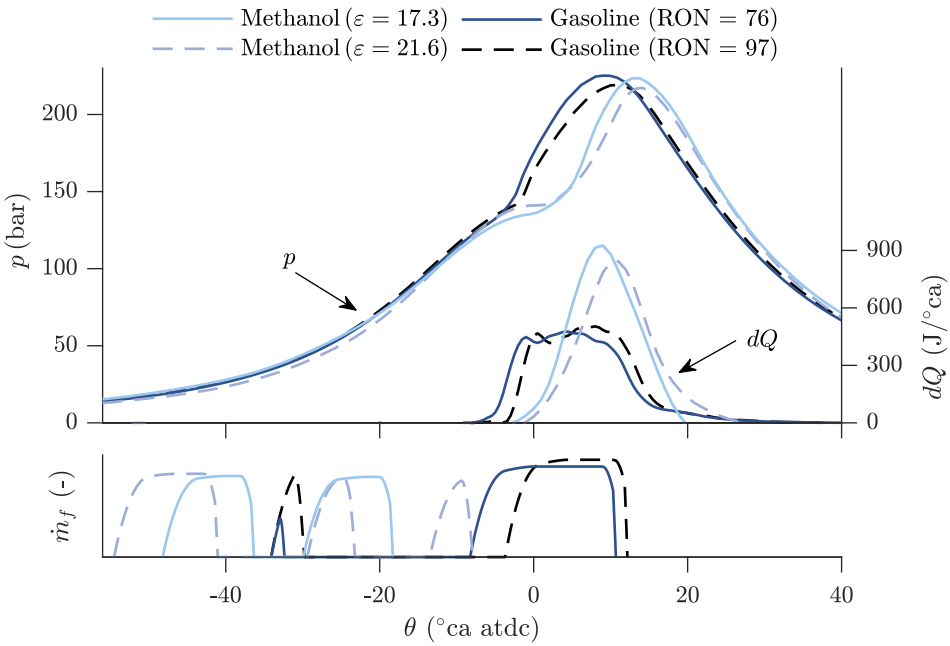

Figure 5.16: In-cylinder pressure (p) and rate of heat release ($\mathrm{d}Q$) for the A75 operating point.

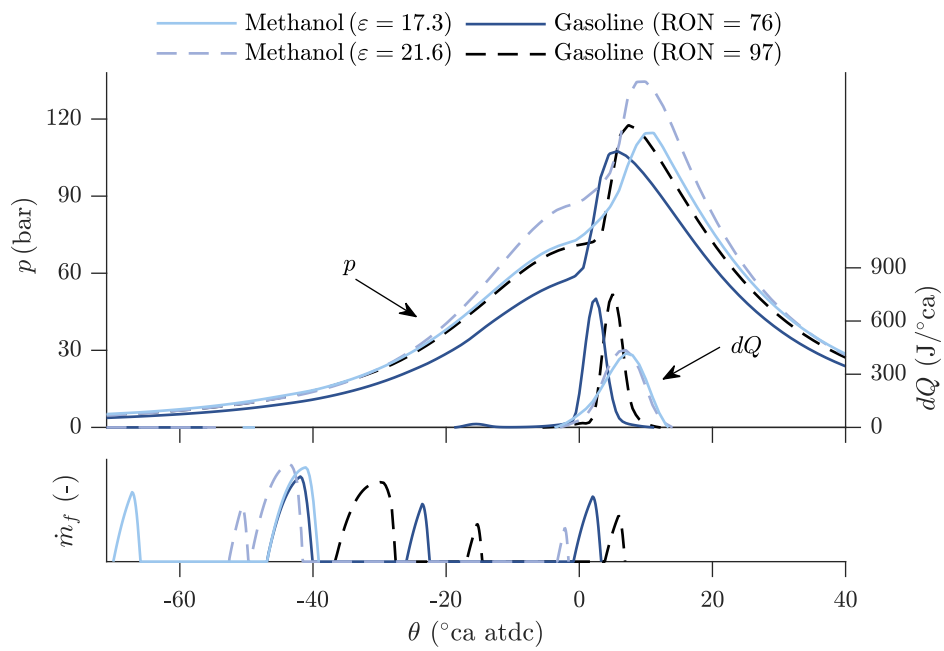

Figure 5.17: In-cylinder pressure (p) and rate of heat release ($\mathrm{d}Q$) for the B25 operating point.

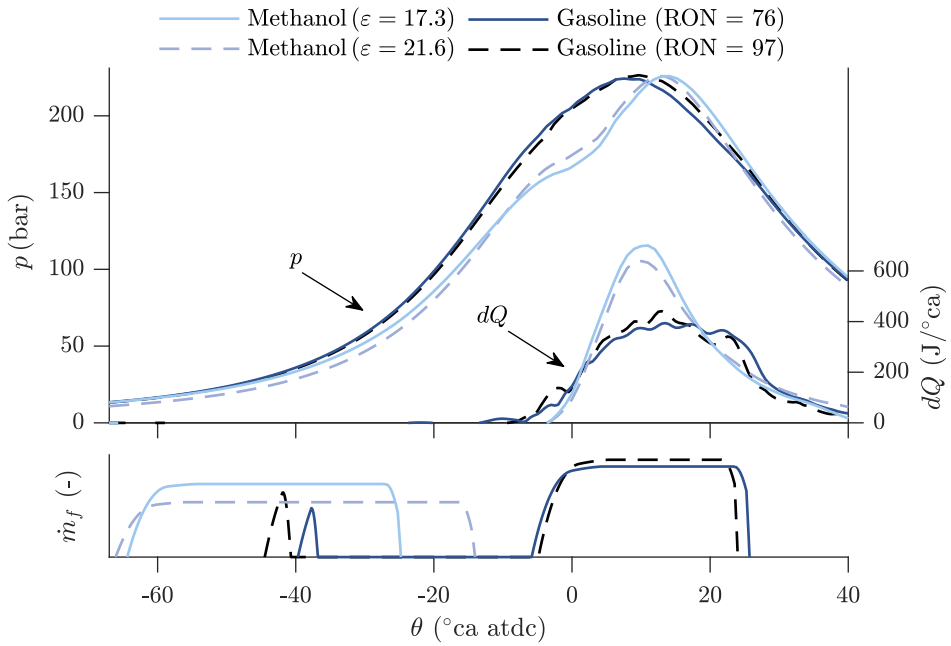

Figure 5.18: In-cylinder pressure (p) and rate of heat release ($\mathrm{d}Q$) for the B100 operating point.

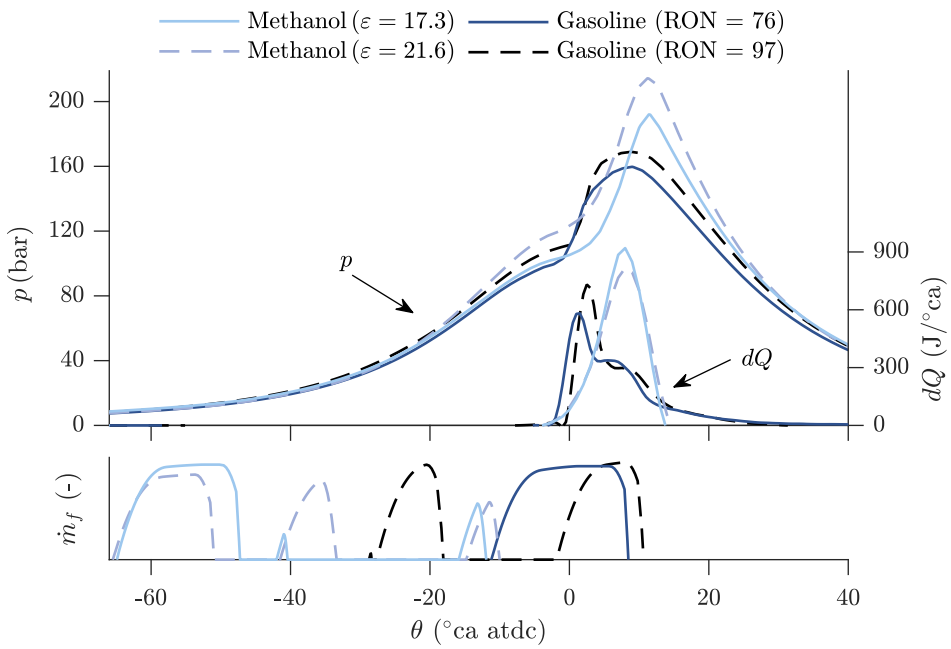

Figure 5.19: In-cylinder pressure (p) and rate of heat release ($\mathrm{d}Q$) for the C50 operating point.

Table 5.4: Combustion timings (°ca aTDC) from Equation (5.8) for all operating points (A75, B25, B100, C50) and all four cases i.e. methanol with $\varepsilon = 17.3$ (M1), methanol with $\varepsilon = 21.6$ (M2), gasoline with RON $= 76$ (G1), and gasoline with RON $= 97$ (G2).

	A75				B25				B100				C50			
	M1	M2	G1	G2	M1	M2	G1	G2	M1	M2	G1	G2	M1	M2	G1	G2
θ_{10}	5.0	5.8	-1.7	0.1	2.8	3.5	0.6	3.8	5.1	5.5	2.8	2.5	3.9	3.8	0.6	2.0
θ_{50}	9.8	11.8	6.1	7.6	7.0	7.1	2.8	5.5	13.4	14.7	16.0	14.5	8.3	8.3	6.0	6.0
θ_{90}	15.7	20.0	19.1	18.8	10.8	10.9	6.0	8.5	28.8	33.5	32.9	31.5	11.0	11.8	20.9	18.0
$\theta_{90} - \theta_{10}$	10.7	14.2	20.8	18.6	7.9	7.4	5.5	4.8	23.8	28.0	30.1	29.0	7.1	7.9	20.3	16.0

i.e. a longer time for the in-cylinder gas to assert force on the piston. However, it is complicated by the fact that the in-cylinder volume has its smallest value just before TDC, and thus heat released at TDC will result in a more rapid and larger pressure and temperature increase. This furthermore means that the in-cylinder heat transfer, and NO_x emissions (which are very sensitive to the highest global and local temperature respectively) increase with an earlier start of combustion. As a result, these effects lead to a compromise between on the one hand acquiring a long time for expansion, and on the other hand minimizing heat transfer and NO_x emissions. Table 5.4 also shows the combustion duration which is defined as $\theta_{90} - \theta_{10}$, that is the time between the end of combustion and the start of combustion. It is interesting to note that, for all operating points except the one with the lowest engine load (B25), the cases with gasoline have a longer combustion duration.

Taking all of this into account, it seems as if it was easier to obtain a better compromise between combustion duration, heat transfer, and NO_x emissions for the cases with methanol. Additionally, in the case of gasoline, it is likely that a longer combustion duration led to the need for an advanced combustion phasing and meant that a higher level of EGR was needed only in order to suppress the higher heat transfer and NO_x emissions. This was not needed with methanol because a shorter combustion duration could be obtained and thus the combustion phasing could be retarded without as much of a penalty in reduced expansion work. This is also likely the reason why there was only a minor difference in heat transfer loss, and why even though the gasoline cases required a lower T_{im} and p_{im}, they still resulted in a lower gas exchange efficiency than for the methanol case with low compression ratio. Table 5.5 shows the maximum global temperature ($T_{\text{max,global}}$), the maximum local temperature ($T_{\text{max,local}}$) and the brake specific NO_x emissions[8]. The above reasoning is further strengthened by noticing that even though more EGR was applied for the cases with gasoline, the earlier start of combustion resulted in a higher maximum local temperature, and thus

[8]The global temperature in this context is the temperature which would be obtained if the equation of state was applied. The local temperature is the temperature of every particle in the SRM, thus varying significantly inside the cylinder for this type of combustion.

Table 5.5: Brake specific NO_x emissions (g/(kW h)), maximum local in-cylinder temperature (K), and global in-cylinder temperature (K), for all operating points (A75, B25, B100, C50) and all four cases i.e. methanol with $\varepsilon = 17.3$ (M1), methanol with $\varepsilon = 21.6$ (M2), gasoline with RON = 76 (G1), and gasoline with RON = 97 (G2).

	A75				B25				B100				C50			
	M1	M2	G1	G2	M1	M2	G1	G2	M1	M2	G1	G2	M1	M2	G1	G2
sNO_x	0.87	0.78	0.89	0.89	0.02	0.02	0.79	0.74	0.30	0.32	0.93	0.89	0.66	1.00	0.78	0.96
T^{max}_{local}	2477	2546	2515	2505	2113	2147	2547	2551	2505	2425	2629	2572	2438	2447	2525	2556
T^{max}_{global}	2004	2056	1956	1941	1808	1798	1912	1804	1876	1886	1814	1878	2095	2133	1862	1861

higher NO_x emissions. But on the other hand, due to a high level of EGR, the global average temperature was on the same level or less in comparison to the cases with methanol.

So far, I have shown the rate of heat release, in-cylinder pressure traces and maximum in-cylinder temperatures for all the cases. The values and shapes of these parameters are of course very much affected by the inlet conditions. But perhaps even more so, by the rate of fuel injection, and particularly when the fuel is injected during the

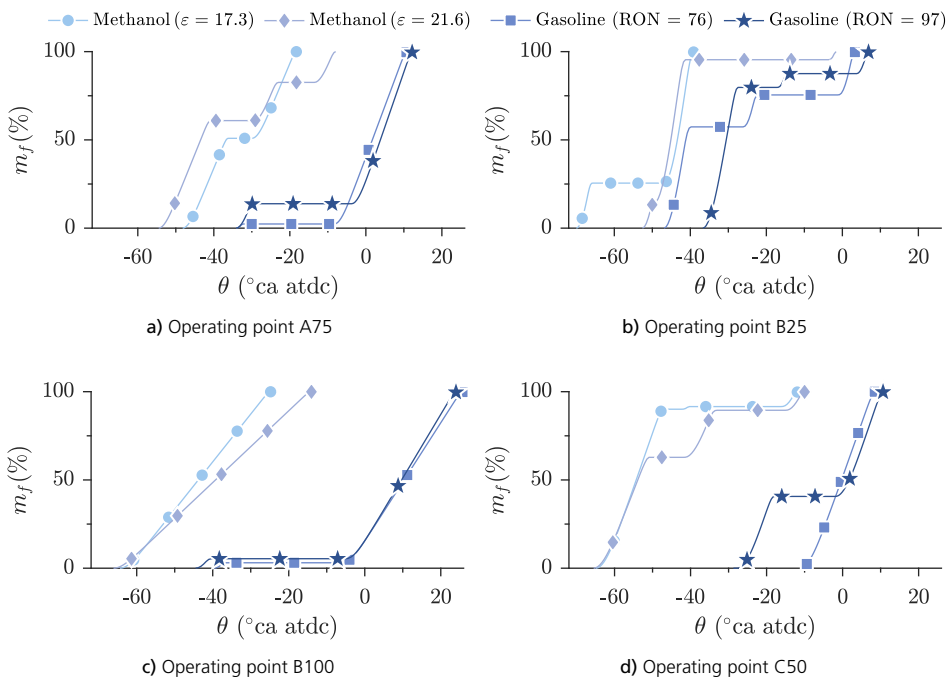

Figure 5.20: Accumulated mass of fuel as a function of crank angle degree for the engine and for all operating points, comparing methanol (with $\varepsilon = 17.3$ and $\varepsilon = 21.6$) and gasoline (with RON = 76 and RON = 97).

Table 5.6: End of injection (θ_{eoi}), start of combustion (θ_{10}) and the corresponding ignition dwell ($\theta_{10} - \theta_{\text{eoi}}$), all in °ca aTDC for all operating points (A75, B25, B100, C50) and all four cases i.e. methanol with $\varepsilon = 17.3$ (M1), methanol with $\varepsilon = 21.6$ (M2), gasoline with RON $= 76$ (G1), and gasoline with RON $= 97$ (G2).

	A75				B25				B100				C50			
	M1	M2	G1	G2	M1	M2	G1	G2	M1	M2	G1	G2	M1	M2	G1	G2
θ_{eoi}	-18.3	-7.9	10.7	12.2	-39.1	-1.6	3.3	6.9	-24.8	-14.0	25.7	24.0	-11.9	-10.0	8.5	10.6
θ_{10}	5.0	5.8	-1.7	0.1	2.8	3.5	0.6	3.8	5.1	5.5	2.8	2.5	3.9	3.8	0.6	2.0
θ_{eoi} - θ_{10}	23.3	13.7	-12.4	-12.0	42.0	5.1	-2.7	-3.1	29.9	19.5	-22.9	-21.5	15.8	13.8	-7.9	-8.6

compression stroke. This is visualized in Figure 5.20 which shows the accumulation of fuel (as it goes from 0 % to 100 % of injected fuel) as a function of crank angle degree, for all the cases and operating points. Moreover, the rate of fuel injection is shown in Figures 5.16 to 5.19. Evidently, there is a large difference between the injection strategy for the cases with methanol, compared to the cases with gasoline. Specifically, the injection of methanol is located earlier than the injection of gasoline for all operating points. The difference is quantified in Table 5.6 which shows the end of injection (θ_{eoi}) for the last injection pulse, start of combustion (θ_{10}) and the corresponding ignition dwell ($\theta_{10} - \theta_{\text{eoi}}$). Interestingly, there is a positive ignition dwell for the methanol cases in all operating points, whereas the cases with gasoline show a negative ignition dwell. The definition of PPC from Chapter 2 stated that there needs to be a positive ignition dwell. Thus for these simulations, we can conclude that only methanol satisfies the definition of PPC. Although neither of the gasoline fuels facilitated a positive ignition dwell, it should be noted that slightly more fuel could be injected before the start of combustion for the gasoline fuel, which had a higher research octane number, which agrees with the discussion from Chapter 2.

5.4 Limitations of the Approach

An attempt to explain the differences in fuel injection and heat release rates, will be presented in the subsequent chapter. Meanwhile, it should be noted that the current version of the stochastic reactor model did not include a model to account for fuel, which might be stuck in various crevice volumes. As a consequence, this part of the fuel will not be oxidized and hence could give rise to a substantial increase in combustion losses, and therefore yield a considerably lower brake efficiency. Although it is uncertain if this effect can be avoided completely, it can likely be somewhat circumvented by using an injector with a more narrow umbrella angle which could lead the fuel into the piston bowl and prevent it from hitting the cylinder wall [102, 103]. Moreover, on a PPC engine, the electronic control unit (ECU) is thought to be able to change the start of injection timings on a cycle-to-cycle basis. This is beneficial from a combustion stability perspective, however, by advancing the fuel injection, the start

of combustion might be less affected by the actual start of injection timing. Instead, it is likely that the start of combustion is more affected by the inlet conditions, such as the inlet temperature and oxygen concentration [39, 63]. Since it is more difficult to achieve as fast control of the inlet conditions, due to the slower dynamics, this can become a practical issue, especially during transient operation, and cause combustion instability.

In light of these issues it would be interesting to know whether the brake efficiency would be significantly reduced by retarding the fuel injection, or if just a slight change would result, and if it thus could be possible to achieve a high combustion stability and brake efficiency at the same time. However, it is difficult to quantify the benefit of early injections on the brake efficiency in the case of methanol, at least just by analyzing the results from the particle swarm optimizer. This is because, as any general optimization algorithm, the particle swarm optimizer will proceed in the direction which minimizes the cost function. Therefore, in order to quantify the effect of early injection timings on the brake efficiency, I constructed a sensitivity study in which I set constraints on the timing of the first injection (θ^1_{soi}). The standard compression ratio was used and because the same trend in injection timings was seen for all operating points, I chose to only use two of them namely A75 and B25. For each operating point, two different cases were run and compared to the original case were the particle swarm optimizer was allowed to set the start of injection without constraints. In the first case, the particle swarm optimizer was only allowed to set the first injection timing as early as –40°ca aTDC, as opposed to anytime during the compression stroke. In the second case, this limitation was made stricter by requiring that the first injection timing, be later than –25°ca aTDC. For clarity, the three resulting cases with their respective constraints are summarized in Equation (5.9).

$$\begin{aligned}
&\text{Case A:} \quad \theta^3_{\text{soi}} > \theta^2_{\text{soi}} > \theta^1_{\text{soi}} > -160°\text{ca aTDC (ivc)} \\
&\text{Case B:} \quad \theta^3_{\text{soi}} > \theta^2_{\text{soi}} > \theta^1_{\text{soi}} > -40°\text{ca aTDC} \\
&\text{Case C:} \quad \theta^3_{\text{soi}} > \theta^2_{\text{soi}} > \theta^1_{\text{soi}} > -25°\text{ca aTDC}
\end{aligned} \tag{5.9}$$

The resulting rate of heat release profiles, fuel injection rate, and in-cylinder pressure traces from this sensitivity study are presented in Figures 5.21 and 5.22, for the A75 and B25 operating points respectively. Furthermore, Table 5.7 shows some of the results which were used previously in this chapter. There is a perceptible difference going from case A to case C. However, for the operating point A75 the largest difference occurs between case B and case C, whereas only a small difference is seen between case A and case B. This stands in contrast to operating point B25, where a much larger difference can be seen going from case A to case B. However, this is not strange because the original θ^1_{soi} of case A for the operating point A75 was –48°ca aTDC, while

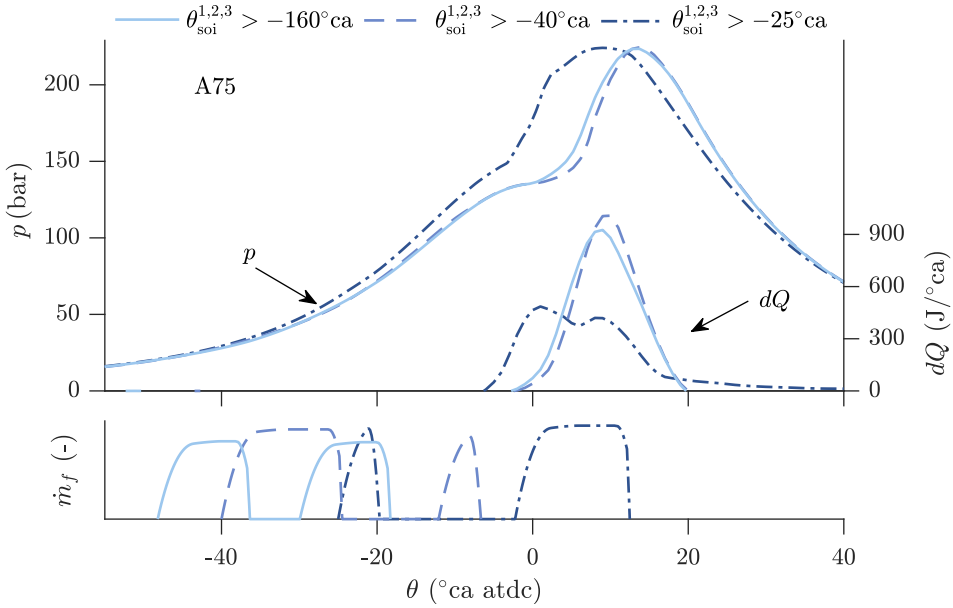

Figure 5.21: In-cylinder pressure (p) and rate of heat release ($\mathrm{d}Q$) for the operating point A75, comparing the three injection strategies defined in Equation (5.9). Methanol with the 17.3 compression ratio was used.

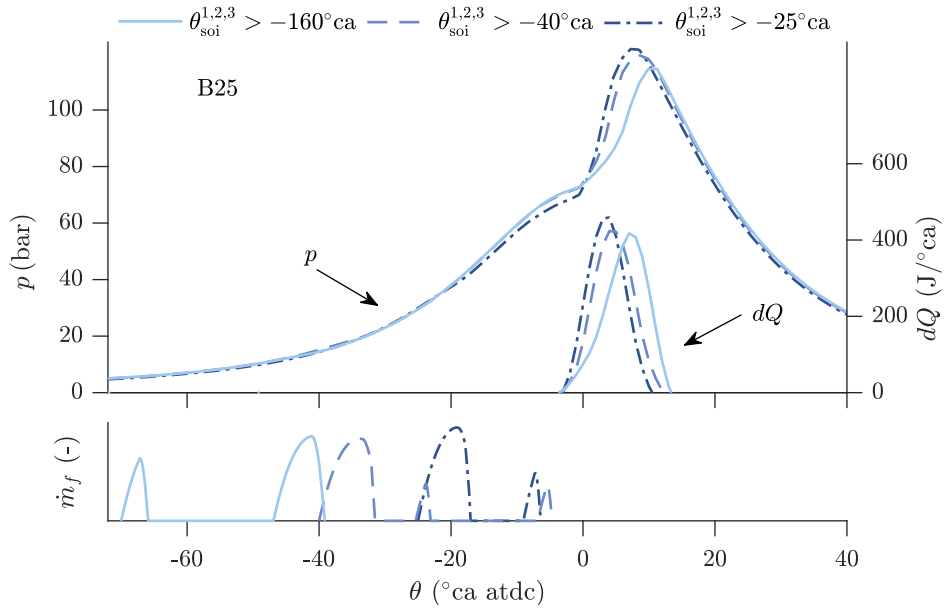

Figure 5.22: In-cylinder pressure (p) and rate of heat release ($\mathrm{d}Q$) for the operating point B25, comparing the three injection strategies defined in Equation (5.9). Methanol with the 17.3 compression ratio was used.

Table 5.7: Resulting input and output values from the optimization of operating point A75.

	Operating point	A75			B25		
	Case	A	B	C	A	B	C
Input ($\boldsymbol{u}$)	EGR %	14.9	14.5	22.2	22.2	22.8	22.0
	T_{im} (K)	366	362	356	398	393	387
	p_{im} (bar)	3.13	3.11	3.19	1.70	1.67	1.59
	p_{inj} (bar)	1110	1480	1720	1620	1530	1980
	θ^1_{soi} (°ca aTDC)	-48.2	-40.0	-25.0	-70.0	-40.0	-25.0
	θ^2_{soi} (°ca aTDC)	-30.0	-12.1	-2.3	-46.9	-25.4	-9.0
	θ^3_{soi} (°ca aTDC)	-	-	-	-	-6.9	-
	r^1_{inj}	0.51	0.81	0.20	0.26	0.84	0.88
	r^2_{inj}	0.49	0.19	0.80	0.74	0.08	0.12
	r^3_{inj}	0.00	0.00	0.00	0.00	0.08	0.00
Output ($\boldsymbol{y}$)	η_{brake} (%)	47.5	47.4	45.3	40.7	40.3	40.2
	p_{max} bar	224	225	225	115	119	122
	p'_{max} (bar/°ca)	13.7	15.0	15.0	7.5	10.1	11.0
	sNO_x (g/(kW h))	0.87	1.00	0.98	0.02	0.13	0.85
Key results	η_{gross} (%)	51.9	51.7	49.7	52.4	52.0	51.6
	θ_{10} (°ca aTDC)	5.0	5.9	0.0	2.8	2.0	1.0
	θ_{50} (°ca aTDC)	9.8	10.4	8.0	7.0	5.0	4.0
	θ_{90} (°ca aTDC)	15.7	15.8	27.3	10.8	9.2	7.8
	θ_{90} - θ_{10} (°ca aTDC)	10.7	9.9	27.3	7.9	7.2	6.8
	θ_{eoi}	-18.3	-6.6	12.5	-39.1	-4.7	-6.4
	θ_{eoi} - θ_{10}	23.3	12.5	-12.5	42.0	6.7	7.4
	$T_{\text{max, local}}$	2477	2501	2623	2113	2329	2572
	$T_{\text{max, global}}$	2004	2008	1779	1808	1811	1857
	Heat loss (%)	12.0	11.9	12.1	16.9	17.1	17.2
	Exhaust loss (%)	36.0	36.2	38.1	30.6	30.8	31.1
	λ	1.66	1.67	1.57	2.29	2.26	2.20

it was –70°ca aTDC for operating point B25. Moreover, it can be seen that case C led to rates of heat release, which look similar to the ones which were obtained for the gasoline fuels in Figures 5.16 and 5.17. In fact, for many of the parameters in Table 5.7, the argumentation that was previously led for the differences between methanol and gasoline can be used to explain the differences between case A and case C. For instance, it can be seen that the operating point A75 experiences a significantly longer combustion duration and an earlier start of combustion with a fuel injection which is located close to TDC. Additionally, the gross and brake efficiencies decrease from case A to case C, even though the largest drop in brake efficiency can be seen for the

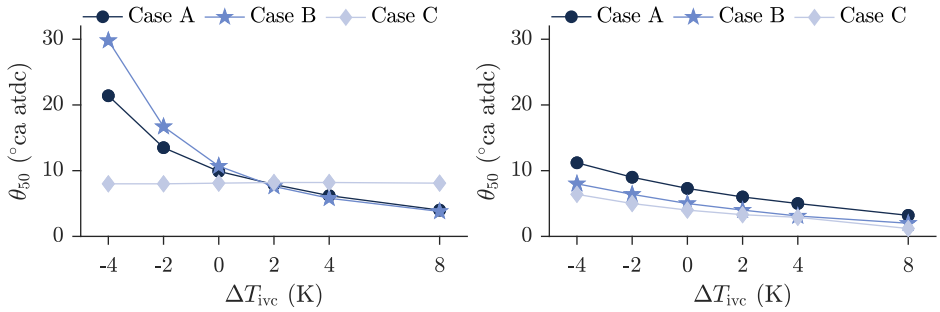

a) Operating point A75. **b)** Operating point B25.

Figure 5.23: Combustion phasing (θ_{50}) as a function of varying inlet valve closing temperature.

high load operating point A75. In fact, the brake efficiency for operating point A75 is comparable to the brake efficiency for the cases with gasoline fuels, i.e. 45.5 % and 45.6 %.

In conclusion, it seems to be worth-while to aim for early injection timings. However, as mentioned earlier, this type of injection strategy would typically increase the sensitivity of inlet conditions on the combustion, and hence on the brake efficiency. To investigate the magnitude of this sensitivity, the inlet valve closing temperature and the start of injection timing of the main injection, were varied from the baseline cases. Figures 5.23 to 5.26 show the variations in combustion phasing (θ_{50}) and maximum in-cylinder pressure (p_{max}). For the operating point with lower engine load, B25, the sensitivity of the start of injection timing is rather insignificant. The sensitivity of inlet temperature is slightly larger, but still relatively low, and thus facilitates an early injection timing strategy. In contrast, the difference in sensitivity, between the injection strategies, of the inlet temperature and start of injection timing, are substantially larger for the operating point A75. For cases A and B, the combustion phasing is advanced by approximately 15°ca for an increase in inlet temperature of 12 K. Furthermore, the

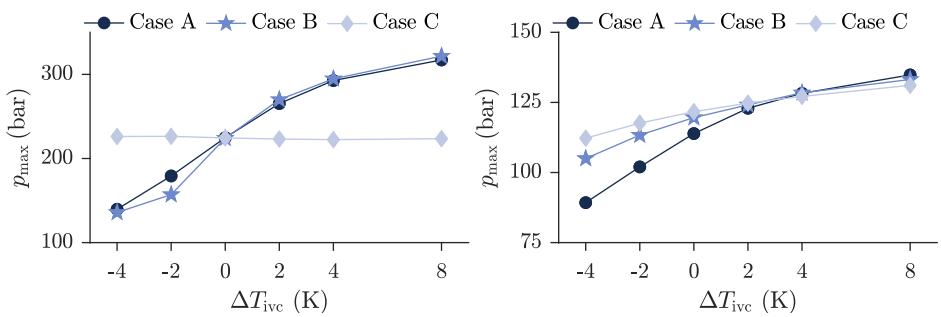

a) Operating point A75. **b)** Operating point B25.

Figure 5.24: Maximum cylinder pressure (p_{max}) as a function of varying inlet valve closing temperature.

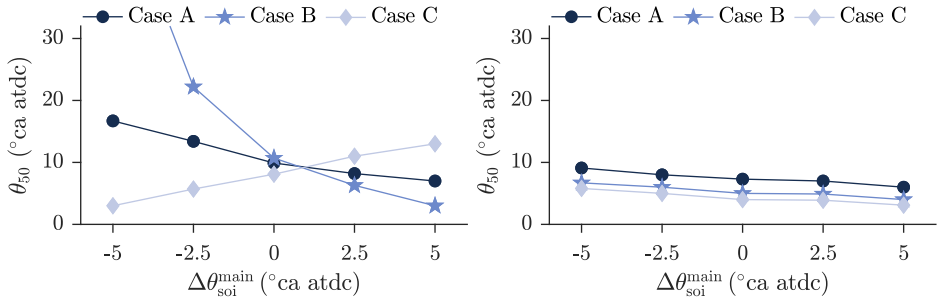

a) Operating point A75. **b)** Operating point B25.

Figure 5.25: Combustion phasing (θ_{50}) as a function of varying start of injection timing of the main injection.

maximum in-cylinder pressure varies, over 150 bar, for the same change in inlet temperature. Moreover, the maximum in-cylinder pressure exceeds 300 bar which would be catastrophic it were to happen in a real engine. On the other hand, for the injection strategy case C, the combustion phasing and the maximum in-cylinder pressure is insensitive to a variation in inlet temperature. This is unfortunate, as Table 5.7 showed that the potential gain in brake efficiency, was higher for this operating point, than for the B25 operating point.

Figures 5.25 and 5.26 reveal an interesting phenomenon. An advance of the start of injection timing, results in an advancement of the combustion phasing in case C, however, in case A and case B, the same advancement yields a retardation of the combustion phasing. The explanation for this interesting observation will be given in the subsequent chapter. Nevertheless, with these results we can conclude that an early injection strategy is likely feasible at lower engine loads. However, for it to work at high engine load, a very precise control of the inlet conditions is necessary.

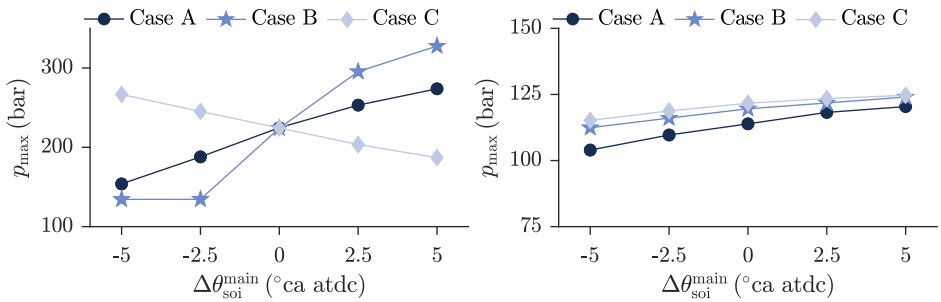

a) Operating point A75. **b)** Operating point B25.

Figure 5.26: Maximum cylinder pressure (p_{max}) as a function of varying start of injection timing of the main injection.

5.5 Influence of Optimization Constraints

The final results from a constrained optimization will change depending on the actual values of these constraints. For this study I tried to choose values which would be applicable to a modern production engine. Nevertheless, it would be of interest to see how sensitive the results actually are to these values. Therefore, this section presents a study, in which the constraints on the air-fuel ratio (λ), the intake manifold temperature, maximum pressure rise rate, and the NO_x emissions are varied.

It is important to see if the results would change for a different constraint on λ, since this constraint was set in order to limit soot emissions implicitly. For instance, if a λ of 1.6 is required to suppress soot, then arguably a reduction in gas exchange efficiency would result. Furthermore, the constraint on the intake manifold temperature was set in order to prevent water condensation. If the condensed water could be taken care of, and therefore enable the removal of this constraint, it would be interesting to see if it could lead to a significant gain in brake efficiency. Moreover, a high λ and a low T_{im} could facilitate PPC. Because there was no constraint on λ for methanol, and the required T_{im} was sufficiently above the limit, only the gasoline fuels were considered for this sensitivity analysis. The gasoline fuel with a research octane number of 76 was chosen and the optimizations were repeated for the operating point A75 with the following constraints: $\lambda > 1.6$ and $T_{\mathrm{im}} > 273\,\mathrm{K}$.

The limit on maximum pressure rise rate was set in order to keep the engine from experience knock. However, PPC is typically found to have higher pressure rise rates than conventional diesel combustion (for the same operating conditions) and thus a too low limit on this constraint, could be the reason the gasoline fuels did not show a PPC-like rate of heat release. Moreover, it would be interesting to quantify the change in brake efficiency due to a change in the pressure rise rate limit. The operating point A75 was chosen for the sensitivity study of this constraint as well, however, the fuel was changed to the gasoline with a RON of 97 because it was thought to be more inclined to change into a PPC mode, compared to the lower RON gasoline. The baseline value of 15 bar/°ca for the maximum pressure rise rate was changed to 7.5 bar/°ca and 30 bar/°ca for this sensitivity study.

The constraint on NO_x emissions was investigated because this limit was thought to have a significant impact on the results. In particular, the required amount of EGR, and consequently the gas exchange efficiency, would likely be affected. The limit of $NO_x < 1.0\,\mathrm{g/(kW\,h)}$, which was used in all optimizations, was changed to $NO_x < 0.4\,\mathrm{g/(kW\,h)}$, as it is the Euro VI regulations limit for heavy-duty trucks. The operating point A75 was chosen for this sensitivity analysis as well, however, for this case both methanol and the gasoline fuel (RON 76) were considered.

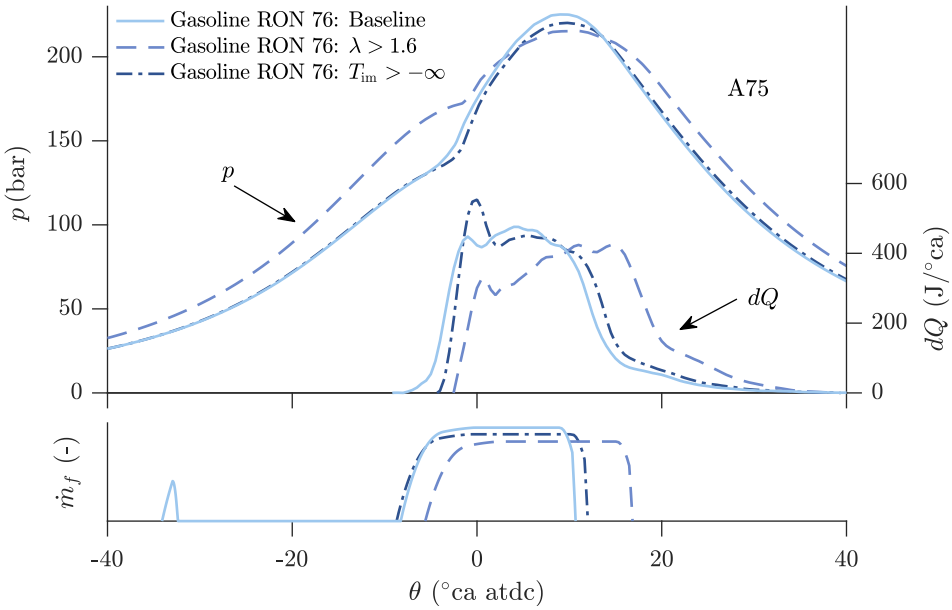

Figure 5.27: In-cylinder pressure (p) and rate of heat release ($\mathrm{d}Q$) from the sensitivity analysis of the constraint variables λ and intake manifold temperature (T_{im}). The optimizations were performed for the operating point A75, and using the gasoline fuel with a research octane number of 76.

Figure 5.27 presents the cylinder pressures, rates of heat release, and fuel injection rates, comparing the baseline optimization for the gasoline fuel, with the case when the required air-fuel ratio was increased, and when there was no constraint on the intake manifold temperature. Moreover, key result parameters are presented in Table 5.8. By increasing the constraint on λ, the amount of required air is increased,

Table 5.8: Results from the sensitivity analysis of the constraint variables λ and intake manifold temperature (T_{im}). The optimizations were performed for the operating point A75, and using the gasoline fuel with a research octane number of 76.

Gasoline RON 76	Baseline	$\lambda > 1.6$	$T_{\text{im}} > -\infty$
η_{brake} (%)	45.4	43.9	45.9
η_{gross} (%)	49.8	49.9	50.5
$\eta_{\text{gas exchange}}$ (%)	98.6	95.3	98.1
λ (-)	1.30	1.60	1.40
EGR (%)	31.1	30.8	29.1
sNO$_x$ (g/(kW h))	0.89	1.00	0.96
T_{im} (K)	336	338	315
p_{im} (bar)	2.85	3.52	2.82
θ_{50}	6.1	11.3	7.1
θ_{eoi} - θ_{10}	-12.4	-15.3	-12.5
$T_{\text{local}}^{\text{max}}$ (K)	2515	2548	2522

hence leading to a higher intake manifold pressure. This is visible in the pressure trace where a significantly higher pressure before the start of combustion is apparent. As a consequence, the combustion phasing had to be retarded, because otherwise the maximum cylinder pressure would have exceeded the constraint of 225 bar. The combustion phasing (θ_{50}) was located at 11.3°ca aTDC, which was a shift by 5.2°ca from the baseline. Furthermore, a later combustion phasing would suggest a decrease in gross indicated efficiency. However, this was counteracted by the fact that the ratio of specific heats was increased and the heat transfer loss was reduced, due to a higher λ and lower global combustion temperature, which therefore led to a minor increase in gross indicated efficiency. Moreover, since the combustion was phased later, the amount of NO_x emissions was reduced, and therefore a lower level of EGR could be applied which could have indicated an increase in the gas exchange efficiency. Nevertheless, due to the substantial increase in λ, and thus dilution, the gas exchange efficiency was reduced by more than 3.0 %pt. Taking into account the large decrease in gas exchange efficiency and the minor increase in gross indicated efficiency, the total effect on the brake efficiency was negative, and it was reduced by 1.5 %pt. This is a substantial reduction in brake efficiency. Furthermore, it is comparable to the reduction in brake efficiency, which was found in Section 4.2.2, when the EGR level was increased.

Removing the limit on the intake manifold temperature, decreases the required temperature with 21 K (from 336 K to 315 K). As a consequence, the gross indicated efficiency and brake efficiency increased by 0.7 %pt., and 0.5 %pt., respectively. This is analogous to the results from Section 4.2.1. Nevertheless, there was not a tremendous difference in terms of rate of heat release or the fuel injection rate. In addition, the small pilot, which was used in the case of higher intake temperature, was removed when the intake temperature was reduced. It is likely that a lower intake temperature led to a higher peak pressure rise rate (keeping everything else the same), which in turn meant that the combustion phasing had to be retarded (a change of 1.0°ca). On the other hand, a retarded combustion phasing, together with the lower intake temperature, led to a slightly lower level of EGR being sufficient to keep the NO_x emissions under the constraint. A lower level of EGR, and a lower intake manifold temperature, should have led to a higher gas exchange efficiency, however, this was not the case. The explanation can probably be found in the air-fuel ratio being higher, increasing the λ from 1.3 to 1.4. Following the previous discussion, a higher air-fuel ratio is generally beneficial for yielding a higher gross indicated efficiency, even though it also leads to a lower gas exchange efficiency. For this particular case, a slightly higher air-fuel ratio was better in terms of brake efficiency. Finally, it is interesting to note that neither the increase of air-fuel ratio, nor a lower intake manifold temperature, led to a relevant difference in ignition dwell. In the case of lower intake temperature, a slightly longer separation between the start of injection and start of combustion was seen, however,

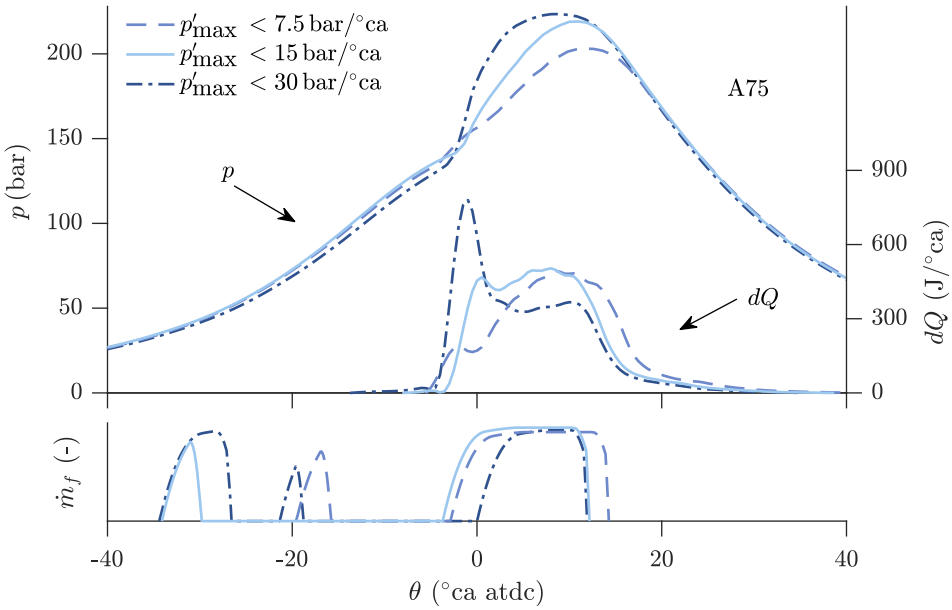

Figure 5.28: In-cylinder pressure (p) and rate of heat release ($\mathrm{d}Q$) from the sensitivity analysis of the constraint on maximum pressure rise rate $p'_{\max}$. The optimizations were performed for the operating point A75, and using the gasoline fuel with a research octane number of 97.

since the optimal injection pressure was lower for this case, the resulting ignition dwell was similar. In the case of higher air-fuel ratio, both the separation between start of injection and start of combustion, and the ignition dwell were similar to the baseline optimization.

Table 5.9: Results from the sensitivity analysis of the maximum pressure rise rate $p'_{\max}$. The constraint on maximum pressure rise rate was changed, from the baseline of 15.0 bar/°ca, to 7.5 bar/°ca and 30.0 bar/°ca. The optimizations were performed for the operating point A75, and using the gasoline fuel with a research octane number of 97.

Case	1	2	3
$p'_{\max}$ **(bar/°ca)**	**6.2**	**12.4**	**20.9**
η_{brake} (%)	45.4	45.5	45.9
η_{gross} (%)	49.6	50.0	50.2
$\eta_{\text{gas exchange}}$ (%)	98.8	98.4	98.8
λ (-)	1.36	1.34	1.34
EGR (%)	28.8	30.7	28.0
sNO_x (g/(kW h))	0.97	0.89	0.96
T_{im} (K)	336	338	334
p_{im} (bar)	2.87	2.93	2.80
θ_{50}	9.5	7.6	5.6
$r_{\text{premixed}}/r_{\text{total}}$ (%)	**10.2**	**13.9**	**40.2**
$T^{\max}_{\text{local}}$ (K)	2560	2505	2578

Figure 5.28 shows the cylinder pressures, rates of heat release, and fuel injection rates, for the sensitivity study on the limit of pressure rise rate. It is noticeable how a higher pressure rise rate leads to more premixed combustion, as depicted from the rate of heat release. This premixedness can be quantified by calculating how much of the fuel is injected before the start of combustion. Table 5.9 shows that the amount of premixedness ($r_{\text{premixed}}/r_{\text{total}}$) goes from 10.2 % to 40.2 % as the maximum pressure rise rate increases from 6.2 bar/°ca to 20.9 bar/°ca. Moreover, the highest pressure rise rate did not reach the constraint limit, instead the optimizer found a significantly lower value as optimum. The brake efficiency increased with an increasing pressure rise rate. The level of EGR was kept around the same value, and the resulting NO_x emissions were below the constraint of 1.0 g/(kW h). Although the combustion phasing was advanced with higher pressure rise rate, the maximum local temperature did not change drastically and thus was the reason for the same level of NO_x emissions.

Figure 5.29 shows the cylinder pressures, rates of heat release, and fuel injection rates, comparing the baseline optimizations for methanol and gasoline, when the constraint on NO_x emissions was set stricter. Minor changes in these traces can be observed. For instance, in the case of methanol, the fuel injection events were advanced. The injection pressure was higher for methanol, but lower for gasoline. As expected, the combustion phasing was shifted later and a higher level of EGR was needed, for both

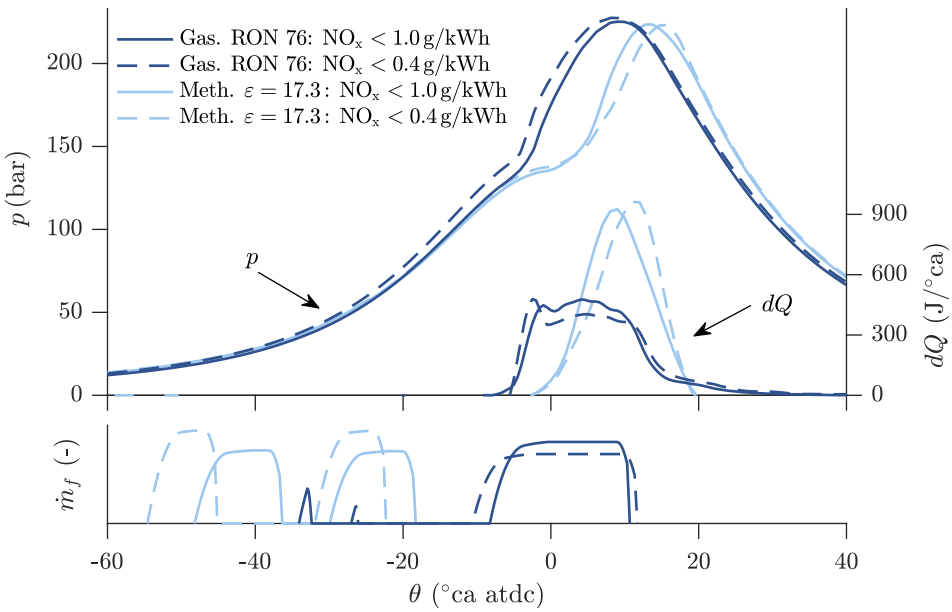

Figure 5.29: Results from the sensitivity analysis of the constraint for NO_x emissions. The optimizations were performed for the operating point A75, and comparing methanol with the gasoline fuel with a research octane number of 76.

Table 5.10: In-cylinder pressure (p) and rate of heat release ($\mathrm{d}Q$) from the sensitivity analysis of the constraint for NO_x emissions. The optimizations were performed for the operating point A75, and comparing methanol with the gasoline fuel with a research octane number of 76.

	Methanol		Gasoline	
sNO_x (g/(kW h))	0.87	0.40	0.89	0.40
η_{brake} (%)	47.5	47.1	45.4	44.0
η_{gross} (%)	51.9	51.6	49.8	49.3
$\eta_{\text{gas exchange}}$ (%)	98.7	98.4	98.6	97.7
λ (-)	1.66	1.56	1.30	1.30
EGR (%)	14.9	20.4	31.1	36.6
T_{im} (K)	366	378	336	342
p_{im} (bar)	3.13	3.23	2.85	3.10
θ_{50}	9.8	11.3	6.1	6.6
$T_{\text{local}}^{\text{max}}$ (K)	2477	2570	2515	2435

fuels, as can be seen in Table 5.10. Interestingly, the local maximum temperature is higher for the NO_x restricted case for methanol. However, this temperature is obtained at a higher equivalence ratio and therefore does not produce more NO_x. Furthermore, both the gross indicated and the gas exchange efficiencies were reduced, leading to a total reduction of the brake efficiency with 0.4 %pt. and 1.4 %pt., for methanol and gasoline respectively. Thus, the decrease was three times as big for the gasoline fuel, even though the same absolute increase in EGR level was applied. However, for the gasoline case, the EGR level increased from an already high level, and therefore led to a larger decrease in gas exchange efficiency. Finally, it can be noted that a higher intake manifold temperature was required due to a higher water concentration in the incoming air-EGR mixture.

5.6 Summary

This chapter has presented results from several engine optimizations. A meta heuristic optimization algorithm, called the particle swarm, was used to optimize a number of engine parameters with the goal of maximizing the brake efficiency. Optimization constraints were put on the maximum cylinder pressure, maximum cylinder pressure rise rate, NO_x emissions, and soot emissions, as well as preventing water condensation. The specific algorithm was chosen because of the complex relationships between the engine parameters and their effect on the engine performance. Results for three different fuels, methanol and gasoline (RON 76 and 97), were presented. In the case of methanol, the compression ratio was optimized to achieve a higher brake efficiency and to enable a lower required intake manifold temperature. It turned out that in-

creasing the compression ratio, from 17.3:1 to 21.6:1, could give an, overall, 1.4 %pt. higher brake efficiency.

The results from the optimizations showed that methanol could yield the highest brake efficiency for this engine and operating conditions. In fact, the arithmetic mean brake efficiency was 2.2 %pt. and 3.6 %pt. higher for the methanol cases, with standard and optimized compression ratio respectively, than for the case with the gasoline fuels. This increase in brake efficiency was mainly due to a higher gross indicated efficiency, and only to a lesser extent to an increase in gas exchange efficiency.

The gross indicated efficiency was higher because of a lower exhaust loss. The reasons for a lower exhaust loss were several. First, an improved compromise between combustion duration, heat transfer and NO_x emissions was obtained for the cases with methanol. Secondly, due to the cooling from fuel vaporization, less energy had to be used under the compression stroke. Finally, the ratio of specific heats were higher in most of the operating points for the cases with methanol due to a lower level of EGR.

The highest efficiency with methanol was obtained when the fuel was injected relatively early in the compression stroke. This led to a long separation between the fuel injection event and the start of combustion, and increased the cooling, due to fuel vaporization, during the compression stroke. The umbrella angle needs to be narrow to avoid wall wetting when injecting early. Moreover, the sensitivity of the inlet conditions on combustion have shown to increase with advanced injection timings. Therefore, it was of interest to quantify the reduction in brake efficiency when the start of injection was set closer to TDC. It was seen, for the A75 operating point, that a brake efficiency penalty of 2.2 %pt. followed, when the start of injection was restricted to be no earlier than 25°ca before TDC. For the operating point B25, this decrease was 0.8 %pt. which is less but not insignificant. Furthermore, the sensitivity of inlet temperature and start of injection timing (of the main injection), was small for the operating point B25, while for the operating point A75, this sensitivity was alarmingly large. Furthermore, the combustion phasing was retarded when advancing the start of injection timing for the early injection strategy. This seemed non intuitive and will therefore be investigated further in the subsequent chapter.

With the gasoline fuels, only the B25 operating point exhibited something which was close to PPC, that is most of the fuel was injected before the start of combustion. Consequently, these results suggest that, for these fuels, conventional diesel combustion should be used, at least when the engine load is higher than 25 %. However, that does not necessarily mean that the PPC concept does not yield higher brake efficiencies than conventional diesel combustion, in general. For instance, it is likely that the constraint on intake manifold temperature meant that the temperature at TDC was too high to avoid early auto-ignition, and thus enable a separation between the fuel

injection and the start of combustion. One thing that speaks against this explanation, is the fact that the optimizer found a similar optimal combination, of fuel injection and combustion, when this constraint was removed. Another reason for not obtaining a positive ignition dwell could be that the constraint on pressure rise rate was set too strict. This was seen in the sensitivity study where the constraint on maximum pressure rise rate was changed. By allowing for a higher pressure rise rate, the brake efficiency increased and a larger percentage of the total fuel mass could be injected before the start of combustion. Still, only 40 % of the fuel was injected before the start of combustion and hence this was not PPC according to the definition used in this thesis. On the other hand, pressure rise rates typically increase with engine load. Thus, a higher limit on the pressure rise rate could potentially have shifted the operating region with PPC to higher loads, perhaps to using PPC at loads below 50 % and conventional diesel combustion at the higher loads.

Yet another reason, for not obtaining a positive ignition dwell, could be that the implicit constraint on soot emissions demoted PPC. The constraint was set on a specific level of air-fuel ratio, namely $\lambda > 1.3$. However, this does not take the level of soot formation into account, instead only an empirical soot oxidation is considered. Thus, it is possible that the diffusion type combustion, which the optimization algorithm found optimal, would not have given the highest brake efficiency, if the soot emissions would have been modeled and thus constrained explicitly. This is especially true when considering that a stricter limit on λ resulted in a substantial penalty in brake efficiency. If instead soot emissions were modeled explicitly, a lower λ could perhaps have been used in combination with a positive ignition dwell, to yield a higher brake efficiency. Simulation of soot emissions with the stochastic reactor model would have required a different kinetic model, which would likely have had to contain more species, and therefore increased the simulation times. On the other hand, if species tabulation of the kinetic model was applied, as shown in [104], then complex kinetic models can be used and thus model soot emissions with the same methodology as in this thesis.

Chapter 6

Emission Formation and Ignition Location on the $T - \phi$ Plane

The previous chapter showed that when optimizing the engine settings for the highest brake efficiency, methanol showed a positive ignition dwell in all operating points, and thus fulfilled the requirement of partially premixed combustion (PPC) (from Chapter 2). On the other hand, the gasoline fuel, with a research octane number (RON) of 76, did not show a positive ignition dwell. Moreover, it was shown that a change of fuel, to a fuel with a RON of 97, did not yield any significant difference in ignition dwell. In fact, the difference in rate of heat release and fuel injection was almost negligible comparing the two fuels. However, the removal of the constraint on maximum in-cylinder pressure rise, did increase the amount of fuel which could be injected before the start of combustion, and resulted in a higher brake efficiency. Furthermore, by investigating the effect of limiting the start of injection timing for methanol it was found that a retarding timing did not yield a later combustion phasing, but an earlier one.

These are all observations warranting further analysis. Further insight could be gained by investigating the stochastic reactor model particle trajectories, that is how the particles move through the temperature and equivalence ($T - \phi$) plane. For instance, it would be possible to determine the location, in the $T - \phi$ domain, at which the ignition occurred. Furthermore, the distribution of temperature and equivalence ratio can be used to qualitatively understand the prevailing combustion conditions and thus the potential emissions formation.

The present chapter will therefore use the results from Chapter 5, but take the analysis one step further for some of the optimized cases. However, before presenting this, the $T - \phi$ plane needs to be constructed which is therefore demonstrated next.

6.1 $T - \phi$ Map Methodology

The concept of $T - \phi$ diagrams originated in [25], and these have since been used widely [11, 26, 27, 105]. Traditionally, these diagrams have been used to illustrate the formation of emissions, mostly NO_x and soot, but also unoxidized fuel species, as well as CO and CO_2. In addition, the ignition delay time can be displayed on a $T-\phi$ diagram to, for example, analyze the ignition location in a premixed combustion event.

6.1.1 Emission Formation

In this work the diagrams, which show emissions formation, have been constructed for neat methanol and a gasoline surrogate. The gasoline surrogate had a calculated RON of 95.6 and consisted of iso-octane (63.1 %), n-heptane (9.8 %), and toluene (27.1 %). Toluene was added to mimic the influence of aromatics on soot formation. The surrogate formulation was taken from [106]. The $T - \phi$ diagrams were constructed using a grid, presented in Table 6.1, consisting of 51 levels of temperature and 77 levels of equivalence ratio leading to a total number of 3927 points. At every grid point, a premixed chemical reaction, between the fuel (in gas phase) and air, was simulated in a homogeneous reactor from the LOGEresearch simulation frame-work [107]. The pressure and temperature were kept constant throughout the simulation, which ran for a residence time of 2.0 ms. A shorter residence time could have been chosen, as the diagrams typically do not change after 0.5 ms [108]. Moreover, 0.5 ms and 2.0 ms, correspond to 3.6°ca and 14.4°ca, respectively. The pressure was 100 bar in all simulations. This particular value was chosen as a compromise between being a relevant pressure for a combustion event inside the engine, and not to be too far outside the kinetic model's validation regime. The resulting emissions could then, through linear interpolation, be viewed on the $T - \phi$ diagram. The detailed kinetic

Table 6.1: The grid used for constructing the $T - \phi$ diagrams which show emission formation. T_{constant} is the constant temperature which was applied during each simulation.

	Min.	Max.	Δ	Levels
T_{constant} (K)	500	3000	50	51
ϕ (-)	0.1	3.9	0.05	77

scheme, developed by Seidel, was used in these simulations as it models combustion of methanol and gasoline surrogates, as well as soot and NO_x formation [28]. Moreover, this reference includes a comprehensive description of the kinetic model and it will therefore not be discussed further here.

The formation of soot and NO_x, for methanol and the gasoline surrogate, are presented in Figure 6.1. The formation yields were converted from species mass fraction (Y) to g/(kW h) (NO_x), and mg/(kW h) (soot), by applying Equation (6.1), which means that they have been normalized with the energy content of the fuel.

$$\begin{aligned} \mathrm{NO_x}\,(\mathrm{g/(kW\,h)}) &= \frac{Y_{\mathrm{NO_x}}}{Y_{\mathrm{fuel}}}\frac{10^3/3.6}{Q_{\mathrm{LHV}}} \\ \mathrm{Soot}\,(\mathrm{mg/(kW\,h)}) &= \frac{Y_{\mathrm{Soot}}}{Y_{\mathrm{fuel}}}\frac{10^6/3.6}{Q_{\mathrm{LHV}}} \end{aligned} \tag{6.1}$$

It is interesting to note that the soot and NO_x emissions form distinct islands in the $T - \phi$ diagram. The soot formation increases with equivalence ratio, however, the highest levels are found for a rather limited range of temperatures. Furthermore, the difference in soot formation, between the fuels, is as expected huge. In fact, the highest level of soot formation for methanol is lower than 1.0 ng/(kW h), and is therefore not displayed. Moreover, this explains why soot emissions are non existent in engine experiments with methanol [50–53]. In contrast, the difference in NO_x formation is small. Instead the NO_x formation is only dependent on the excess of oxygen and the temperature. The NO_x formation increases with increasing temperature and decreas-

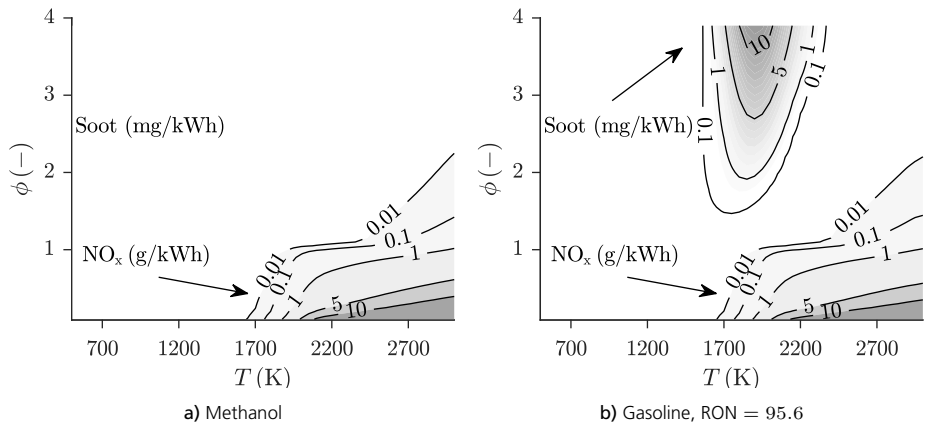

Figure 6.1: Soot and NO_x formation for methanol and the gasoline surrogate. Combustion with methanol did not yield any soot.

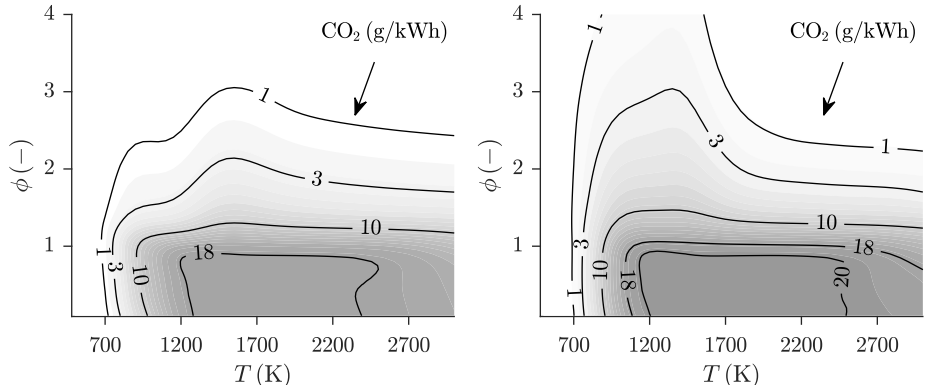

Figure 6.2: CO_2 formation for methanol and the gasoline surrogate.

ing equivalence ratio. Due to a difference in energy content of the fuels, a slightly higher NO_x formation for methanol can be distinguished.

NO_x and soot emissions are naturally of most interest when considering direct injection, compression ignition engines. Nevertheless, it can be useful to illustrate other species as well. For instance, the formation of CO and CO_2 emissions are shown in Figures 6.2 and 6.3. They were also converted to g/(kW h), by the same formula as the NO_x emissions. At low temperatures, the oxidation of the fuel does not get started, and thus there is no formation of either CO or CO_2. Instead, the formation of CO_2 and CO starts to appear after 700 K. The reason is that, the higher the temperature, the faster are the chemical reaction rates, and thus more of the fuel can be oxidized to completion, that is from fuel and O_2, through CO, to CO_2. This can be seen as

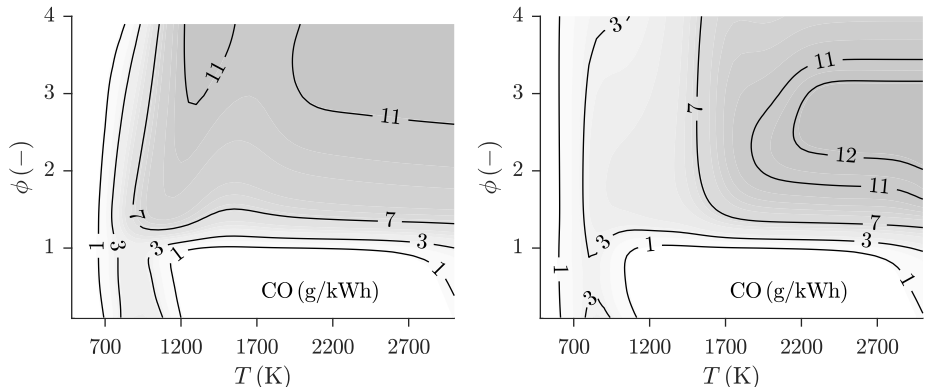

Figure 6.3: CO formation for methanol and the gasoline surrogate.

increasing the temperature, at an equivalence ratio below one, yields an increase in both CO and CO_2, until a temperature of 1000 K, after which the formation of CO reduces and the formation of CO_2 increases. Close to complete oxidation then occurs for all temperatures up to 2400 K, after which dissociation comes into play, and hence CO formation increases. Furthermore, at an equivalence ratio above one, there is not enough oxygen to complete the oxidation step, that is going from CO to CO_2.

The $T-\phi$ diagrams can be used to analyze the particle trajectories, and hence the combustion. It should, however, be noted that full advantage of the emission formation maps is prohibited by the fact that there is no mixing within the maps. By contrast, the combustion in an engine involves mixing of burned and unburned species. Nonetheless, it is likely that the more premixed the reactants are before the combustion starts, the more can these maps be used to quantify the emissions formation.

6.1.2 Ignition Delay Time

The ignition delay time can also be displayed on the $T-\phi$ diagram. As it is common practice, the ignition delay was simulated in an adiabatic constant volume reactor. In a constant volume reactor, the initial pressure and temperature are set and the combustion of fuel and air is allowed to proceed. Because it is a constant volume, the pressure and temperature increase due to combustion. In this work, the ignition delay time was defined as the time it takes for the pressure rise rate to reach its highest value. In contrast to the simulations in the constant pressure reactor, these simulations were conducted on a different grid, see Table 6.2. One thing to note is that the initial pressure was 60 bar in all simulations. This value was chosen because it represented an average of the pressure, before start of combustion, for the simulated cases in Chapter 5. Nevertheless, the ignition delay time changes with pressure, but as was seen in Figure 5.1, the sensitivity, at an initial pressure above 50 bar, is small. Moreover, this analysis is more concerned about the trends and it is likely that they will not change with, for instance, an increase in initial pressure. It should also be noted that these simulations were initialized with the fuel in gas phase. As the ignition delay time will be used to analyze the particle trajectories from the stochastic reactor model, the same chemical mechanisms were used. That means the reduced form of the AramcoMech 2.0 mechanism [77], and the full chemical kinetic model from [78]

Table 6.2: The grid used for constructing the $T-\phi$ diagrams which show ignition delay time. T_{initial} is the initial temperature.

	Min.	Max.	Δ	Levels
T_{initial} (K)	600	1300	10	71
ϕ (-)	0.1	3.0	0.1	30

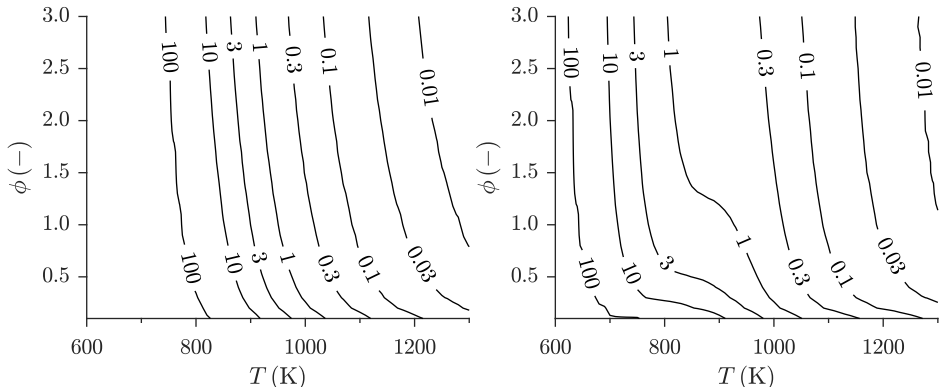

a) Methanol b) Gasoline, RON = 97

Figure 6.4: Contours of constant ignition delay time (ms), for methanol and the gasoline surrogate, as a function of initial temperature and equivalence ratio. The ignition delay time was simulated in a constant volume homogeneous reactor at a pressure of 60 bar.

were used. Furthermore, these simulations were performed with neat methanol and the gasoline surrogate with a calculated RON of 97 from Chapter 5.

Figure 6.4 shows contours of simulated constant ignition delay time (ms), for both fuels, as a function of initial temperature and equivalence ratio. For methanol, the ignition delay time reduces exponentially with higher temperatures. Furthermore, going from a high to a low equivalence ratio, along a constant temperature, yields a shorter ignition delay time, and this trend is especially pronounced at an equivalence ratio below one. For the gasoline fuel, almost the same trends can be observed, although the absolute values are reduced which means that a shorter ignition delay time is obtained for the same combination of initial temperature and equivalence ratio, compared to methanol. In addition, between a constant ignition delay of 3 ms to 0.3 ms, there is evidence of low temperature chemistry. However at this initial pressure, there is no sign of a negative temperature coefficient behavior because the contours do not cross.

6.2 SRM Particle Trajectories during Optimal Combustion

The emission formation and the contours of ignition delay time are valuable tools, when analyzing the way that the stochastic reactor model particles move before and during the combustion. This section will expand on the analysis from Chapter 5, and look at the difference of the ignition and combustion processes, between methanol and the gasoline fuel with a RON of 97.

As most of the differences for the ignition and combustion are assumed to be dependent on the engine load, the B25 and B100 operating points were chosen as they are at the ends of the simulated load range. In these simulations, a number of 5000 particles were used. To display all of these particles would have made the $T - \phi$ figures cluttered. For this reason, these figures will only show the particles which are at the Pareto front in terms of temperature and equivalence ratio. Furthermore, note that the markers in these figures do not represent stochastic reactor model particles, but instead are used for distinguishing between different Pareto fronts.

The ignition timing, and location in the $T - \phi$-diagrams, was determined by tracking the particles' instantaneous rate of heat release. When there was a particle with a sufficient rate of heat release (decided by a relevant threshold), this was used as the ignition. For methanol this was trivial. However, for the gasoline fuel low temperature chemistry led to an early, and premature, rate of heat release without any substantial increase in cylinder temperature. Therefore, this low temperature reaction heat release was neglected when determining the ignition location.

Figure 6.5 shows the particle Pareto fronts just after ignition, at two different crank angle degrees, namely $\theta_{0.1}$ and θ_1 (cf. Equation (5.8)), comparing methanol (left) and gasoline (right), for the B25 operating point. There are two distinct differences comparing the two fuels. First, the span in temperature is significantly larger for methanol, than it is for gasoline. Thermal stratification is commonly used to describe this temperature difference. The reason for the large thermal stratification in the case of methanol, is the large latent heat of the fuel which cause particles which have more fuel to be colder, and particles with less fuel to be warmer. Secondly, the ignition for methanol is located at the leanest equivalence ratio, while it is located at the richest

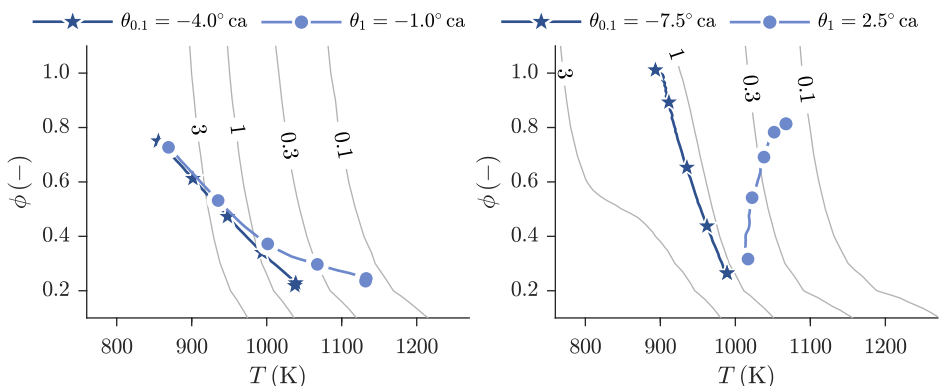

a) Methanol **b)** Gasoline, RON = 97

Figure 6.5: Stochastic reactor model particle Pareto fronts, at $\theta_{0.1}$ and θ_1, for the B25 operating point. The contours of constant ignition delay time from Figure 6.4 are visible.

equivalence ratio for gasoline. Naturally, there is a coupling between the ignition delay time and these two observations. In the case of methanol, a large thermal stratification leads to the fact that the particles which contain the least fuel, cross the ignition delay contours first, and therefore they have a shorter ignition delay time, and hence ignite first. In contrast, for the gasoline fuel, due to the lack of a large thermal stratification, the ignition delay time contours and the particle Pareto front are aligned and thus the particles with the most fuel have the shortest ignition delay time. Moreover, the small thermal stratification that exists, decreases because low temperature chemistry reactions heat up the richest particles.

The combustion process is visualized in Figure 6.6 which shows the particle Pareto fronts at the locations for 10 % and 50 % heat released (θ_{10} and θ_{50}). In the case of methanol the combustion proceeds from the leanest equivalence ratios to the richest and, as was noticeable in Figure 5.17, this yields a rather smooth rate of heat release profile with a low peak. Furthermore, the highest local temperature, at θ_{50}, is low and thus the particles do not penetrate far into the NO_x island, which therefore explains why this case generated low NO_x emissions. On the other hand, the combustion proceeds oppositely in the case of gasoline. The richest particles ignite first, and the combustion proceeds toward the leanest particles. Moreover, the third fuel injection is located after θ_{10} and this fuel is therefore injected when there is already a high cylinder temperature. This can be seen to yield particles which are burning at an equivalence ratio of one and thus at high temperatures. Moreover, these high local temperatures are seen to result in a deeper penetration of the NO_x island, and therefore lead to much higher NO_x emissions.

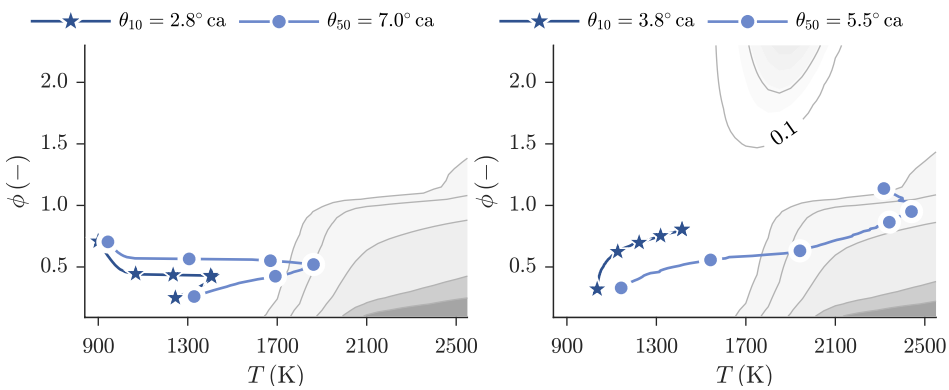

Figure 6.6: Stochastic reactor model particle Pareto fronts, at θ_{10} and θ_{50}, for the B25 operating point. The emission formation of NO_x and soot, from Figure 6.1, are visible.

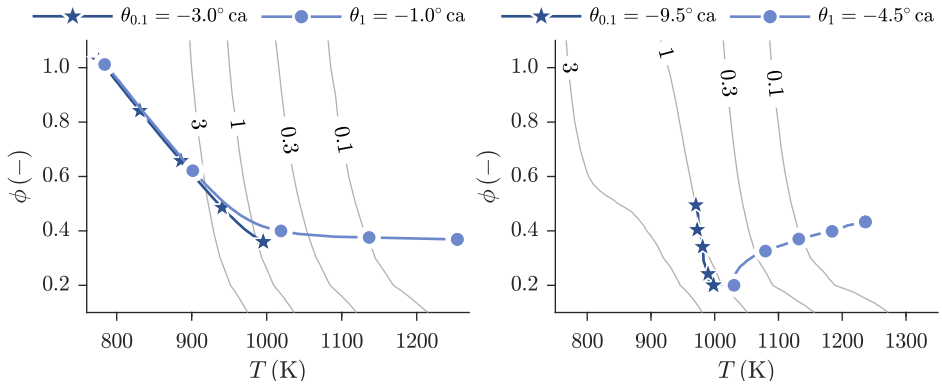

Figure 6.7: Stochastic reactor model particle Pareto fronts, at $\theta_{0.1}$ and θ_1, for the B100 operating point. The contours of constant ignition delay time from Figure 6.4 are visible.

Moving on to the B100 operating point, Figure 6.7 shows the particle Pareto fronts at $\theta_{0.1}$ and θ_1. For methanol, the thermal stratification is even larger, compared to B25, which is to be expected due to the increased fuel mass and lower level of dilution (cf. Figures 5.7 and 5.8). Like the B25 operating point, the ignition occurs at the leanest equivalence ratio. In the case of the gasoline fuel, only the fuel in the pilot injection is visible because the pilot ignited before the start of the main injection. Thus, the overall equivalence ratio is rather lean. Nevertheless, this pilot ignites where it is the richest. Figure 6.8 then shows the particle Pareto fronts at θ_{10} and θ_{50}. The combustion with methanol, similarly to the B25 operating point, goes from particles with leanest equivalence ratio to the ones with richest, which results in a smooth increase in the rate of heat release profile (cf. Figure 5.18). In contrast, the combustion with gasoline

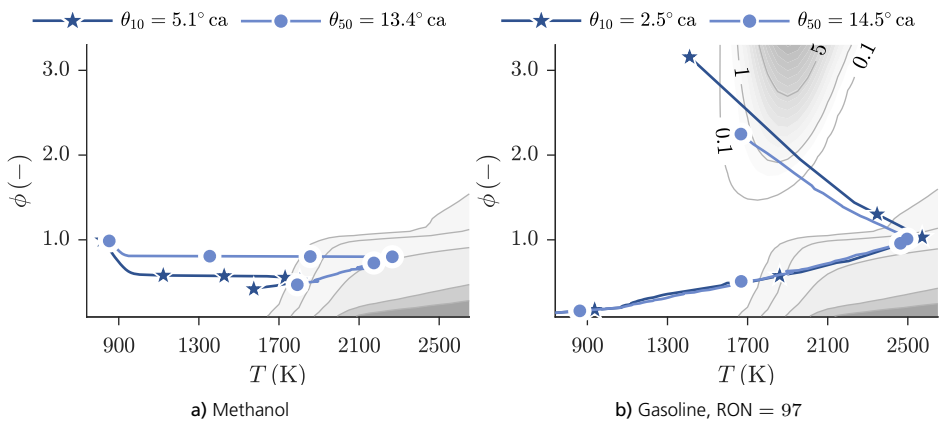

Figure 6.8: Stochastic reactor model particle Pareto fronts, at θ_{10} and θ_{50}, for the B100 operating point. The emission formation of NO_x and soot, from Figure 6.1, are visible.

is set off by the pilot and is then governed by the large main injection which burns in a depicted mixing-controlled manner. As is apparent, all the fuel particles move through the soot island as combustion goes on, and therefore it is most likely that this case forms substantial amounts of soot. As has been mentioned earlier in this thesis, this is not to say that the amount of soot emissions in the exhaust is large, as soot oxidation is still to occur. Finally, as the peak temperature at θ_{50} is significantly larger for the gasoline case, it is not surprising that the resulting NO_x emissions are larger.

6.3 Sensitivity of Start of Injection on Ignition Timing

In Section 5.4 it was shown, for methanol, that for the early injection strategy (case A) and operating point A75, an advancement of the start of injection timing resulted in a retardation of the combustion phasing. This was intuitively difficult to understand because the opposite is typically true, at least for conventional diesel combustion. As a matter of fact, for the injection strategy which employed later timings, the combustion phasing was completely controlled by the phasing of the main injection. The particle Pareto fronts can be used to understand why this difference occurred. The left subfigure of Figure 6.9 shows the particle Pareto fronts, just before ignition and at θ_{50}, for when the start of injection timing of the main injection is moved, –5°ca and 5°ca, compared to the baseline (–48°ca). It can be seen that, when the injection timing is advanced, there is more time for the fuel to mix with the bulk gas. This results in a reduction of the thermal stratification, and therefore the particles which have the leanest equivalence ratio (where ignition occurs) have a lower temperature, than the ones in the case with later injection timing, and hence ignite later. Furthermore, due to a later combustion phasing for the advanced start of injection case, the resulting

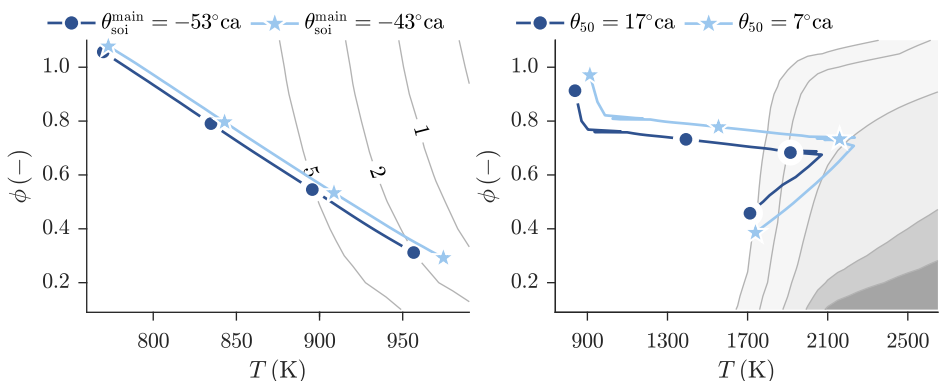

Figure 6.9: Stochastic reactor model particle Pareto fronts, just before ignition (left) and at θ_{50} (right), for when the start of injection timing of the main injection is moved, –5°ca and 5°ca, compared to the baseline (–48°ca) for injection strategy case A, the A75 operating point, and methanol.

maximum in-cylinder temperature is lower and this yields lower NO_x emissions which is apparent in the right sub-figure of Figure 6.9.

6.4 The Effect of Thermal Stratification

From the content presented thus far, thermal stratification has been used to explain many of the differences, in the ignition and combustion processes, between methanol and gasoline. Furthermore, as the rate of heat release profiles for methanol show a smoother rise, it is possible that there is a link between thermal stratification and maximum pressure rise rate, which in turn was the reason for not obtaining PPC conditions in the case of gasoline.

The concept of thermal stratification is not new. In engines applying the homogeneous charge compression ignition (HCCI) concept, it has been shown to be the mechanism behind reducing pressure rise rates, as it leads to a sequential series of auto-ignition events [109]. To expand the load range of HCCI, researchers have therefore attempted to increase the level of thermal stratification. These attempts include reducing the engine coolant temperature to reduce wall temperatures [110], different heating of the intake ports [111], or reducing the mixing of residual and incoming fresh charge [112]. However, they have shown minor success because they only moderately change the thermal stratification of the bulk gas, which has been shown to be the dominating factor in reducing pressure rise rates [113]. The use of ethanol, on the other hand, was shown to be successful in increasing the thermal stratification of the bulk gas due to fuel-vaporization cooling [114]. Thus, it is likely that methanol, which has a higher latent heat than ethanol, will be even better. Analyzing the results from the optimizations in Chapter 5, in order to study the effect of thermal stratification on methanol and gasoline PPC, is complicated for two reasons. First, these optimizations used multiple injections, which have shown to effectively reduce pressure rise rates by itself [19, 41]. Second, as mentioned repeatedly, the cases with gasoline had the fuel injection located after the start of combustion, when the role of thermal stratification is arguably inconsequential.

The present investigation will instead use a sweep of start of injection timings, to investigate the role of thermal stratification on the ignition and combustion processes, for methanol and gasoline. The start of injection timing was varied between –100°ca to –15°ca aTDC, and was chosen as the dominating parameter, because it was thought to be the most influencing factor. Furthermore, two levels of global equivalence ratio was used, because as is seen in HCCI engines, an increase in global dilution is beneficial for reducing the absolute level of pressure rise rate. The two levels of global equivalence ratio that were used were $\phi = 0.4$ and $\phi = 0.8$. Moreover, the level of thermal

stratification is likely to decrease with increasing dilution, as there is more mass to cool. This numerical experiment was conducted as follows. The combustion phasing was kept constant at 8°ca aTDC. This was done by changing the intake manifold temperature, similarly to [63]. However, a change in temperature changes the trapped mass at inlet valve closing, and therefore the degree of dilution. In order to keep the global ϕ constant, without changing the intake manifold pressure, the level of EGR was varied and set to a suitable value. The operating point corresponded to A25 from Figure 5.3, which meant an engine load of 25 % and an engine speed of 1100 rpm. To keep the influence of different lower heating value (and thus different fuel injection profiles) to a minimum, the number of injector nozzle holes and nozzle hole diameter were adjusted, as it was thought that changing the fuel injection pressure would affect the induced turbulence and thermal stratification more. The fuel injection pressure was set to 800 bar in accordance with what was done in [63].

The particle Pareto fronts are shown in Figures 6.10 to 6.12, for the crank angle degrees corresponding to just before ignition (light blue symbols) and at ignition (dark blue symbols). Figure 6.10 corresponds to the cases with a start of injection timing of –100°ca aTDC, whereas Figures 6.11 and 6.12 show the cases with a start of injection timing of –50°ca aTDC and –15°ca aTDC, respectively. The difference between the fuels, in thermal stratification, is apparent at all these start of injection timings. However, there are similarities as well. For example, at the –100°ca aTDC start of injection timing, both fuels ignite at almost the same equivalence ratio. Although it should be noted that the stratification in equivalence ratio is rather small, as the fuel and bulk gas have had sufficient time to mix, for this case. Moreover, both levels of dilution

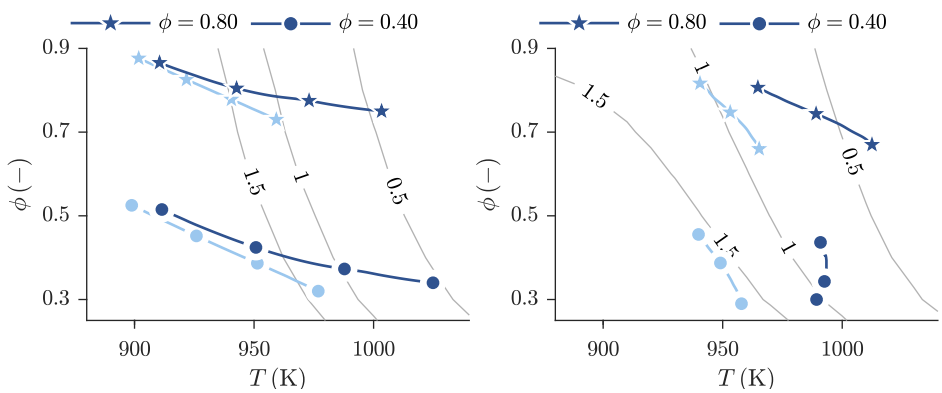

Figure 6.10: Stochastic reactor model particle Pareto fronts, just before the start of combustion (light blue symbols), and at the crank angle of start of combustion (dark blue symbols), for a start of injection timing of $\theta_{soi} = -100$°ca aTDC. The contours of constant ignition delay time from Figure 6.4 are visible.

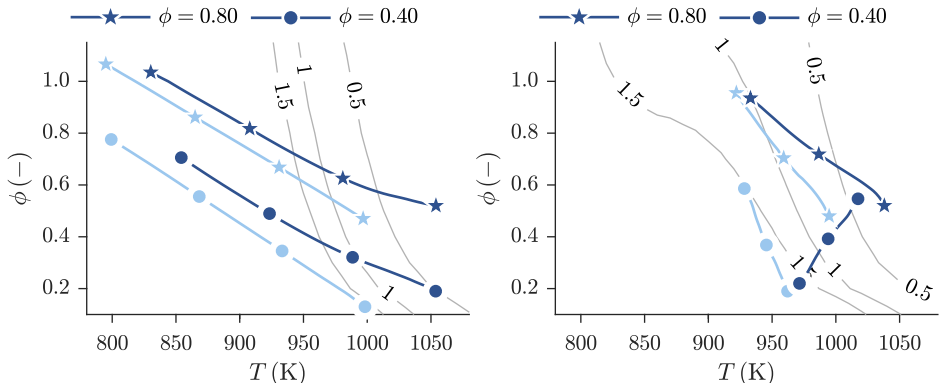

Figure 6.11: Stochastic reactor model particle Pareto fronts, just before the start of combustion (light blue symbols), and at the crank angle of start of combustion (dark blue symbols), for a start of injection timing of $\theta_{soi} = -50$°ca aTDC. The contours of constant ignition delay time from Figure 6.4 are visible.

yield a lean ignition location for methanol, whereas the ignition for the gasoline fuel, for the high level of dilution case, occurs at the richest equivalence ratio.

Looking at the −50°ca aTDC start of injection case (Figure 6.11), the degree of thermal stratification has increased for the methanol, whereas it, in relative terms, has not changed much for the gasoline cases. Methanol again ignites at the leanest equivalence ratio. In contrast, now there is clearly ignition at the richest equivalence ratio for the gasoline case with high dilution. In addition, the value of equivalence ratio at ignition, is the same for both the gasoline cases, even though it happens at the opposite ends of the Pareto fronts.

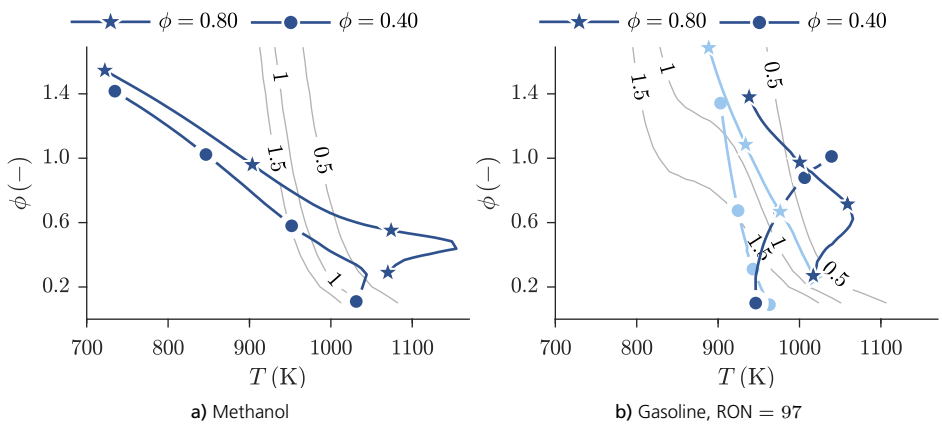

Figure 6.12: Stochastic reactor model particle Pareto fronts, just before the start of combustion (light blue symbols), and at the crank angle of start of combustion (dark blue symbols), for a start of injection timing of $\theta_{soi} = -15$°ca aTDC. The contours of constant ignition delay time from Figure 6.4 are visible.

Finally for the –15°ca aTDC start of injection case (Figure 6.12), there is an even larger degree of thermal stratification for methanol[1]. In contrast to the other start of injection timings, the equivalence ratio of ignition is not at the lean end. Instead, the ignition occurs at a slightly higher equivalence ratio, even though this equivalence ratio is lower than for the preceding cases. For the gasoline, and the case with the highest level of dilution, the particle Pareto front looks similar to the one in Figure 6.5. This is not strange, as the conditions for these two cases are very alike, albeit having a different speed and a slightly different combustion phasing.

This analysis and the observations can be extended by analyzing the trends of maximum pressure rise rate, equivalence ratio at the ignition location, and the level of thermal stratification. Figures 6.13 to 6.15 show these results for all considered start of injection timings. The level of thermal stratification, in Figure 6.15, is taken as the difference in temperature on the Pareto front, just before ignition. As was observed from the particle Pareto fronts on the $T - \phi$ diagrams, the level of thermal stratification increases to a larger extent with methanol, going from early to late start of injection timings, than with gasoline. In contrast, the increase in thermal stratification is negligible with gasoline, in comparison to methanol. Furthermore the ignition equivalence ratio shows opposite trends comparing methanol and gasoline. With methanol, the equivalence ratio becomes leaner and leaner, while the opposite is true for the gasoline. The resulting pressure rise rate with gasoline is constant as a function of start of injection timing, and only depends on the level of dilution, which is consistent with the HCCI literature. In fact, for the gasoline, pressure rise rate correlates perfectly with dilution for these cases ($R^2 = 0.98$). Methanol, on the other hand, reduces the pressure rise rate with retarding start of injection timing. Moreover, in the case of methanol, thermal stratification, inlet valve closing temperature, and equivalence ratio at ignition are needed to find a good correlation with pressure rise rate ($R^2 = 0.91$ and $R^2 = 0.94$), while dilution in fact reduces the correlation. Furthermore, for methanol, the value of pressure rise rate passes 15 bar/°ca at a start of injection timing of –70°ca aTDC, which could be the reason why the optimizer in Chapter 5 did not find an earlier timing (for any of the operating points) than –70°ca aTDC. Contrastingly, the pressure rise rate rarely goes below 15 bar/°ca, even at the higher level of dilution, for gasoline, but stays around 15 bar/°ca for the higher dilution case, and 35 bar/°ca for the lower dilution case.

[1]Note that for methanol (left sub-figure) the Pareto front just before start of combustion is not shown because there is practically no difference between the light-blue and dark blue lines.

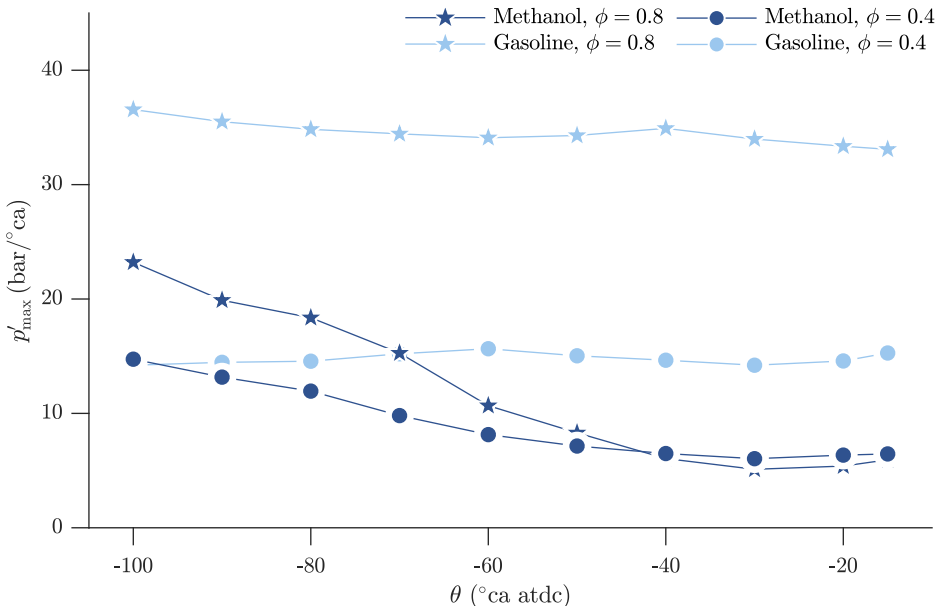

Figure 6.13: Maximum pressure rise rate as a function of start of injection, comparing methanol to gasoline, and for two different levels of dilution.

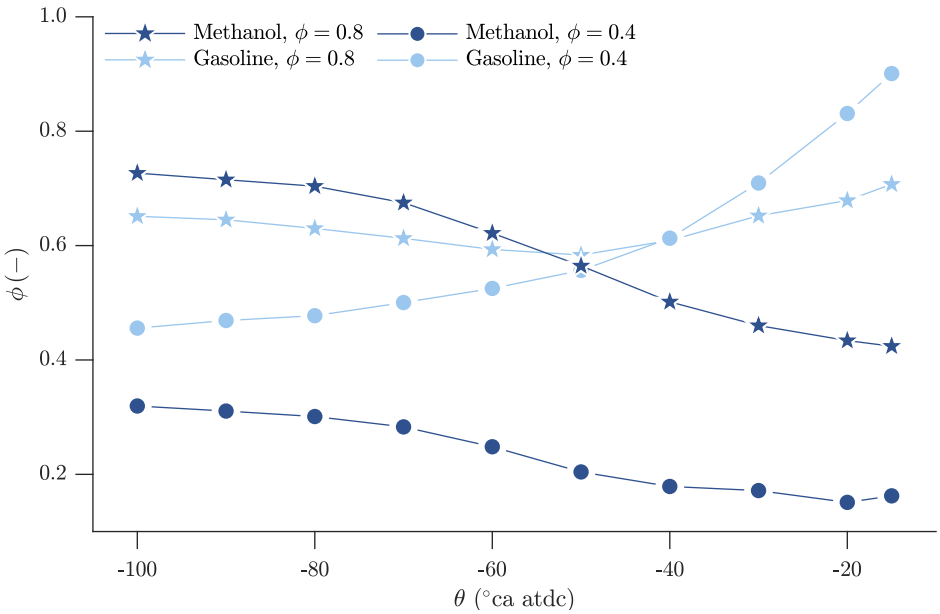

Figure 6.14: The equivalence ratio value at ignition, as a function of start of injection, comparing methanol to gasoline, and for two different levels of dilution.

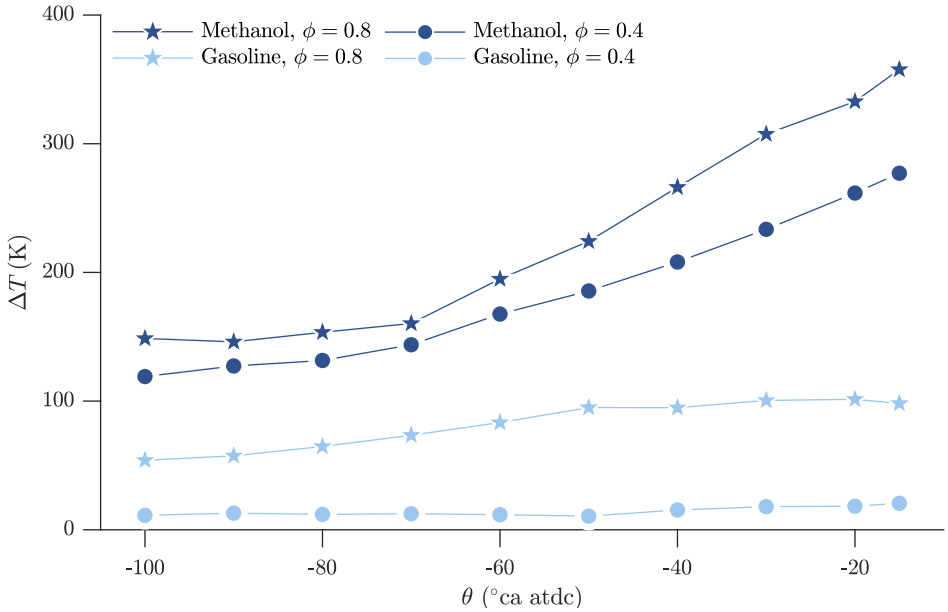

Figure 6.15: Thermal stratification as a function of start of injection, comparing methanol to gasoline, and for two different levels of dilution.

6.5 Summary

This chapter extended the analysis from Chapter 5, by analyzing the ignition and combustion processes, using $T - \phi$ diagrams. The emissions formation of soot, NO_x, CO, and CO_2 emissions, as well as ignition delay time, were displayed on these diagrams. It was depicted that methanol does not show any tendency to form soot, and could thus explain why no soot emissions are found in engine experiments with neat methanol. Gasoline, on the other hand, due to its aromatic content, showed a large propensity for soot formation. Ignition delay times were generally shorter with the gasoline fuel, as a function of temperature and equivalence ratio, compared to methanol.

Furthermore, the emissions formation and ignition delay time could then be used, together with the stochastic reactor model particle trajectories, to analyze the ignition and combustion processes. These figures could for instance, explain the reason for low NO_x emissions in the case of methanol. Moreover, with the contours of constant ignition delay time, it was possible to conclude that thermal stratification plays a major role when it comes to explaining the location of ignition, in terms of equivalence ratio.

The effect of thermal stratification was later investigated, using a sweep of start of injection timings, going from early to late ones. For the case of gasoline, it was seen

that thermal stratification is negligible, and consequently the maximum pressure rise rate correlated only with the overall dilution level. In contrast, pressure rise rate correlated well with thermal stratification for methanol, although also the inlet valve closing temperature, and equivalence ratio at ignition, were needed to obtain a good correlation.

Chapter 7

Summary and Conclusions

This chapter contains a brief summary of the main contributions and observations of the work presented in this thesis.

7.1 Contributions

Previously, the main focus of the work on the partially premixed combustion (PPC) concept has been on maximizing gross indicated efficiency. This work has expanded that picture by looking at ways of maximizing the brake efficiency. The main contributions have been:

- Three turbocharger configurations (two single-stage and a two-stage) were evaluated for the PPC concept. It was shown that only a small benefit in brake efficiency could be obtained with the two-stage turbocharger, however, a higher engine load could be obtained because the compression and expansion were divided.
- By using a combined low and high-pressure EGR system it was possible to increase the gas exchange efficiency by 4.0 %pt.
- The first PPC coupling of the stochastic reactor model and GT-suite was presented to enable full cycle simulation. Furthermore, the particle swarm algorithm was applied to conduct engine operating point optimizations with methanol and gasoline. With methanol it was possible to obtain a 2.2 %pt. higher brake efficiency compared to gasoline. Moreover, if the engine com-

pression ratio was increased to 21.6:1 (compared to the standard of 17.3:1) the brake efficiency increased 1.4 %pt. further.

- A significant increase in brake efficiency was obtained by applying an early injection strategy with methanol. However, it was found that the sensitivity of combustion to inlet conditions was large for these early injection strategies.
- Soot formation was confirmed to be insignificant with methanol, by visualizing the formation of soot and NO_x on a $T - \phi$ diagram.
- The large degree of thermal stratification was found to be responsible for the lower maximum pressure rise rates with methanol.

Chapters 4 to 6 have presented studies aimed at expanding the system boundary, going from a gross to a brake perspective, of the partially premixed combustion concept. The focus has been on the gas exchange performance, differences between fuels, and the in-cylinder conditions in the temperature and equivalence ratio ($T - \phi$) domain.

An evaluation of the choice of turbocharger, for the partially premixed combustion concept was presented in Chapter 4. Of the three turbocharger configurations which were studied, a two-stage turbocharger provided the highest brake efficiency as well as the highest attainable engine load. In addition, the influence of intake manifold temperature was investigated, and showed that both the brake and thermodynamic efficiencies, reduce with an increasing temperature. Finally, a sweep of the level of exhaust gas recirculation, revealed a significant mismatch between the turbine and compressor impeller sizes. It was found that due to the low exhaust temperature, which comes from a high level of dilution, the turbine has a substantially smaller effective mass flow than the compressor, and would therefore benefit from a design with a smaller wheel diameter.

Chapter 4 furthermore presented a comparison between three different exhaust gas recirculation configurations: a high pressure, a low pressure, and a combined high and low pressure one. The turbocharger comprised a single stage, with a variable geometry turbine, and was resized to be optimal for the three different EGR configurations. The combined low and high-pressure configuration showed the highest brake efficiency, due to an overall higher compressor efficiency, which was made possible because the mass flow could be adjusted between the low and high pressure circuits.

Chapter 5 presented an optimization study, in which the maximum brake efficiency was simulated, for methanol and two gasoline fuels (RON $= 76$ and RON $= 97$). The high RON fuel was chosen because a higher RON typically facilitates partially premixed combustion. However, it has been shown that the combustion stability at

low loads typically reduces with high RON, and the maximum pressure rise rate increases. Therefore, the gasoline fuel with RON = 76 was chosen for a comparison. On the other hand, the use of renewables are arguably the fastest way to reduce the CO_2 emissions from heavy-duty vehicles. Consequently, methanol was chosen as it is the simplest fuel which can be produced from renewable sources and which is liquid (and of sufficient energy density) at atmospheric conditions. For the optimizations, constraints were put on the maximum cylinder pressure, maximum cylinder pressure rise rate, NO_x emissions, and soot emissions, as well as preventing water condensation. The optimization algorithm came from a group of meta-heuristic methods, called the particle swarm, which was chosen because of the complex relationships between the engine parameters and their effect on the engine performance. In addition, the engine compression ratio was optimized for methanol, leading to four investigated cases. The highest brake efficiency was obtained for methanol with the optimized compression ratio, followed by methanol with standard compression ratio, while the brake efficiencies for the two gasoline fuels were the lowest. The reason for a higher brake efficiency for methanol, was due to an improved compromise between combustion duration, in-cylinder heat transfer, and NO_x emissions. Moreover, an increased cooling of the bulk gas reduced the compression work. Finally, because less EGR was needed to suppress NO_x emissions, the ratio of specific heats was often higher for methanol, despite methanol requiring a higher inlet temperature.

Despite dissimilar boundary conditions, the most noticeable difference between the cases with methanol and the gasoline fuels, was found in the resulting fuel injection strategy. For methanol, it was possible to use a significantly earlier start of injection, while the gasoline fuels had to be injected closer to top dead center, for a larger part of the tested engine operating points. In fact, a positive ignition dwell was not shown to be optimal for the gasoline fuels in any of the operating points. In contrast, this could be achieved for the cases with methanol. A sensitivity study of the optimization constraints revealed that neither a higher air-fuel ratio nor a reduced intake manifold, led to a positive ignition dwell for the gasoline cases. On the other hand, a higher air-fuel ratio led to a reduced brake efficiency, while a lower intake manifold temperature led to an increased one. Additionally, the removal of the constraint on pressure rise rate was investigated for the gasoline fuel with the highest research octane number. A higher pressure rise rate allowed for 40 % of the fuel to be injected before the start of combustion and enabled a higher brake efficiency. Still, a positive ignition dwell was not achieved which was the definition, used in this thesis, for partially premixed combustion. As the maximum pressure rise rate typically increases with engine load, due to a lower degree of dilution, it is possible that the operating points with 25 % and 50 % load would facilitate partially premixed combustion if the constraint on pressure rise rate was set to a higher value.

An injection strategy with relatively early start of injection timings (–70°ca aTDC to –50°ca aTDC), was found to be optimum in all operating points with methanol. It is likely that the umbrella angle of the injector needs to be made very narrow in order to avoid high amounts of unburned hydrocarbon and CO emissions due to partially oxidized fuel which is stuck in various crevice volumes. Moreover, a sensitivity analysis, presented in this work, revealed that the sensitivity of combustion stability to inlet conditions was high. For instance, for the A75 operating point, the combustion phasing changed by 15°ca for a change in the inlet temperature of 12 K. In addition, the maximum in-cylinder pressure exceeded 300 bar for the earliest combustion phasing. Finally, the results suggested that this sensitivity increased with engine load.

In Chapter 6, emissions formation were simulated in a constant pressure, homogeneous reactor, in order to study the potential levels of soot, NO_x, CO, and CO_2 emissions, from methanol and a gasoline fuel. The results showed that methanol does not form soot at typical engine conditions. Contrastingly the gasoline fuel, due to its aromatic content, had a large propensity for soot formation. Moreover, the ignition delay time as a function of temperature and equivalence ratio, was simulated for both fuels. The results of emissions formation and ignition delay time, facilitated and extended the analysis on the results from Chapter 5, by enabling a depiction of the stochastic reactor model particle trajectories, in the temperature and equivalence ratio domain. This analysis showed that thermal stratification, due to vaporization cooling, can reduce the pressure rise rates for methanol. Furthermore, this could be used to explain why the optimal injection timing, for methanol, was as early as –70°ca aTDC. In the case of gasoline, thermal stratification did not play a role, instead the pressure rise rate was only influenced by the global level of dilution.

7.2 Outlook

The following are several recommendations for further study based on the results presented in this thesis.

The results in Chapter 4 suggested a mismatch between the compressor and turbine wheel diameters. Thus, designing a turbocharger aimed for partially premixed combustion could potentially increase the gas exchange efficiency and allow for higher dilution levels. On the other hand, the optimum boundary conditions, found in Chapter 5, for the engine when it was run on methanol, differed significantly from the ones with gasoline. Moreover, the turbocharger used in these optimizations was not chosen for the conditions which were found optimum with methanol. Thus, a redesign of the turbocharger to use with methanol would also warrant an investigation.

The results found in Chapter 5 require validation and verification. This can be done experimentally or with higher fidelity models such as 3-D computational fluid dynamics (CFD). Especially, the early injection strategies which were found optimal with methanol, should be verified. A CFD model could be used to validate the vaporization of the fuel and the mixing model used with the stochastic reactor model. Initial CFD simulations have been conducted which suggest that the stochastic reactor model achieves a good prediction of the mixing, but also show that the results depend greatly on the chosen spray model parameters in the CFD model. Additionally, the optimum injector umbrella angle could be found with a CFD simulation and then used to investigate the trade-off between start of injection timing and combustion efficiency.

Further investigation needs to be conducted to verify the large sensitivity of the combustion stability to inlet conditions when the engine is run with early start of injection timings and methanol. If the sensitivity is as large as suggested from the results in this thesis, algorithms for improved control of the inlet conditions are required.

It was hypothesized in Chapter 5 that the reason for not obtaining partially premixed combustion with the gasoline fuel, could have been that the soot emissions were not modeled explicitly. The kinetic model used in Chapter 6 could be applied and combined with the stochastic reactor model and the optimization algorithm, to investigate this hypothesis. Naturally, such an investigation would need verification and validation against measured soot emissions before conducting the optimizations. As the kinetic model is large, the tabulation technique described in [104], could be utilized and enable a significant reduction of the total simulation time needed.

Appendix

Table A1: Experimental data from the heavy-duty multi cylinder Scania diesel engine. Engine compression ratio (ε), engine speed (n), gross imep ($\text{imep}_{\text{gross}}$), intake manifold temperature (T_{im}), intake manifold pressure (p_{im}), normalized air-fuel-ratio (λ), EGR, crank angle at which 50 % of the fuel has burned (θ_{50}), and start of injection (θ^1_{soi}).

	ε (-)	n (rpm)	$\text{imep}_{\text{gross}}$ (bar)	T_{im} (K)	p_{im} (bar)	λ (-)	EGR (%)	θ_{50} (°ca)	θ^1_{soi} (°ca)
1	17.3	1300	5	297	1.24	1.9	49	5.5	-30
2	17.3	1300	8	295	1.54	1.5	46	8.5	-24
3	17.3	1300	10	296	1.77	1.3	47	6.6	-10
4	17.3	1300	12	296	2.03	1.5	42	5.9	-9
5	17.3	1300	13	296	2.18	1.5	44	5.7	-9
6	17.3	1300	15	295	2.42	1.4	44	5.9	-10
7	17.3	1300	19	295	2.89	1.2	45	8	-8
8	17.3	1400	5	294	1.21	1.7	53	7.5	-35
9	17.3	1400	7	295	1.3	1.3	51	8.4	-35
10	17.3	1400	10	294	1.62	1.3	47	6.4	-37
11	17.3	1400	13	294	1.97	1.2	47	5.9	-37
12	17.3	1400	19	295	2.52	1.3	42	5.7	-10
13	17.3	1600	5	296	1.27	1.8	50	6.4	-24
14	17.3	1600	8	296	1.49	1.4	49	6.6	-18
15	17.3	1600	10	296	1.81	1.5	50	6.1	-16
16	17.3	1600	13	295	2.19	1.4	46	5.6	-12
17	17.3	1600	16	295	2.45	1.2	47	5.6	-12

Table A2: Experimental data from the heavy-duty single cylinder Scania D13 engine. Engine compression ratio (ε), engine speed (n), gross imep ($\text{imep}_{\text{gross}}$), intake manifold temperature (T_{im}), intake manifold pressure (p_{im}), normalized air-fuel-ratio (λ), EGR, crank angle at which 50 % of the fuel has burned (θ_{50}), and start of injection θ^1_{soi}.

	ε (-)	n (rpm)	$\text{imep}_{\text{gross}}$ (bar)	T_{im} (K)	p_{im} (bar)	λ (-)	EGR (%)	θ_{50} (°ca)	θ^1_{soi} (°ca)
1	17.3	1250	10.3	428	2.84	2.0	33	5.7	-9.8
2	17.3	1250	10.3	429	2.62	1.8	35	5.4	-10.4
3	17.3	1250	9.4	438	1.85	1.3	34	6.5	-10.4
4	17.3	1250	10.4	428	2.89	1.7	43	5.3	-10.6
5	17.3	1250	10.1	428	2.53	1.6	42	6.0	-10.0

Table A2 continued from previous page

	ε (-)	n (rpm)	$imep_{gross}$ (bar)	T_{im} (K)	p_{im} (bar)	λ (-)	EGR (%)	θ_{50} (°ca)	θ^1_{soi} (°ca)
6	17.3	1250	8.9	437	1.92	1.2	44	6.1	-12.6
7	17.3	1250	10.0	416	2.75	1.5	54	6.0	-10.0
8	17.3	1250	9.6	429	2.65	1.3	53	5.9	-12.0
9	17.3	1250	8.8	435	1.97	1.1	53	6.3	-18.0
10	17.3	800	5.2	464	1.04	2.0	0	6.6	-11.9
11	17.3	800	5.4	453	1.31	2.5	0	6.4	-9.0
12	17.3	800	5.4	445	1.51	3.0	0	6.5	-8.0
13	17.3	800	5.3	440	1.76	3.5	0	6.4	-6.8
14	17.3	800	5.3	435	2.03	4.1	0	6.8	-5.6
15	17.3	800	15.2	426	2.97	2.0	0	8.6	0.0
16	17.3	800	15.3	428	2.65	1.8	0	8.9	0.0
17	17.3	800	15.5	431	2.44	1.6	0	9.0	-0.2
18	17.3	800	15.4	432	2.23	1.4	0	9.2	-0.4
19	17.3	800	14.8	435	2.04	1.2	0	9.4	-0.4
20	17.3	1600	5.2	436	1.00	2.0	0	7.2	-12.9
21	17.3	1600	5.2	428	1.21	2.6	0	7.2	-12.9
22	17.3	1600	5.2	426	1.41	3.0	0	6.7	-12.5
23	17.3	1600	5.3	421	1.63	3.5	0	6.8	-11.7
24	17.3	1600	5.3	419	1.89	4.1	0	6.9	-10.8
25	17.3	1200	6.8	391	2.27	4.1	0	8.9	-12.0
26	17.3	1200	6.4	409	2.09	3.9	0	7.0	-14.0
27	27	1200	6.3	321	1.05	2.0	0	8.6	-3.8
28	27	1200	6.4	326	1.37	2.0	26	6.3	-6.4
29	27	1200	6.3	329	1.38	2.0	27	10.8	-2.8
30	27	1200	6.3	330	1.15	1.6	29	5.8	-10.0
31	27	1200	6.3	338	1.20	1.6	29	9.9	-5.8
32	27	1200	6.3	340	1.24	1.6	29	6.3	-5.4
33	27	1200	6.4	334	1.22	1.6	28	10.8	-1.4
34	27	1200	6.3	337	1.19	1.6	27	8.2	-4.8
35	27	1200	6.5	337	1.78	1.6	54	8.3	-4.4
36	27	1200	6.3	334	1.40	1.2	55	7.4	-6.6
37	15	1200	6.3	457	1.85	1.3	52	4.9	-16.0
38	15	1200	6.2	478	1.85	1.3	52	4.8	-13.0
39	15	1200	6.4	472	1.85	1.4	50	6.1	-13.0
40	15	1200	6.4	475	1.84	1.4	50	5.7	-12.0
41	15	1200	6.4	475	1.85	1.4	51	5.9	-11.0
42	15	1200	6.4	477	1.85	1.4	50	6.0	-14.0
43	15	1200	6.4	464	1.86	1.6	46	5.8	-15.0
44	15	1200	6.2	470	1.85	1.6	46	5.9	-12.0
45	15	1200	6.0	478	1.85	1.6	45	5.8	-10.0
46	15	1200	5.9	486	1.84	1.6	45	5.6	-9.0
47	15	1200	6.4	480	1.85	2.7	0	6.6	-5.5
48	15	1200	6.5	481	1.85	2.7	0	6.4	-5.5
49	15	1200	6.6	481	1.85	2.4	10	6.4	-5.5
50	15	1200	6.4	479	1.85	2.0	30	6.2	-6.5
51	15	1200	6.3	478	1.85	2.2	23	6.6	-6.0
52	15	1200	6.3	479	1.85	1.8	36	6.0	-7.5

Table A2 continued from previous page

	ε (-)	n (rpm)	$\text{imep}_{\text{gross}}$ (bar)	T_{im} (K)	p_{im} (bar)	λ (-)	EGR (%)	θ_{50} (°ca)	θ^{1}_{soi} (°ca)
53	15	1200	6.4	480	1.85	1.7	38	6.4	-7.5
54	15	1200	6.3	477	1.85	1.7	42	6.3	-8.5
55	15	1200	6.2	477	1.85	1.6	45	6.0	-9.5
56	15	1200	6.3	478	1.85	1.5	48	5.7	-10.5
57	15	1200	6.4	474	1.85	1.4	51	5.2	-13.0
58	15	1200	6.6	466	1.85	1.2	54	5.4	-17.5
59	15	1200	13.1	434	2.00	1.5	0	4.7	-12.5
60	15	1200	13.2	434	2.00	1.4	8	4.9	-12.5
61	15	1200	13.2	433	2.00	1.3	13	4.4	-13.0
62	15	1200	13.2	432	2.01	1.2	20	3.8	-13.5
63	15	1200	12.8	432	1.99	1.1	25	3.6	-13.5
64	15	1200	12.4	434	1.99	1.1	30	3.4	-14.0
65	15	1200	9.6	483	1.85	1.8	0	7.0	-15.0
66	15	1200	9.6	478	1.85	1.7	11	7.1	-15.0
67	15	1200	9.6	479	1.85	1.6	16	7.2	-15.0
68	15	1200	9.5	479	1.85	1.4	24	7.6	-15.0
69	15	1200	9.5	477	1.85	1.3	30	7.9	-15.0
70	15	1200	9.4	477	1.85	1.2	33	8.2	-15.0
71	15	1200	9.2	477	1.85	1.1	38	8.6	-15.0
72	15	1200	6.3	482	1.85	2.8	0	6.2	-6.0
73	17.3	1200	4.8	397	2.00	5.7	0	5.5	-10.0
74	17.3	1200	5.0	383	2.00	5.7	0	5.5	-20.0
75	17.3	1200	4.9	380	2.00	5.5	0	5.5	-30.0
76	17.3	1200	4.4	391	2.00	6.0	0	5.5	-40.0
77	17.3	1200	4.1	399	2.00	6.1	0	5.5	-60.0
78	17.3	1200	4.3	390	2.00	5.9	0	5.5	-80.0

References

[1] Leo Meyer, Sander Brinkman, Line van Kesteren, Noëmie Leprince-Ringuet, et al. *IPCC, 2014: Climate Change 2014: Synthesis Report. Contribution of Working Groups I, II and III to the Fifth Assessment Report of the Intergovernmental Panel on Climate Change*. Tech. rep. Geneva, Switzerland, 2014, pp. 3–87.

[2] International Energy Agency. *CO2 Emissions from Fuel Combustion 2018*. 2018, p. 515.

[3] International Energy Agency. *Energy, Climate Change and Environment 2016 Insights*. Special Report. International Energy Agency, 2016, p. 133.

[4] Donald W. Stanton. *Systematic Development of Highly Efficient and Clean Engines to Meet Future Commercial Vehicle Greenhouse Gas Regulations*. 2013.

[5] Ingo Mikulic, Reggie Zhan, and Scott Eakle. "Dependence of Fuel Consumption on Engine Backpressure Generated by a DPF". In: *SAE 2010 World Congress & Exhibition*. SAE International, 2010.

[6] R H Thring. "Homogeneous-Charge Compression-Ignition (HCCI) Engines". In: *SAE Technical Paper*. SAE International, 1989.

[7] Magnus Christensen, Bengt Johansson, and Patrik Einewall. "Homogeneous Charge Compression Ignition (HCCI) Using Isooctane, Ethanol and Natural Gas - A Comparison with Spark Ignition Operation". In: *SAE Technical Paper*. SAE International, 1997.

[8] Jan-Ola Olsson, Per Tunestål, and Bengt Johansson. "Closed-Loop Control of an HCCI Engine". In: *SAE Technical Paper*. SAE International, 2001.

[9] Magnus Lewander, Bengt Johansson, Per Tunestål, Nathan Keeler, et al. "Evaluation of the Operating Range of Partially Premixed Combustion in a Multi Cylinder Heavy Duty Engine with Extensive EGR". In: *SAE Technical Paper*. SAE International, 2009.

[10] Christof Noehre, Magnus Andersson, Bengt Johansson, and Anders Hultqvist. "Characterization of Partially Premixed Combustion". In: *SAE Technical Paper*. SAE International, 2006.

[11] John E Dec. "Advanced compression-ignition engines understanding the in-cylinder processes". In: *Proceedings of the Combustion Institute* 32.2 (2009), pp. 2727–2742. ISSN: 1540-7489.

[12] Gautam T Kalghatgi, Per Risberg, and Hans-Erik Ångström. "Advantages of Fuels with High Resistance to Auto-ignition in Late-injection, Low-temperature, Compression Ignition Combustion". In: *Powertrain & Fluid Systems Conference and Exhibition*. SAE International, 2006.

[13] Gautam T Kalghatgi, Per Risberg, and Hans-Erik Ångström. "Partially Pre-Mixed Auto-Ignition of Gasoline to Attain Low Smoke and Low NOx at High Load in a Compression Ignition Engine and Comparison with a Diesel Fuel". In: *SAE Technical Paper*. SAE International, 2007.

[14] Gautam Kalghatgi, Leif Hildingsson, and Bengt Johansson. "Low NOx and Low Smoke Operation of a Diesel Engine Using Gasoline-Like Fuels". In: *ASME 2009 Internal Combustion Engine Division Spring Technical Conference*. ASME, 2009. ISBN: 978-0-7918-4340-6.

[15] Helgi Fridriksson, Bengt Sunden, Shahrokh Hajireza, and Martin Tuner. "CFD Investigation of Heat Transfer in a Diesel Engine with Diesel and PPC Combustion Modes". In: *SAE Technical Paper*. SAE International, 2011.

[16] Yu Zhang, Praveen Kumar, Yuanjiang Pei, Michael Traver, et al. "An Experimental and Computational Investigation of Gasoline Compression Ignition Using Conventional and Higher Reactivity Gasolines in a Multi-Cylinder Heavy-Duty Diesel Engine". In: *WCX World Congress Experience*. SAE International, 2018.

[17] Bishwadipa Das Adhikary, Rolf D Reitz, and Stephen Ciatti. "Study of In-Cylinder Combustion and Multi-Cylinder Light Duty Compression Ignition Engine Performance Using Different RON Fuels at Light Load Conditions". In: *SAE 2013 World Congress & Exhibition*. SAE International, 2013.

[18] Hadeel Solaka Aronsson, Martin Tuner, and Bengt Johansson. "Using Oxygenated Gasoline Surrogate Compositions to Map RON and MON". In: *SAE 2014 World Congress & Exhibition*. SAE International, 2014.

[19] Praveen Kumar, Yu Zhang, Michael Traver, and David Cleary. "Simulation-Guided Air System Design for a Low Reactivity Gasoline-Like Fuel under Partially-Premixed Combustion in a Heavy-Duty Diesel Engine". In: *WCX™17: SAE World Congress Experience*. SAE International, 2017.

[20] Christopher P Kolodziej, Mark Sellnau, Kukwon Cho, and David Cleary. "Operation of a Gasoline Direct Injection Compression Ignition Engine on Naphtha and E10 Gasoline Fuels". In: *SAE International Journal of Engines* 9.2 (2016), pp. 979–1001. ISSN: 1946-3944.

[21] Gautam Kalghatgi and Bengt Johansson. “Gasoline compression ignition approach to efficient, clean and affordable future engines”. In: *Proceedings of the Institution of Mechanical Engineers, Part D: Journal of Automobile Engineering* 232.1 (2018), pp. 118–138.

[22] George A Olah. “Beyond Oil and Gas: The Methanol Economy”. In: *Angewandte Chemie International Edition* 44.18 (2005), pp. 2636–2639. ISSN: 1521-3773.

[23] Sebastian Verhelst, James W G Turner, Louis Sileghem, and Jeroen Vancoillie. “Methanol as a fuel for internal combustion engines”. In: *Progress in Energy and Combustion Science* 70 (2019), pp. 43–88. ISSN: 0360-1285.

[24] Magnus Lewander, Bengt Johansson, and Per Tunestål. “Investigation and Comparison of Multi Cylinder Partially Premixed Combustion Characteristics for Diesel and Gasoline Fuels”. In: *SAE International Powertrains, Fuels and Lubricants Meeting*. SAE International, 2011.

[25] Takeyuki Kamimoto and Myurng-hoan Bae. “High Combustion Temperature for the Reduction of Particulate in Diesel Engines”. In: *SAE Technifcal Paper*.

[26] Kazuhiro Akihama, Yoshiki Takatori, Kazuhisa Inagaki, Shizuo Sasaki, et al. “Mechanism of the Smokeless Rich Diesel Combustion by Reducing Temperature”. In: *SAE Technical Paper 2001-01-0655*. 2001.

[27] Henrik Salsing, Valeri Golovitchev, and Ingemar Denbratt. “Numerical Analysis of Combustion and Emissions Formation in a Heavy Duty DME Engine”. In: *SAE Technical Paper 2012-01-0156*. 2012.

[28] Lars Seidel. “Development and reduction of a multicomponent reference fuel for gasoline”. Doctoral thesis. BTU Cottbus - Senftenberg, 2017.

[29] Guillaume Lequien, Öivind Andersson, Per Tunestål, and Magnus Lewander. “A Correlation Analysis of the Roles of Soot Formation and Oxidation in a Heavy-Duty Diesel Engine”. In: *SAE/KSAE 2013 International Powertrains, Fuels & Lubricants Meeting*. SAE International, 2013.

[30] John E Dec. “A Conceptual Model of DI Diesel Combustion Based on Laser-Sheet Imaging*”. In: *SAE Technical Paper*. SAE International, 1997.

[31] Ming Zheng, Graham T Reader, and J.Gary Hawley. “Diesel engine exhaust gas recirculation—a review on advanced and novel concepts”. In: *Energy Conversion and Management* 45.6 (2004), pp. 883–900. ISSN: 0196-8904.

[32] J Thangaraja and C Kannan. “Effect of exhaust gas recirculation on advanced diesel combustion and alternate fuels - A review”. In: *Applied Energy* 180 (2016), pp. 169–184. ISSN: 0306-2619.

[33] N Ladommatos, S Abdelhalim, and H Zhao. "The effects of exhaust gas recirculation on diesel combustion and emissions". In: *International Journal of Engine Research* 1.1 (2000), pp. 107–126.

[34] Magnus Lewander, Kent Ekholm, Bengt Johansson, Per Tunestål, et al. *Investigation of the Combustion Characteristics with Focus on Partially Premixed Combustion in a Heavy Duty Engine*. 2008.

[35] Mengqin Shen, Martin Tuner, Bengt Johansson, and William Cannella. "Effects of EGR and Intake Pressure on PPC of Conventional Diesel, Gasoline and Ethanol in a Heavy Duty Diesel Engine". In: *SAE Technical Paper*. SAE International, 2013.

[36] Magnus Sjöberg, John E. Dec, and Wontae Hwang. "Thermodynamic and Chemical Effects of EGR and Its Constituents on HCCI Autoignition". In: *SAE World Congress & Exhibition*. SAE International, 2007.

[37] Christopher Chadwell, Terrence Alger, Charles Roberts, and Steven Arnold. "Boosting Simulation of High Efficiency Alternative Combustion Mode Engines". In: *SAE Int. J. Engines* 4 (2011), pp. 375–393.

[38] Nhut Lam, Per Tunestål, and Arne Andersson. "Analyzing Factors Affecting Gross Indicated Efficiency When Inlet Temperature Is Changed". In: *International Powertrains, Fuels & Lubricants Meeting*. SAE International, 2018.

[39] Morteza Fathi, Rahim Khoshbakhti Saray, Mohsen Pourfallah, Javad Kheyrollahi, et al. "EGR and Intake Charge Temperature Effects on Dual-Fuel HCCI Combustion and Emissions Characteristics". In: *10th International Conference on Engines & Vehicles*. SAE International, 2011.

[40] José Ramón Serrano, Pedro Piqueras, Emanuele Angiolini, Cesare Meano, et al. "On Cooler and Mixing Condensation Phenomena in the Long-Route Exhaust Gas Recirculation Line". In: *SAE Technical Paper*. SAE International, 2015.

[41] Gabriel Ingesson, Lianhao Yin, Rolf Johansson, and Per Tunestål. "A Double-Injection Control Strategy For Partially Premixed Combustion". In: *IFAC-PapersOnLine* 49.11 (2016), pp. 353–360. ISSN: 2405-8963.

[42] Kenan Muric, Per Tunestål, and Ingemar Magnusson. "Medium and High Load Performance of Partially Premixed Combustion in a Wave-Piston Multi-Cylinder Engine With Diesel and PRF70 Fuel". In: *Volume 1: Large Bore Engines; Fuels; Advanced Combustion*. ASME, 2018, V001T03A005. ISBN: 978-0-7918-5198-2.

[43] Stena Line. *Stena Line launches the world's first methanol ferry*. 2015. URL: http://news.stenaline.co.uk/pressreleases/stena-line-launches-the-world-s-first-methanol-ferry-1137516.

[44] Lennart Haraldson. *Methanol as fuel*. Methanol as Fuel & Energy Storage Workshop. 2015.

[45] MAN. *MAN demonstrates two-stroke methanol engine*. 2015. URL: http://www.motorship.com/news101/engines-and-propulsion/man-demonstrates-two-stroke-methanol-engine.

[46] Hao Chen, Lu Yang, Peng-hui Zhang, and Andrew Harrison. "The controversial fuel methanol strategy in China and its evaluation". In: *Energy Strategy Reviews* 4 (2014), pp. 28–33. ISSN: 2211-467X.

[47] Matthew Brusstar, Mark Stuhldreher, David Swain, and William Pidgeon. "High Efficiency and Low Emissions from a Port-Injected Engine with Neat Alcohol Fuels". In: *SAE Technical Paper*. SAE International, 2002.

[48] Matthew J Brusstar and Charles L Gray. "High Efficiency with Future Alcohol Fuels in a Stoichiometric Medium Duty Spark Ignition Engine". In: *Powertrain & Fluid Systems Conference and Exhibition*. SAE International, 2007.

[49] James P. Szybist, Kalyana Chakravathy, and C. Stuart Daw. "Analysis of the Impact of Selected Fuel Thermochemical Properties on Internal Combustion Engine Efficiency". In: *Energy & Fuels* 26.5 (2012), pp. 2798–2810. eprint: https://doi.org/10.1021/ef2019879.

[50] Gregory Roberts, Bernard Johnson, and Chris Edwards. "Prospects for High-Temperature Combustion, Neat Alcohol-Fueled Diesel Engines". In: *SAE International Journal of Engines* 7.1 (2014), pp. 448–457. ISSN: 1946-3944.

[51] Sam Shamun, Maja Novakovic, Vilhelm B Malmborg, Calle Preger, et al. "Detailed Characterization of Particulate Matter in Alcohol Exhaust Emissions". In: *The Proceedings of the International symposium on diagnostics and modeling of combustion in internal combustion engines* 2017.9 (2017), B304.

[52] Sam Shamun, Mengqin Shen, Bengt Johansson, Martin Tuner, et al. "Exhaust PM Emissions Analysis of Alcohol Fueled Heavy-Duty Engine Utilizing PPC". In: *SAE International Journal of Engines* 9.4 (2016), pp. 2142–2152. ISSN: 1946-3944.

[53] Sam Shamun, Can Hasimoglu, Ahmet Murcak, Öivind Andersson, et al. "Experimental investigation of methanol compression ignition in a high compression ratio HD engine using a Box-Behnken design". In: *Fuel* 209 (2017), pp. 624–633. ISSN: 0016-2361.

[54] Gamma Technologies LLC. *GT SUITE v2018*. https://www.gtisoft.com/gt-suite/gt-suite-overview/.

[55] D A Kouremenos, C D Rakopoulos, D T Hountalas, and T K Zannis. "Development of a Detailed Friction Model to Predict Mechanical Losses at Elevated Maximum Combustion Pressures". In: *SAE Technical Paper*. SAE International, 2001.

[56] Thomas Morel and Rifat Keribar. "A Model for Predicting Spatially and Time Resolved Convective Heat Transfer in Bowl-in-Piston Combustion Chambers". In: *SAE Technical Paper*. SAE International, 1985.

[57] Stijn Broekaert. "A study of the heat transfer in low temperature combustion engines". PhD thesis. Ghent University, 2018, p. 252. ISBN: 978-94-6355-091-8.

[58] Günter F Hohenberg. "Advanced Approaches for Heat Transfer Calculations". In: *1979 SAE International Off-Highway and Powerplant Congress and Exposition*. SAE International, 1979.

[59] Lianhao Yin, Gabriel Ingesson, Per Tunestål, Rolf Johansson, et al. "An Experimental Investigation of a Multi-Cylinder Engine with Gasoline-Like Fuel towards a High Engine Efficiency". In: *SAE Technical Paper*. SAE International, 2016.

[60] Lianhao Yin, Gabriel Ingesson, Rolf Johansson, Per Tunestål, et al. "Partially premixed combustion multi-cylinder engine cycle-to-cycle-oriented temperature estimation and control". In: *International Journal of Powertrains* 6.1 (2017), p. 5. ISSN: 1742-4267.

[61] Gabriel Ingesson, Lianhao Yin, Rolf Johansson, and Per Tunestål. "Simultaneous Control of Combustion Timing and Ignition Delay in Multi-Cylinder Partially Premixed Combustion". In: *SAE Int. J. Engines* 8 (2015), pp. 2089–2098.

[62] Gabriel Ingesson, Lianhao Yin, Rolf Johansson, and Per Tunestål. "Evaluation of Nonlinear Estimation Methods for Calibration of a Heat-Release Model". In: *SAE International Journal of Engines* 9.2 (2016), pp. 1191–1200. ISSN: 1946-3944.

[63] Changle Li, Lianhao Yin, Sam Shamun, Martin Tuner, et al. "Transition from HCCI to PPC: the Sensitivity of Combustion Phasing to the Intake Temperature and the Injection Timing with and without EGR". In: *SAE 2016 World Congress and Exhibition*. SAE International, 2016.

[64] Andrew Smallbone, Amit Bhave, Aaron R. Coble, Sebastian Mosbach, et al. "Identifying Optimal Operating Points in Terms of Engineering Constraints and Regulated Emissions in Modern Diesel Engines". In: *SAE 2011 World Congress & Exhibition*. SAE International, 2011.

[65] Andrew Smallbone, Amit Bhave, Michael Hillman, Allan Saville, et al. "Virtual Performance and Emissions Mapping for Diesel Engine Design Optimization". In: *SAE 2013 World Congress & Exhibition*. SAE International, 2013.

[66] Guillaume Bernard, Mark Scaife, Amit Bhave, David Ooi, et al. "Application of the SRM Engine Suite over the Entire Load-Speed Operation of a U.S. EPA Tier 4 Capable IC Engine". In: *SAE 2016 World Congress and Exhibition*. SAE International, 2016.

[67] LOGE AB. *LOGEsoft*. http://logesoft.com/loge-software/.

[68] J. Janicka, W. Kolbe, and W. Kollmann. "Closure of the Transport Equation for the Probability Density Funcfion of Turbulent Scalar Fields". In: *Journal of Non-Equilibrium Thermodynamics* 4.1 (1979), pp. 47–66. ISSN: 0340-0204.

[69] Tim Franken, Arnd Sommerhoff, Werner Willems, Andrea Matrisciano, et al. "Advanced Predictive Diesel Combustion Simulation Using Turbulence Model and Stochastic Reactor Model". In: *WCX™17: SAE World Congress Experience*. SAE International, 2017.

[70] Michal Pasternak, Fabian Mauss, Cathleen Perlman, and Harry Lehtiniemi. "Aspects of 0D and 3D Modeling of Soot Formation for Diesel Engines". In: *Combustion Science and Technology* 186.10-11 (2014), pp. 1517–1535. eprint: https://doi.org/10.1080/00102202.2014.935213.

[71] Michal Pasternak, Fabian Mauss, and Henry Bensler. "Diesel Engine Cycle Simulation with a Reduced Set of Modeling Parameters Based on Detailed Kinetics". In: *SAE Technical Paper*. SAE International, 2009.

[72] Michal Pasternak, Fabian Mauss, Gábor Janiga, and Dominique Thévenin. "Self-Calibrating Model for Diesel Engine Simulations". In: *SAE Technical Paper*. SAE International, 2012.

[73] Michal Pasternak, Fabian Mauss, Christian Klauer, and Andrea Matrisciano. "Diesel engine performance mapping using a parametrized mixing time model". In: *International Journal of Engine Research* 19.2 (2018), pp. 202–213. ISSN: 1468-0874.

[74] Tim Franken and Fabian Mauss. "Development of Methodology for Predictive Diesel Combustion Simulation Using 0D Stochastic Reactor Model". In: 2016.

[75] Martin Tunér, Karin Frojd, Lars Seidel, and Fabian Mauss. "Diesel-PPC engine: Predictive Full Cycle Modeling with Reduced and Detailed Chemistry". In: *SAE Technical Paper*. 2011.

[76] Peter Kozuch. "Phenomenological model for a combined nitric oxide and soot emission calculation in DI diesel engines". Ph.D. Thesis. University of Stuttgart.

[77] *AramcoMech 2.0 Chemical Mechanism*. URL: http://www.nuigalway.ie/c3/aramco2/frontmatter.html.

[78] Hu Wang, Adam B Dempsey, Mingfa Yao, Ming Jia, et al. "Kinetic and Numerical Study on the Effects of Di-tert-butyl Peroxide Additive on the Reactivity of Methanol and Ethanol". In: *Energy & Fuels* 28.8 (2014), pp. 5480–5488.

[79] Y B Zel'dovich. "The Oxidation of Nitrogen in Combustion Explosions". In: *Acta Physicochimica U.S.S.R.* 21 (1946), pp. 577–628.

[80] Leilei Xu, Xue-Song Bai, Ming Jia, Yong Qian, et al. "Experimental and modeling study of liquid fuel injection and combustion in diesel engines with a common rail injection system". In: *Applied Energy* 230 (2018), pp. 287–304. ISSN: 0306-2619.

[81] H. Saravanamuttoo, G. Rogers, H. Cohen, and P. Straznicky. *Gas Turbine Theory*. 2009. Chap. 2.

[82] Martin Tuner. "Potential ESC Performance of a Multi-Cylinder Heavy Duty PPC Truck Engine: System Simulations based on Single Cylinder Experiments". In: *SAE Technical Paper*. SAE International, 2013.

[83] Benedikt Ernst, Jasper Kammeyer, and Joerg R. Seume. "Improved Map Scaling Methods for Small Turbocharger Compressors". In: *Volume 3: Controls, Diagnostics and Instrumentation; Education; Electric Power; Microturbines and Small Turbomachinery; Solar Brayton and Rankine Cycle*. ASME, 2011, pp. 733–744. ISBN: 978-0-7918-5463-1.

[84] Borislav Sirakov and Michael Casey. "Evaluation of Heat Transfer Effects on Turbocharger Performance". In: *Journal of Turbomachinery* 135.2 (2012), p. 021011. ISSN: 0889-504X.

[85] José Ramón Serrano, Pablo Olmeda, Francisco J. Arnau, Artem Dombrovsky, et al. "Turbocharger heat transfer and mechanical losses influence in predicting engines performance by using one-dimensional simulation codes". In: *Energy* 86 (2015), pp. 204–218. ISSN: 0360-5442.

[86] John B Heywood. *Internal Combustion Engine Fundamentals*. McGraw Hill Book Co.

[87] N Watson and M S Janota. *Turbocharging the internal combustion engine*. Macmillan; Wiley London: New York, 1982. ISBN: 0333242904.

[88] Hiereth H. and Prenninger P. *Charging the Internal Combustion Engine*. Springer-Verlag Wien, 2007. ISBN: 978-3-211-33033-3.

[89] Hany Moustapha, Mark F. Zelesky, Nicholas C. Baines, and David Japikse. *Axial and Radial Turbines*. Concepts NREC, 2003. ISBN: 0-933283-12-0.

[90] Bernhardt Lüddecke, Dietmar Filsinger, and Jan Ehrhard. "On Mixed Flow Turbines for Automotive Turbocharger Applications". In: *International Journal of Rotating Machinery* 2012 (2012), pp. 1–14. ISSN: 1023-621X.

[91] Carl Fredriksson and Nick Baines. "The Mixed Flow Forward Swept Turbine for Next Generation Turbocharged Downsized Automotive Engines". In: *Volume 5: Industrial and Cogeneration; Microturbines and Small Turbomachinery; Oil and Gas Applications; Wind Turbine Technology*. ASME, 2010, pp. 559–563. ISBN: 978-0-7918-4400-7.

[92] Bin Mao, Mingfa Yao, Zunqing Zheng, Yongzhi Li, et al. "Effects of Dual Loop EGR on Performance and Emissions of a Diesel Engine". In: *SAE Technical Paper*. SAE International, 2015.

[93] Bin Mao, Mingfa Yao, Zunqing Zheng, and Haifeng Liu. "Effects of Dual Loop EGR and Variable Geometry Turbocharger on Performance and Emissions of a Diesel Engine". In: *SAE Technical Paper*. SAE International, 2016.

[94] Giorgio Zamboni, Simone Moggia, and Massimo Capobianco. "Hybrid EGR and turbocharging systems control for low NOX and fuel consumption in an automotive diesel engine". In: *Applied Energy* 165 (2016), pp. 839–848. ISSN: 0306-2619.

[95] James E. Anderson, Thomas G. Leone, Michael H. Shelby, Timothy J. Wallington, et al. "Octane Numbers of Ethanol-Gasoline Blends: Measurements and Novel Estimation Method from Molar Composition". In: *SAE 2012 World Congress & Exhibition*. SAE International, 2012.

[96] Andy Yates, Arthur Bell, and Andre Swarts. "Insights relating to the autoignition characteristics of alcohol fuels". In: *Fuel* 89.1 (2010), pp. 83 –93. ISSN: 0016-2361.

[97] Paul C Miles and Öivind Andersson. "A review of design considerations for light-duty diesel combustion systems". In: *International Journal of Engine Research* 17.1 (2016), pp. 6–15.

[98] DieselNet. *European Stationary Cycle (ESC)*. URL: https://dieselnet.com/standards/cycles/esc.php.

[99] Mengqin Shen, Martin Tuner, and Bengt Johansson. "Close to Stoichiometric Partially Premixed Combustion -The Benefit of Ethanol in Comparison to Conventional Fuels". In: *SAE Technical Paper*. SAE International, 2013.

[100] Carl Magnus Lewander, Bengt Johansson, and Per Tunestål. "Extending the Operating Region of Multi-Cylinder Partially Premixed Combustion using High Octane Number Fuel". In: *SAE 2011 World Congress & Exhibition*. SAE International, 2011.

[101] James Kennedy. "Particle Swarm Optimization". In: *Encyclopedia of Machine Learning*. Ed. by Claude Sammut and Geoffrey I Webb. Boston, MA: Springer US, 2010, pp. 760–766. ISBN: 978-0-387-30164-8.

[102] Bruno Walter and Bertrand Gatellier. "Development of the High Power NADI™Concept Using Dual Mode Diesel Combustion to Achieve Zero NOx and Particulate Emissions". In: *Spring Fuels & Lubricants Meeting & Exhibition*. SAE International, 2002.

[103] Yong Sun and Rolf D. Reitz. "Adaptive Injection Strategies (AIS) for Ultra-Low Emissions Diesel Engines". In: *SAE World Congress & Exhibition*. SAE International, 2008.

[104] Andrea Matrisciano, Tim Franken, Cathleen Perlman, Anders Borg, et al. "Development of a Computationally Efficient Progress Variable Approach for a Direct Injection Stochastic Reactor Model". In: *WCX™17: SAE World Congress Experience*. SAE International, 2017.

[105] Sang-Kyu Kim, Tomoyuki Wakisaka, and Yujo Aoyagi. "A numerical study of the effects of boost pressure and exhaust gas recirculation ratio on the combustion process and exhaust emissions in a diesel engine". In: *International Journal of Engine Research* 8.2 (2007), pp. 147–162.

[106] Corinna Netzer, Lars Seidel, Michal Patsernak, Christian Klauer, et al. "Impact of Gasoline Octane Rating on Engine Knock using Detailed Chemistry and a Quasi-dimensional Stochastic Reaktior Model". In: *Digital Proceedings of the 8th European Combustion Meeting (ECM 2017), Dubrovnik, Croatia*. 2017, pp. 493 –498.

[107] LOGE AB. *Manual Book 1 "Thermodynamic and Chemical Kinetics"*. LOGE AB.

[108] Erik Svensson, Changle Li, Sam Shamun, Bengt Johansson, et al. "Potential Levels of Soot, NO_x , HC and CO for Methanol Combustion". In: 2016.

[109] Magnus Sjöberg, John E. Dec, and Nicholas P. Cernansky. "Potential of Thermal Stratification and Combustion Retard for Reducing Pressure-Rise Rates in HCCI Engines, Based on Multi-Zone Modeling and Experiments". In: *SAE 2005 World Congress & Exhibition*. SAE International, 2005.

[110] Magnus Sjöberg, John E. Dec, Aristotelis Babajimopoulos, and Dennis N. Assanis. "Comparing Enhanced Natural Thermal Stratification Against Retarded Combustion Phasing for Smoothing of HCCI Heat-Release Rates". In: *2004 Powertrain & Fluid Systems Conference & Exhibition*. SAE International, 2004.

[111] R. E. Herold and J. B. Ghandhi. "Investigation of Bulk In-Cylinder Stratification with Split Intake Runners". In: *Powertrain & Fluid Systems Conference and Exhibition*. SAE International, 2007.

[112] B. Thirouard, J. Cherel, and V. Knop. “Investigation of Mixture Quality Effect on CAI Combustion”. In: *SAE 2005 World Congress & Exhibition*. SAE International, 2005.

[113] John E. Dec, Wontae Hwang, and Magnus Sjöberg. “An Investigation of Thermal Stratification in HCCI Engines Using Chemiluminescence Imaging”. In: *SAE 2006 World Congress & Exhibition*. SAE International, 2006.

[114] Magnus Sjöberg and John E. Dec. *Smoothing HCCI Heat Release with Vaporization-Cooling-Induced Thermal Stratification using Ethanol*. 2011.

Summary of Papers

Paper I: Evaluation of Different Turbocharger Configurations for a Heavy-Duty Partially Premixed Combustion Engine

E. Svensson, L. Yin, P. Tunestål, M. Thern, M. Tunér

SAE International Journal of Engines vol. 10, no. 5 (2017)

This paper evaluated the performance of four different turbochargers while applying the partially premixed combustion concept to a heavy-duty compression ignition engine. The multi cylinder engine model, which is presented in Chapter 3, was used in all simulations to predict the gas dynamic phenomena while rate of heat release profiles were taken from experiments in order to simulate the combustion. The highest brake efficiency of 45.2 % was achieved with a two-stage turbocharger. Furthermore, the intake temperature had a significant influence on both brake efficiency and the highest achievable load. The use of high rates of EGR (45 % to 55 %) was seen to reduce the brake efficiency significantly, as well as lower the exhaust temperatures.

I built and validated the 1-D gas dynamic multi cylinder engine model in the modeling framework GT-suite and designed and performed the simulations. Lianhao Yin performed the experiments and post-processed the experimental results under the supervision of Per Tunestål. I wrote the paper and Marcus Thern and Martin Tunér reviewed the paper before submission.

Paper II: Combined Low and High Pressure EGR for Higher Brake Efficiency with Partially Premixed Combustion

E. Svensson, L. Yin, P. Tunestål, M. Tunér

SAE Technical Paper, 2017-01-2267, 2017

This paper investigated the benefit of combining low and high pressure EGR, compared to applying only high pressure or low pressure EGR, to a heavy-duty compression ignition engine. The multi cylinder engine model, which is presented in Chapter 3, was used in all simulations to predict the gas dynamic phenomena while rate of heat release profiles were taken from experiments in order to simulate the combustion. A significant improvement in brake efficiency was achieved for the combined EGR configuration. The reason for this improvement was that it was possible to control the mass flow through the compressor and hence achieve a higher gas exchange efficiency.

I built and validated the 1-D gas dynamic multi cylinder engine model in the modeling framework GT-suite and designed and performed the simulations. Lianhao Yin performed the experiments and post-processed the experimental results under the supervision of Per Tunestål. I wrote the paper and Martin Tunér reviewed the paper before submission.

Paper III: Simulation Based Investigation of achieving Low Temperature Combustion with Methanol in a Direct Injected Compression Ignition Engine

E. Svensson, S. Verhelst

SAE Technical Paper, 2019-01-1152, 2019

This paper built on the findings from paper I and paper II which showed an apparent penalty in brake efficiency caused by high levels of dilution for the partially premixed combustion concept. An optimization study was conducted in order to investigate which engine settings should be used in order to maximize the brake efficiency while limiting emissions such as soot and NO_x. This investigation was performed on two different fuels. A gasoline fuel with a research octane number of 76 was chosen because such a fuel had been advocated in previous research as the best fuel for the partially premixed combustion concept. This gasoline fuel was compared to methanol as it is necessary to move away from fossil fuels and methanol is a liquid fuel with reasonably high energy content. Four operating points from the European stationary cycle were chosen which meant that the engine performance could be evaluated over a broad range of engine speed and load. The multi cylinder engine model, which is presented in Chapter 3, was used in all simulations to predict the gas dynamic phenomena while

the combustion was predicted with the stochastic reactor model presented in Chapter 3. The resulting brake efficiency was on average 2.4 %pt. higher with methanol than with the gasoline fuel. The explanation for this difference stemmed from a higher ratio of specific heats and a more favorable rate of heat release profile. In contrast, the resulting gas exchange efficiency was comparable between the two fuels, even though it was necessary to apply a significantly higher level of EGR in the case of gasoline.

I built and validated the 1-D gas dynamic engine models, calibrated and validated the stochastic reactor model, implemented the coupling for pre-processing, engine simulation, optimization and post-processing in Matlab as well as designed and performed the simulations. I wrote the paper and Sebastian Verhelst reviewed the paper before submission.

Paper IV: Numerical Optimization of Compression Ratio for a PPC Engine running on Methanol

E. Svensson, S. Verhelst

Paper accepted for publication at JSAE/SAE PFL, Kyoto, Japan

This paper investigated the effect of compression ratio for a heavy-duty compression ignition engine fueled with methanol. Specifically, it was thought that a higher compression ratio would lead to a lower required inlet temperature which then could be beneficial from both the perspective of brake efficiency but also ease cold starts. The compression ratio was optimized numerically with the purpose of finding the highest brake efficiency. Constraints were set on NO_x emissions, maximum in-cylinder pressure and maximum in-cylinder pressure rise rate. The multi cylinder engine model, which is presented in Chapter 3, was used in all simulations to predict the gas dynamic phenomena while the combustion was predicted with the stochastic reactor model presented in Chapter 3. The results showed that the optimal compression ratio was 21.6:1 for this engine and simulation conditions, which was substantially higher than the standard compression ratio of 17.3:1. The higher compression ratio resulted in a higher brake efficiency at low engine loads due to a higher ratio of specifics heats and lower inlet temperature. The reason why the optimal compression ratio was not higher is that at high engine loads, the air-to-fuel ratio could not be maintained and the combustion phasing had to be retarded in order to meet the constraint on maximum in-cylinder pressure, both of which led to a lower brake efficiency.

I built and validated the 1-D gas dynamic engine models, calibrated and validated the stochastic reactor model, implemented the coupling for pre-processing, engine simulation, optimization and post-processing in Matlab as well as designed and performed the simulations. I wrote the paper and Sebastian Verhelst reviewed the paper before submission.

Paper v: Evaluation of Injection Strategies at Maximum Brake Efficiency for a Methanol PPC Engine

E. Svensson, M. Tunér, S. Verhelst

Paper submitted to NASAE/SAE, Capri, Italy

This paper investigates the influence of different injection strategies for a heavy-duty compression ignition engine fueled with methanol. It was found in paper III and paper IV that a relatively earlier injection strategy yielded the highest brake efficiencies with methanol. A potential issue is that the start of combustion could be less affected by the actual injection timing and more by the inlet conditions such as pressure, temperature and composition. Thus it was of interest to see if a high brake efficiency could still be achieved with a retarded injection strategy. The multi cylinder engine model, which is presented in Chapter 3, was used in all simulations to predict the gas dynamic phenomena while the combustion was predicted with the stochastic reactor model presented in Chapter 3. The simulations were conducted on two different operating points: one with low engine load and one with high load. The results showed that the engine brake efficiency reduces with a retarded injection strategy. The largest reduction was found for the operating point with high engine load.

I built and validated the 1-D gas dynamic engine models, calibrated and validated the stochastic reactor model, implemented the coupling for pre-processing, engine simulation, optimization and post-processing in Matlab as well as designed and performed the simulations. I wrote the paper and Sebastian Verhelst and Martin Tunér reviewed the paper before submission.

Paper vi: Potential Levels of Soot, NO_x, HC and CO for Methanol Combustion

E. Svensson, C. Li, S. Shamun, B. Johansson, M. Tunér, C. Perlman, H. Lehtiniemi, F. Mauss,

SAE Technical Paper, 2016-01-0887, 2016

This paper investigates the potential levels of soot, oxides of nitrogen, unburned hydrocarbons and CO for a heavy-duty compression ignition engine fueled with methanol. The emission levels were compared to a diesel surrogate consisting of n-heptane and toluene. Temperature-equivalence ratio maps were constructed for both fuels which showed theoretical emission yields. This analysis revealed that the potential of producing soot from methanol is close to non-existing. Furthermore, formaldehyde can likely be insignificant if direct injection is applied. No substantial difference in the

levels of CO and NO_x were found when comparing methanol to diesel. A simulation of the closed part of the cycle was conducted with the stochastic reactor model in order to couple the emissions maps to actual engine conditions. The main finding from this simulation was that the ignition for methanol occurs at lean air-fuel conditions.

I calibrated and validated the stochastic reactor model and designed and performed the constant pressure reactor simulations as well as the engine simulations. Changle Li and Sam Shamun performed the engine experiments under the supervision of Bengt Johansson and Martin Tunér. Cathleen Perlman helped with support in the LOGEsoft framework. Harry Lehtiniemi and Fabian Mauss helped with the analysis of the results. I wrote the main part of the paper with the help of Harry Lehtiniemi who wrote the section about the chemical mechanism and soot modeling and Martin Tunér who wrote the main part of the introduction.